



**Calhoun: The NPS Institutional Archive**

---

Theses and Dissertations

Thesis Collection

---

1989

An electromagnetic radome model using an interactive micro-computer finite element algorithm.

Vince, Robert Johnston

Monterey, California. Naval Postgraduate School

---

<http://hdl.handle.net/10945/25893>



Calhoun is a project of the Dudley Knox Library at NPS, furthering the precepts and goals of open government and government transparency. All information contained herein has been approved for release by the NPS Public Affairs Officer.

**Dudley Knox Library / Naval Postgraduate School**  
**411 Dyer Road / 1 University Circle**  
**Monterey, California USA 93943**

<http://www.nps.edu/library>









# NAVAL POSTGRADUATE SCHOOL

## Monterey, California



# THESIS

V 684

AN ELECTROMAGNETIC RADOME MODEL USING AN  
INTERACTIVE MICRO-COMPUTER FINITE ELEMENT ALGORITHM

by

Robert Johnston Vince

December 1989

Thesis Co-Advisors:

Michael A. Morgan  
James P. Hauser

Approved for public release; distribution is unlimited

T248139

T248121



## REPORT DOCUMENTATION PAGE

REPORT SECURITY CLASSIFICATION UNCLASSIFIED		1b RESTRICTIVE MARKINGS	
SECURITY CLASSIFICATION AUTHORITY		3. DISTRIBUTION / AVAILABILITY OF REPORT Approved for public release; distribution is unlimited	
DECLASSIFICATION / DOWNGRADING SCHEDULE		5. MONITORING ORGANIZATION REPORT NUMBER(S)	
PERFORMING ORGANIZATION REPORT NUMBER(S)		7a. NAME OF MONITORING ORGANIZATION NAVAL POSTGRADUATE SCHOOL	
NAME OF PERFORMING ORGANIZATION NAVAL POSTGRADUATE SCHOOL	6b OFFICE SYMBOL (If applicable) 62	7b. ADDRESS (City, State, and ZIP Code) MONTEREY, CALIFORNIA 93943-5000	
ADDRESS (City, State, and ZIP Code) MONTEREY, CALIFORNIA 93943-5000		9. PROCUREMENT INSTRUMENT IDENTIFICATION NUMBER	
NAME OF FUNDING / SPONSORING ORGANIZATION	8b. OFFICE SYMBOL (If applicable)	10. SOURCE OF FUNDING NUMBERS	
ADDRESS (City, State, and ZIP Code)		PROGRAM ELEMENT NO.	PROJECT NO.
		TASK NO.	WORK UNIT ACCESSION NO.
TITLE (Include Security Classification) AN ELECTROMAGNETIC RADOME MODEL USING AN INTERACTIVE MICRO-COMPUTER FINITE ELEMENT ALGORITHM			
PERSONAL AUTHOR(S) ROBERT JOHNSTON VINCE			
TYPE OF REPORT MASTER'S THESIS	13b TIME COVERED FROM _____ TO _____	14. DATE OF REPORT (Year, Month, Day) 1989 DECEMBER	15 PAGE COUNT 175
SUPPLEMENTARY NOTATION THE VIEWS EXPRESSED IN THIS THESIS ARE THOSE OF THE AUTHOR AND DO NOT REFLECT THE OFFICIAL POLICY OR POSITION OF THE DEPARTMENT OF DEFENSE OR THE U.S. GOVERNMENT			
COSATI CODES		18 SUBJECT TERMS (Continue on reverse if necessary and identify by block number)	
FIELD	GROUP	Finite element algorithm; Computer aided design; Radome model; Azimuthal potentials	
ABSTRACT (Continue on reverse if necessary and identify by block number)			
<p>The goal of this thesis was to develop and validate a set of microcomputer programs using, in part, a previously written finite-element algorithm to analyze the perturbation of an incident electromagnetic field as it penetrates a missile radome. An interactive program was developed to design the radome structure using aerodynamic shaping functions and provide structure and material files as input to the finite-element code. A second program was developed to use the spherical harmonic expansion coefficients provided by the finite-element code to assemble the electromagnetic fields within the radome core and to display the fields that appear across a planar antenna with three-dimensional graphics for any orientation of the antenna. Algorithms were included which compare the computed field components to the theoretical incident plane wave for each stipulated angle of incidence, in order to determine the perturbation due to the presence of the radome. Validation of the computational method was attempted by analyzing the perturbation indicated for an ideal radome with relative permittivity of unity. The attempted validation showed phase errors in the computed fields which were minimal for axial incidence, but became significant for highly canted incidence.</p>			
DISTRIBUTION / AVAILABILITY OF ABSTRACT UNCLASSIFIED/UNLIMITED <input type="checkbox"/> SAME AS RPT. <input type="checkbox"/> DTIC USERS		21. ABSTRACT SECURITY CLASSIFICATION UNCLASSIFIED	
NAME OF RESPONSIBLE INDIVIDUAL Prof. M.A. Morgan		22b TELEPHONE (Include Area Code) 408-646-2677	22c. OFFICE SYMBOL 62Mo



Approved for public release; distribution is unlimited

An Electromagnetic Radome Model  
Using An Interactive Micro-Computer Finite Element Algorithm

by

Robert Johnston Vince  
Lieutenant, United States Navy  
B.S. Math, Tulane University, 1983

Submitted in partial fulfillment of the  
requirements for the degrees of

MASTER OF SCIENCE IN ELECTRICAL ENGINEERING

and

MASTER OF SCIENCE IN ENGINEERING SCIENCE (AERONAUTICS)

from the

NAVAL POSTGRADUATE SCHOOL

December 1989

## ABSTRACT

The goal of this thesis was to develop and validate a set of microcomputer programs using, in part, a previously written finite-element algorithm to analyze the perturbation of an incident electromagnetic field as it penetrates a missile radome. An interactive program was developed to design the radome structure using aerodynamic shaping functions and provide structure and material files as input to the finite-element code. A second program was developed to use the spherical harmonic expansion coefficients provided by the finite-element code to assemble the electromagnetic fields within the radome core and to display the fields that appear across a planar antenna with three-dimensional graphics for any orientation of the antenna. Algorithms were included which compare the computed field components to the theoretical incident plane wave for each stipulated angle of incidence, in order to determine the perturbation due to the presence of the radome. Validation of the computational method was attempted by analyzing the perturbation indicated for an ideal radome with relative permittivity of unity. The attempted validation showed phase errors in the computed fields which were minimal for axial incidence, but became significant for highly canted incidence.

TABLE OF CONTENTS

I.	INTRODUCTION .....	1
II.	RADOME DESIGN .....	6
	A.    RADOME DESIGN METHODOLOGY .....	6
	B.    RADOME SHAPING FUNCTIONS .....	8
	C.    RADOME WALL CONSTRUCTION .....	12
	D.    MATERIALS FOR RADOME CONSTRUCTION .....	16
III.	ELECTROMAGNETIC FIELD THEORY .....	21
	A.    BACKGROUND .....	21
	B.    GENERATION OF THE CORE REGION FIELDS .....	24
	C.    CANTING THE PLANAR ARRAY .....	37
IV.	PROGRAM EXECUTION AND DATA FLOW .....	41
	A.    THE RADOME MODEL DESIGN PROCESS .....	41
	B.    RADSHP EXECUTION .....	43
	C.    RADOME CONSTRUCTION VERIFICATION .....	49
	D.    EMRAD EXECUTION .....	52
	E.    CORFLD EXECUTION .....	62
V.	PROGRAM VALIDATION AND RESULTS .....	73
VI	CONCLUSIONS .....	93
	APPENDIX A - EMRAD FIELD THEORY .....	95
	APPENDIX B - RADSHP PROGRAM CODE .....	110
	APPENDIX C - CORFLD PROGRAM CODE .....	130
	APPENDIX D - SOFTWARE SOURCES .....	164

LIST OF REFERENCES .....165  
INITIAL DISTRIBUTION LIST .....167



## I. INTRODUCTION

Radome design is a composite discipline evolved from aeronautical, electrical, mechanical and materials engineering. The word radome was coined during World War II as a composite of two words, radar and dome [Ref. 1:p. ix]. The term radome originally described the family of dome-shaped structures designed and built to house and protect the radar antennas on aircraft, but now the term is applied to any structure that protects a radio frequency antenna system. The structure is designed to provide maximum protection to the antenna with minimum interference to the antenna's electrical performance.

Radomes on missiles are presently designed to meet many diverse specifications. These specification requirements can be divided into two categories, electrical and aero-mechanical. Electrical design problems include those that have to do with the radome's ability to act as a window, ideally transparent, to the electromagnetic energy that must pass through the radome to be used by the missile's antenna system. This energy is of a specific frequency range and intensity that is within the operating parameters of the antenna system. The magnitude and form of the electromagnetic energy will be dependent on range from the source, polarization, and incident angle. Aero-mechanical design problems address not only the design of the structure of the radome, but also the ability of the

radome to withstand environmental conditions and battle damage. Environmental conditions vary with scenario, and include: normal pressure force and viscosity, wind loads, inertial loads, temperature variations, moisture resistance, resistance to rain erosion, and other diverse factors. Design of a radome for use in battle may require that the aero-mechanical design consider resistance to nuclear radiation and laser weapons.

As in any engineering design, there are tradeoffs between the various requirements, such that each interrelated component design factor must be weighted and considered in the overall system design. Numerical models of environmental conditions assist in the analysis of the tradeoffs for the aero-mechanical design. Numerical models to aid in the electrical design analysis of a radome to protect missile antenna systems which operate at high frequencies are available, such as the ray-tracing algorithms described by Hirsch and Grove in Ref. 2. When a missile antenna system requires operation in the resonance region of frequencies for the radome parameters, a numerical model is required that can solve the radome interaction problem.

The subject of this thesis is the development of a generalized, interactive set of programs to be used in the analysis of the interaction between an actual or proposed radome structure and incident electromagnetic fields at the lower frequencies of interest, where strong resonance characteristics exist. In order to analyze a specified radome, a numerical model is constructed using the interactive program, RADSHP. This radome generation program

provides geometric shaping functions to allow the user to construct a multilayer radome model of specified materials. Chapter II provides a discussion of radome design methodology, the aerodynamic shaping functions available in this package, radome wall constructions, and material specification.

This thesis work is an application of the programs developed for use on a personal computer by Morgan [Ref. 3] and Connolly [Ref. 4] to calculate electromagnetic scattering by inhomogeneous dielectric and/or magnetic bodies of revolution. As discussed in Chapter II, radomes are manufactured using dielectric materials in order to provide a radio frequency window to the antenna housed in the radome's interior. An axisymmetric missile radome structure meets the physical structure requirement for rotational symmetry. The numerical analysis of the interaction of the specified radome structure and the incident electromagnetic energy is performed by the code developed by Morgan, EMCAD. Modifications to this code resulted in the program EMRAD, which provides data file generation to store the modal expansion coefficients which are used by the program CORFLD to determine the electromagnetic fields within the radome interior. In Chapter III, the theory required for the formulation of the computed interior fields of the radome by the program CORFLD is discussed.

The programs developed by Morgan use an optimized variational finite-element algorithm in conjunction with a tri-regional unimoment method to provide scattering solutions for each of multiple incident fields impinging on the specified structure.



The programs represent a significant improvement in computational speed and versatility over computer codes which find the solution to the electromagnetic resonance behavior by use of surface current integral equation formulations. An overview of the finite element scattering algorithm, along with the concepts embodied in the coupled azimuthal potentials and the unimoment method are included in Appendix A. Further information is available in references 3, 4, 5, 6, and 7.

Chapter IV discusses the flow of data between the programs which have been developed. The general use of the RADSHIP program to construct the radome data files is discussed, as well as the data files generated and their uses. The flow of information into and out of the radome analysis program EMRAD is analyzed. The execution and operation of CORFLD is discussed.

In Chapter V, the validation of the interior field computation is discussed, wherein the numerically generated fields are compared to the incident fields for a radome constructed of air. The results produced for radomes constructed of materials presently used in the radome industry are presented and discussed.

The conclusions in Chapter VI will summarize the work previously presented, as well as provide recommendations for future modifications to the interactive package of programs being used.

Additional Appendices are included to provide copies of the source code for the computer programs, RADSHIP and CORFLD, which were written as part of this thesis effort. Source listings for additional programs, such as EMCADIN, EMESH, and EMRAD are

available upon request from Prof. Michael A. Morgan. His address is given in Appendix D, Software Sources.

## II. RADOME DESIGN

### A. RADOME DESIGN METHODOLOGY

The configuration of a radome for high-speed missiles must combine high aerodynamic performance with a highly accurate transmission of electromagnetic energy through the radome to the missile seeker. As described in Ref. 2, the methodology for establishing radome performance requirements is an iterative process. Figure 2.1 shows the process as a set of design procedure loops that begin with a statement of desired performance, and include analytical studies, hardware development, and hardware evaluation. These result in a set of optimized radome requirements, which is the blueprint from which a radome can be constructed. Computer software tools help to maximize the benefit of the work done in analytical studies, thereby minimizing the number of iterations required for the hardware development and evaluation. The programs described in this thesis are designed to analyze the interaction between the aerodynamic considerations in radome design and the electrical performance of the radome.

The aerodynamic considerations in the design of a radome structure are three-fold: shape-generated drag, thermal stress from aerodynamic heating, and structural performance. These three

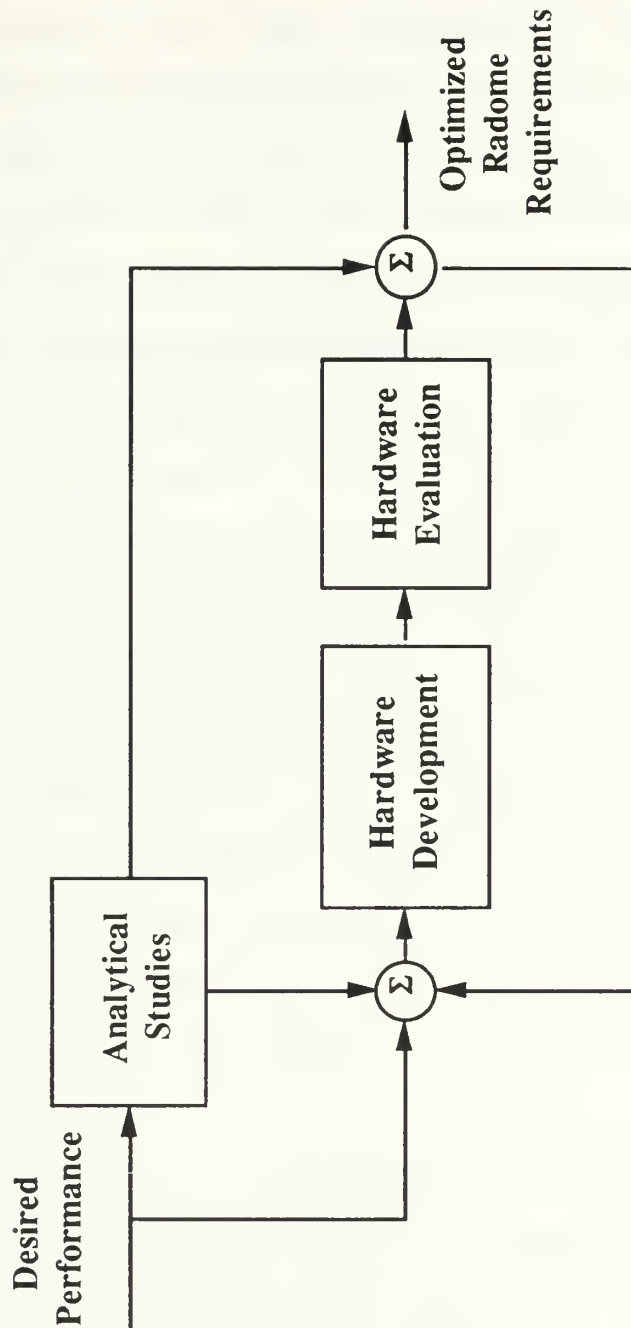


Figure 2.1 Methodology for establishing radome requirements

parameters are not independent of each other, and the electrical performance of the radome is a strong function of these aerodynamic factors. The outer shape of the radome has a large impact on how the missile will fly through the air. It is this outer conformation that will, along with speed of travel and angle of attack, determine the forces that act on the radome structure during flight. The forces generated during flight determine the design requirements on the radome structure for material strength and thermal stress. Fortunately, the shapes that result in the best drag performance are those that can also be used to develop radomes that match the structural requirements. Unfortunately, the shapes that best meet the drag requirements are not necessarily the best for maximizing the electrical performance. The programs developed in this thesis include the computer aided design (CAD) functions to analyze several shaping functions that aerodynamicists have developed to minimize the aerodynamic drag forces with respect to radome structure parameters.

## B. RADOME SHAPING FUNCTIONS

An ogive shaping function is one of the most common used in radome designs. The ogive shape is popular because it is easily fabricated and has relatively acceptable aerodynamic performance at high speeds. It is defined [Ref. 1:p. 48] as a segment of the arc of a circle, whose radius,  $F_1$ , is greater than the radius of the radome base. A pointed ogive is generated when the circle's radius,  $F_1$ , is

large enough so that the arc reaches the radome's axis of symmetry. The ogive shaping function is described by

$$x = \sqrt{F_1^2 - ((H-z)-F_2)^2} - F_3 , \quad (2.1)$$

where  $F_2$  and  $F_3$  determine the position of the circular shaping arc, as illustrated in Fig. 2.2. The ogive shaping function degenerates to a hemisphere when the shaping factors,  $F_2$  and  $F_3$ , are defined as  $F_2 = F_1$  and  $F_3 = 0$ .

A tangent ogive shaping function generates a radome shape such that the surface of the radome is tangent at the base of the radome, providing a smooth transition to the missile body [Ref. 8]. A tangent ogive shaping function is determined such that

$$x = 4 \left( \sqrt{F_4^2 - z^2} - F_5 \right) , \quad (2.2)$$

where

$$F_4 = \frac{R}{2} + 2 \frac{H^2}{R} \quad (2.3)$$

and

$$F_5 = F_4 - \frac{R}{4} . \quad (2.4)$$

A shaping function that provides maximum volume-to-drag ratio at high flight speeds is the von Karman function [Ref. 1:p. 48] ,

$$x = \frac{1}{R\sqrt{\pi}} \left[ F_z - \frac{1}{2} \sin(2F_z) \right]^{\frac{1}{2}} , \quad (2.5)$$

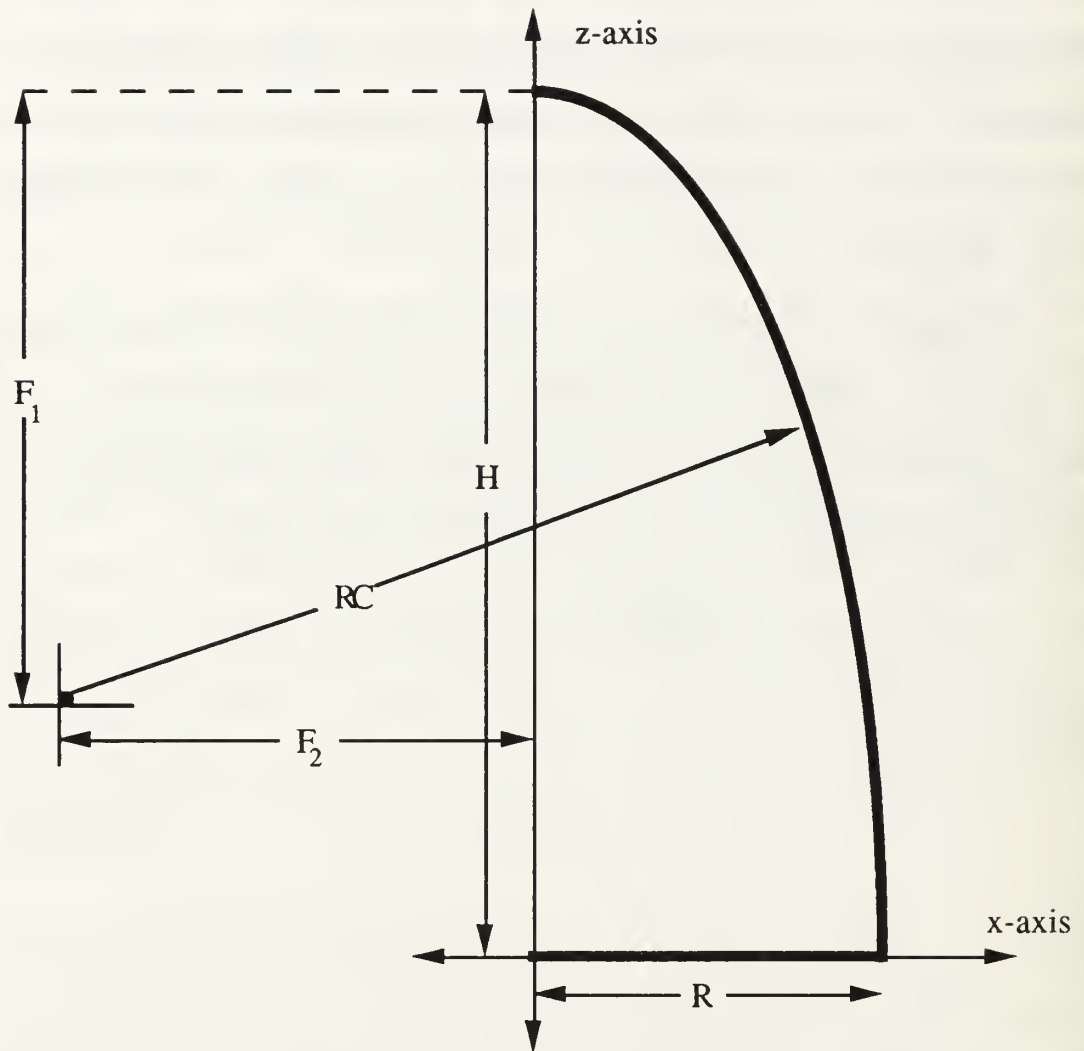


Figure 2.2 Radome shape - nomenclature

where

$$F_z = \cos^{-1} \left[ 1 - 2 \frac{(H-z)}{H} \right] . \quad (2.6)$$

Radomes described by this von Karman shaping function have a limited application due to fabrication difficulties related to the complex shape.

In order to minimize drag for a given height-to-radius ratio, a Newtonian contour is used. This contour is approximated by the power series radome shaping function [Ref. 1:p. 49],

$$x = R \left( \frac{(H-z)}{H} \right)^{F_6} . \quad (2.7)$$

The exponent,  $F_6$ , provides for shaping. When  $F_6 = 1.0$ , the radome shape generated is conical. Aerodynamicists normally use  $F_6 = 0.75$  to approximate the Newtonian contour.

A shaping function analyzed by Hirsch and Grove [Ref. 2] uses a parabolic basis function for the radome shape,

$$x^2 = F_7 - z . \quad (2.8)$$

The rounded effect developed at the tip of the radome by the parabolic shape function can be eliminated by the creation of a mathematical "deadzone" for points within a region about the radome's apex. The parabolic shaping coefficient,  $F_7$ , determines the extent of the "dead zone" and thereby controls the slope of the parabolic surface. The radome shape is determined in terms of the shaping coefficient, then scaled to the radome size parameters. The



unscaled shaping function,

$$x = \sqrt{F_7 - z} , \quad (2.9)$$

is used to generate a parabolic radome shape with a height of  $F_7$ . In order to eliminate the parabolic rounding of the apex, the "deadzone" is established for any points for the unscaled  $z$  value within 1.0 of  $F_7$ . Within this deadzone,  $z > ( F_7 - 1 )$ , the radome shape is determined at a line of constant slope, converging at a height of  $z = F_7 + 1.0$ . This results in the marrying of a pointed apex onto the parabolic radome shape, with the magnitude of the shaping coefficient,  $F_7$ , determining the relative magnitude of the apex to the total radome height.

This project contains coding in RADSHP to generate radomes of multiple layers for the shaping functions described: the general ogive, the tangent ogive, the von Karman shape, the power series radome, and the parabolic radome with pointed apex. RADSHP can generate a complex radome construction model using different shaping functions for each layer. RADSHP generates a material data file appropriate for input to the numerical analysis program, EMRAD, and a structure data file that can be viewed and modified using CURVE DIGITIZER (Appendix 2), then translated by EMCADIN into an input structure data file for EMRAD.

### C. RADOME WALL CONSTRUCTION

If a material existed which was mechanically strong enough to sustain the aerodynamic forces that the radome experiences during

flight, and that same material had the electromagnetic properties of a vacuum, then the radome could be built to ideally meet all requirements. Such a material does not exist, and, in general, as the requirement for material strength increases, the electromagnetic properties tend to strongly deviate from the properties of the ideal vacuum. The transmissivity of the radome tends to decrease as the dielectric constants of the construction materials increase. In order to meet strength requirements, while minimizing the perturbation caused to the electromagnetic field, layer construction of radomes has been developed.

Lamination construction methods allow for an alternating combination of thin layers of high density, high strength materials of high dielectric constants, with thicker layers of low density, lower strength materials of low dielectric constants. Electromagnetic design of laminated radomes is more complex than the design of monolithic radomes in that there is a greater number of boundary conditions to be considered in establishing the lamination layer thicknesses. The EMRAD program developed by Morgan [Ref. 3] currently handles layered dielectrics with up to five layers.

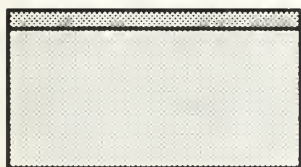
Figure 2.3, adapted from the Radome Engineering Handbook [Ref. 1:p. 46], shows several types of laminated wall construction that exhibit the alternation of layers of low dielectric constant and high dielectric constant materials. The two-ply sandwich is the simplest form of lamination construction with a thin skin of strong, dense material of high dielectric constant, supported internally by a thicker

layer of porous material of low dielectric constant. This design is especially attractive at low frequencies as the lateral dimension of the thin layer of dense material is only a fraction of the longer wavelength.

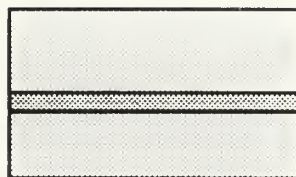
The A-sandwich and B-sandwich are two variations of a stronger three-layer construction. Although the A-sandwich is superior electrically to the B-sandwich, while the placement of the high density material in the center of the layer construction will strengthen the radome wall by making it stiffer, the porous, low density material on the exterior of the radome wall will not sustain the aerodynamic forces during flight.

The B-sandwich's inner and outer skin of high density material and the core of low dielectric material provide stiffness and strength to the radome structure while providing a dense outer skin. This construction has a higher strength-to-weight ratio than a monolithic construction. The core thickness is determined by the strength requirements and provides spacing between the inner and outer skin. Optimal electrical spacing between the skins would be frequency dependent at a core thickness of a quarter wavelength [Ref 1:p. 45].

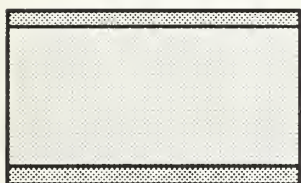
The C-sandwich and multilayer radome wall constructions provide for very high strength levels which may be required at high



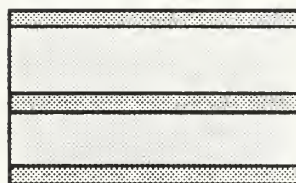
**Two-Ply Sandwich**



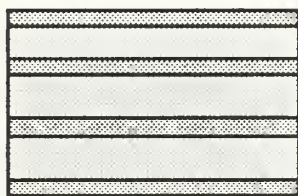
**A-Sandwich**



**B-Sandwich**



**C-Sandwich**



**Multilayer**



**Dense Material**



**Porous Material**

Figure 2.3 Laminated radome wall construction

operating speeds or for use in inclement weather. The layer material may consist of plastic laminates and ceramics. Multilayered construction is attractive where extreme structural rigidity or broadband capabilities are primary requirements. [Ref. 1:p. 46]

The radome interacts with the electromagnetic field as a lens, modifying the field as it passes through the radome structure. At higher frequencies, this interaction can be predicted by the use of ray-tracing techniques, similar to optical lens analysis [Refs. 2 and 8]. Studies have been conducted at higher frequencies to design a layer of dielectric material within the radome's interior structure to act as a correcting lens [Ref. 8] as shown in Fig. 2.4 . This package of programs will allow similar analysis of lens construction at lower frequencies, where the radome and lens parameters are within the resonance region of the electromagnetic fields.

#### D. MATERIALS FOR RADOME CONSTRUCTION

The choice of material for construction of a radome is another engineering design decision. As material science engineers continue to develop new materials, particularly low-weight, high-strength ceramics, the range of materials available to the radome designer increases. The general properties of the three groups of materials which are in common use are listed in Ref. 9, and is used here as a source for material selection. The groups of materials discussed are fiber-reinforced organic resins, refractory oxides, and glass ceramics. Physical properties are listed in Table 2.1.

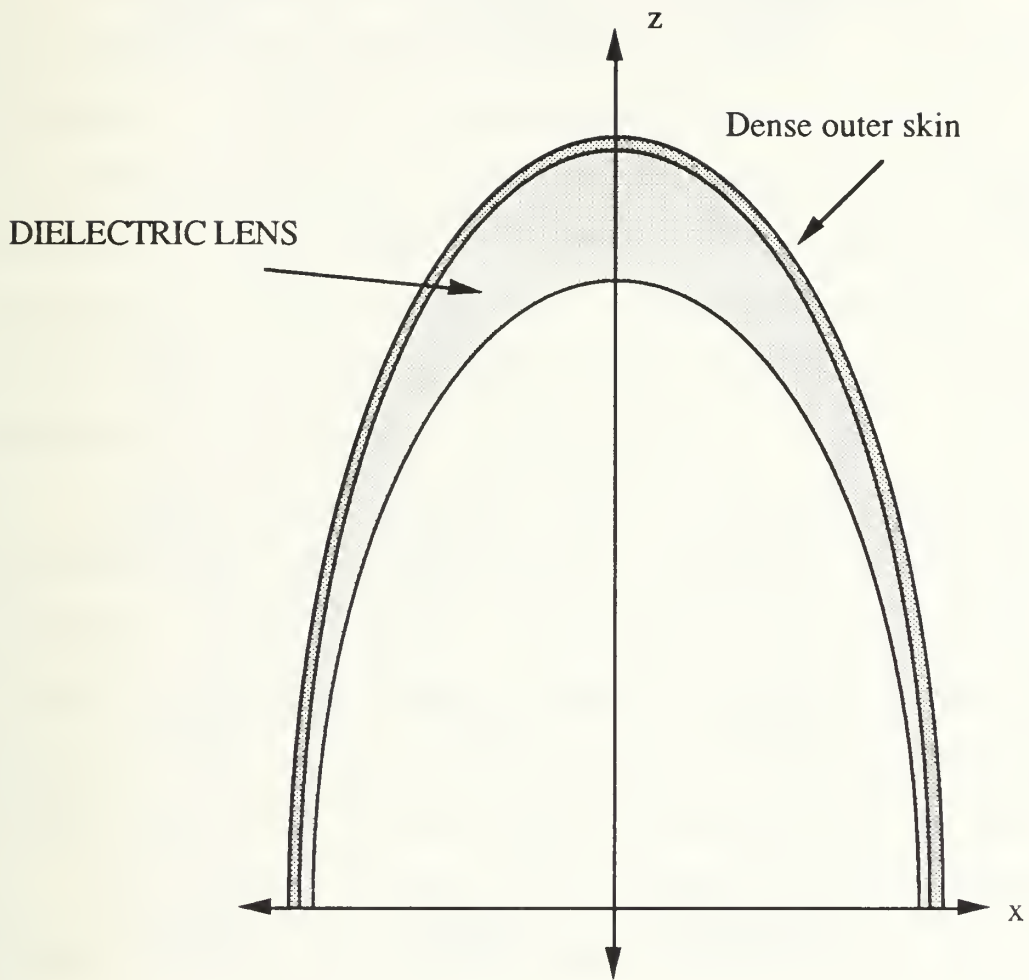


Figure 2.4 Interior radome lens of dielectric material

TABLE 2.1

## RADOME MATERIAL PROPERTIES

	FIBER REINFORCED RESINS	GLASS CERAMICS	REFRACTORY OXIDES
Relative permittivity ( $\epsilon_r$ )	4-6	5.5	8-9
Loss tangent ( $\tan \delta$ )	0.01	0.003	0.002
Density	N/A	160 lb/ft <sup>3</sup>	220 lb/ft <sup>3</sup>
Ultimate Tensile Strength (UTS)	40 kpsi	7 kpsi	27 kpsi
Compressive Strength	20-40 kpsi	35 kpsi	280 kpsi
Maximum Temperature	260 ° C	500 ° C	1700 ° C

In fiber-reinforced organic resins, a variety of resin types are used to impregnate fiberglass. Organic resins, such as phenolic, polyester, and epoxy are used with the fiber to construct the radome. They are then thermally treated to set the structure. Several manufacturing techniques are discussed in Ref. 1. Control of layer thickness is difficult to maintain and requires finishing to avoid aberration. Radomes constructed of these materials have poor resistance to rain erosion, but are relatively cheap and easy to manufacture, even in large sizes. Maximum temperatures that the material can sustain limit use of these materials to missiles with speed of less than Mach 1.5 to Mach 2.0.

Typical glass ceramics used in radome construction are Pyrocream and glass-bonded mica. Compared to organic radome materials, ceramic materials have much higher resistance to rain erosion at supersonic speeds. Ceramics are brittle materials and the controls needed during manufacturing to ensure structural integrity of the radomes makes them expensive to build [Ref. 1:p. 242].

The refractory oxide used in radome construction is usually alumina ( $\text{Al}_2\text{O}_3$ ), but magnesia ( $\text{MgO}$ ) and fused silica ( $\text{SiO}_2$ ) are also used. Refractory oxide manufacturing is also expensive due to the high temperatures used in forming these materials to the desired radome shape. These materials have high dielectric constants, that can undergo a change of up to ten percent between room temperature and 1700 °C. Some of the methods by which refractory oxide radomes are manufactured are slip casting, isostatic pressing,



and flame spraying [Ref. 1:pp. 298-313]. Oxides have a high resistance to rain erosion and wall thickness can be controlled to within 0.002 inches, allowing for extreme control of aberration. Although the dielectric constant of these materials is high, they provide the highest degree of thermal protection and place the least restriction on missile speed.

### III. ELECTROMAGNETIC FIELD THEORY

#### A. BACKGROUND

The analysis of the interaction between a missile's radome and the electromagnetic signal that is radiated or received by that missile's radar is a problem similar to those undergoing intensive investigation in electromagnetic interaction with other physical medium. Ongoing study of medium interactions include other military weapons and weapons platforms, forested areas, bodies of water, rain, and biological tissues [Refs. 3, 5, and 10]. The study of electromagnetic wave penetration through missile radomes allows for a special approach to the solution of the problem for the common case of rotational symmetry in the construction of the radome. In the high-frequency regime, the solution may be found as described by Hirsch and Grove [Ref. 2], with application of an asymptotic approach using the geometrical theory of diffraction (GTD), which incorporates ray-tracing. When lower frequencies are considered, and the interaction problem is in the resonance region, a complete solution of Maxwell's equations is required. The asymptotic GTD method yields unsatisfactory results.

The solution of Maxwell's equations for the radome used within this project is divided into three regions as illustrated in Fig. 3.1. The three regions are the homogenous spherical inner radome core (designated Region I); the transition region, where a semi-annular conformal mesh is generated for field analysis (designated Region II);

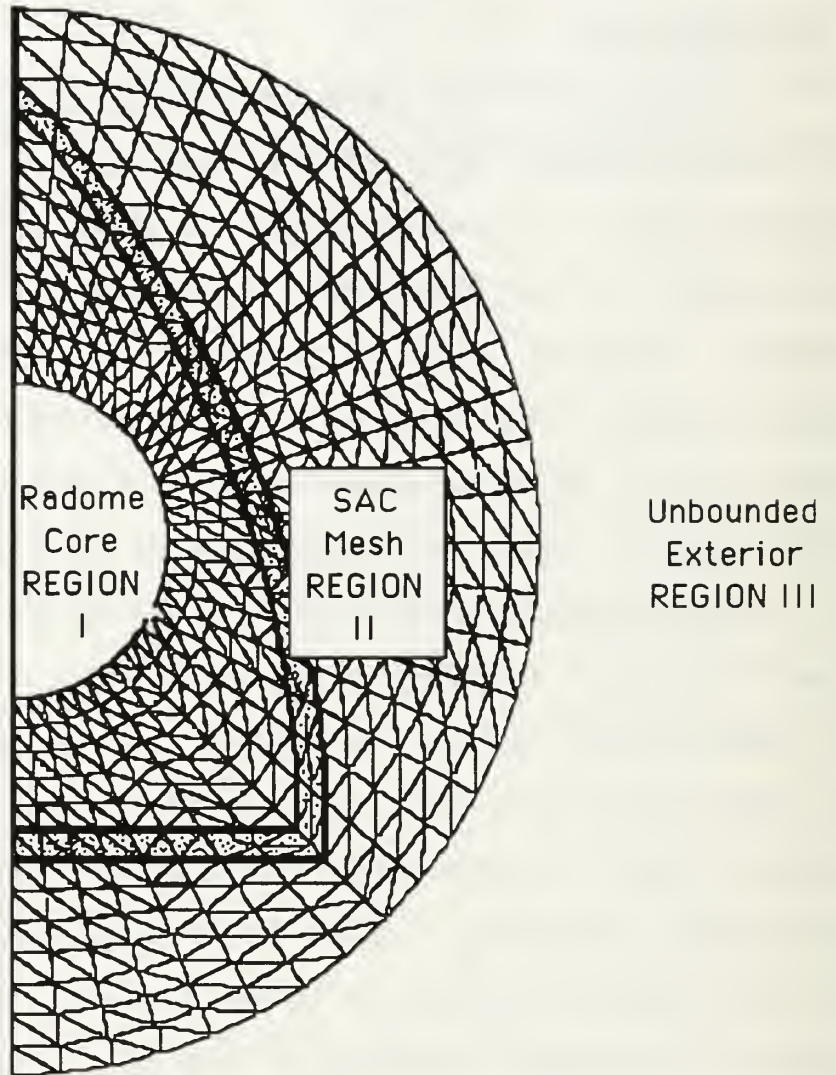


Figure 3.1 Three spatial radome regions for electromagnetic field analysis

and an unbounded exterior scattering region (designated Region III). The total solutions for the fields in the core, Region I, and the scattered fields in the exterior region, Region III, are produced via separate spherical harmonic expansions. Using the unimoment method (Appendix A), the modes in these expansions are applied as boundary conditions on the inner and outer spherical surfaces bounding the mesh and the resultant fields for each such mode are found using the finite element method. A similar analysis is performed for the incident fields on the outer surface.

Using superposition, the finite element solutions are then combined using the same unknown coefficients as in the original expressions. The combined finite element solution is equated, in the least squares sense, to the original expressions along the inner and outer surfaces. Enforcement of this equality allows solution of the expansion coefficients for the core and exterior regions.

The exterior expansion coefficients are used by EMRAD to assemble the scattered fields and bistatic radar cross sections (see Refs. 3 and 4). The core region spherical harmonic expansion coefficients are used to construct the fields that penetrate the radome to illuminate the enclosed antenna. The details of how these interior region fields are generated, using the core region spherical harmonics, is the topic of the next section. An overview of the theory used by Morgan in EMRAD is included in Appendix A. Further information is available in Refs. 3, 4, 5, 6, and 7.

## B. GENERATION OF THE CORE REGION FIELDS

In this section we will consider the construction of the core region fields using the expansion coefficients provided by EMRAD. These fields are assembled and plotted in various ways over user-selected planar surfaces by CORFLD.

Within the spherical core, the source-free phasor Maxwell's curl equations, with suppressed  $e^{j\omega t}$  time variation, are

$$-\nabla \times \mathbf{E} = j\omega \mu \mathbf{H} \quad (3.1)$$

and

$$\nabla \times \mathbf{H} = j\omega \epsilon \mathbf{E} \quad (3.2)$$

where  $\mu$  and  $\epsilon$  are the respective permeability and permittivity. The  $\mu$  and  $\epsilon$  will usually be those of free-space for the case of the core region in a radome.

In a homogenous, source-free spherical region, such as the radome core, it can be shown [Ref. 11] that the vector electromagnetic field can be represented by the combination of two types of spherical harmonic fields, transverse magnetic (TM) and transverse electric (TE). Using the spherical coordinates of Fig. 3.2, these TM and TE fields have the respective properties that  $H_r = 0$  and  $E_r = 0$ . Furthermore, the TM and TE vector fields can be generated from radially directed vector potentials, such that for the TM fields,

$$\mathbf{A} = A_r \mathbf{r} \quad (3.3)$$

and

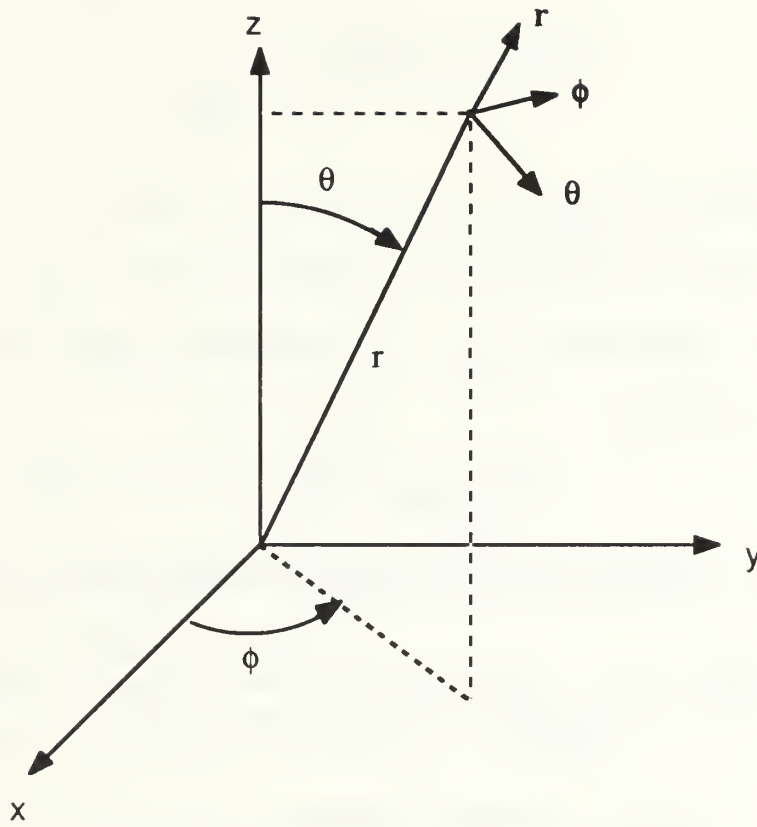


Figure 3.2 Spherical coordinates with unit vectors

$$\mathbf{F} = F_r \mathbf{r} , \quad (3.4)$$

where the radial components satisfy

$$\nabla^2 \left( \frac{A_r}{r} \right) + k^2 \left( \frac{A_r}{r} \right) = 0 \quad (3.5)$$

and

$$\nabla^2 \left( \frac{F_r}{r} \right) + k^2 \left( \frac{F_r}{r} \right) = 0 . \quad (3.6)$$

These equations are in the form of the complex scalar Helmholtz equation,

$$\nabla^2 \Psi + k^2 \Psi = 0 . \quad (3.7)$$

In spherical coordinates, the Helmholtz equation becomes [Ref. 11],

$$\frac{1}{r^2} \frac{\partial}{\partial r} \left( r^2 \frac{\partial \Psi}{\partial r} \right) + \frac{1}{r^2 \sin \theta} \frac{\partial}{\partial \theta} \left( \sin \theta \frac{\partial \Psi}{\partial \theta} \right) + \frac{1}{r^2 \sin^2 \theta} \frac{\partial^2 \Psi}{\partial \phi^2} + k^2 \Psi = 0 . \quad (3.8)$$

To find a solution to this differential equation, the method of separation of variables is used. Letting

$$\Psi = R(r) \Theta(\theta) \Phi(\phi) , \quad (3.9)$$

the separation of variables procedure yields the system of ordinary differential equations:

$$\frac{d}{dr} \left( r^2 \frac{dR}{dr} \right) + [k^2 r^2 - n(n+1)] R = 0 , \quad (3.10)$$

$$\frac{1}{\sin\theta} \frac{d}{d\theta} \left( \sin\theta \frac{d\Theta}{d\theta} \right) + \left[ n(n+1) - \frac{m^2}{\sin^2\theta} \right] \Theta = 0 , \quad (3.1 1)$$

and

$$\frac{d\Phi^2}{d\phi^2} + m^2 \Phi = 0 . \quad (3.1 2)$$

The R equation is related to Bessel's equation, and its solutions are in the form of spherical Bessel functions. Spherical Bessel functions,  $b_n$  , are related to ordinary Bessel functions,  $B_n$ , as indicated.

$$R(r) = b_n(kr) = \sqrt{\frac{\pi}{2kr}} B_{\left(n+\frac{1}{2}\right)}(kr) . \quad (3.1 3)$$

The  $\Theta$  equation is related to Legendre's equation and its solutions are the associated Legendre functions,

$$\Theta(\theta) = L_n^m(\cos\theta) \rightarrow P_n^m(\cos\theta) , Q_n^m(\cos\theta) , \quad (3.14)$$

where  $P_n^m(\cos\theta)$  are the associated Legendre functions of the first kind and  $Q_n^m(\cos\theta)$  are the associated Legendre functions of the second kind. The associated Legendre functions of the second kind tend toward infinity at points along the z-axis and must be excluded for solutions which include this region.



The  $\Phi$  equation has harmonic sinusoidal type solutions

$$\begin{aligned}\Phi(\phi) &= h(m\phi) \rightarrow \cos(m\phi), \sin(m\phi), e^{\pm jm\phi} \\ &= c_1 \cos(m\phi) + c_2 \sin(m\phi) \\ &= c_3 e^{+jm\phi} + c_4 e^{-jm\phi} .\end{aligned}\tag{3.15}$$

Together, these separated solutions form the product solutions to the Helmholtz equation as

$$\Psi_{m,n} = b_n(kr) P_n^m(\cos\theta) h(m\phi) .\tag{3.16}$$

Equations of this type form the elementary spherical harmonic wave functions. The general solution to the Helmholtz equation is formed by summation of linear combinations of these elementary functions, one for the TM fields and one for the TE fields. Each of these solutions will be of the form

$$\Psi(r,\theta,\phi) = \sum_m \sum_n b_n(kr) P_n^m(\cos\theta) h(m\phi) .\tag{3.17}$$

The summation over all possible  $m$  and  $n$  is limited by the nature of the Legendre polynomial of the first kind in that  $P_n^m = 0$  for  $n < m$ . The summation is also limited by the restriction that  $n$  will not equal zero when  $m$  is zero. For both  $n$  and  $m$  equal to zero, then the field evaluated is zero, therefore this solution is also excluded. Then  $m$  is zero and the summation over  $n$  will start with  $n$  equal to one. This leads to the scalar field expansion

$$\Psi(r, \theta, \phi) = \sum_{m=0}^{\infty} \sum_{\substack{n=m \\ n \neq 0}}^{\infty} (c_{mn} \cos m\phi + d_{mn} \sin m\phi) P_n^m(\cos\theta) b_n(kr). \quad (3.18)$$

As the Helmholtz equation under consideration is given as

$$\nabla^2 \Psi + k^2 \Psi = 0, \quad (3.19)$$

then for the TM case

$$\Psi = \frac{A_r}{r}, \quad (3.20)$$

and for the TE case

$$\Psi = \frac{F_r}{r}. \quad (3.21)$$

The spherical harmonic solutions of the Helmholtz equations for these sets of modes are then of the form

$$\left\{ \begin{array}{c} A_r \\ F_r \end{array} \right\} = r \Psi_{m,n} = [(kr) b_n(kr)] P_n^m(\cos\theta) h(m\phi). \quad (3.22)$$

In this renormalized form of the solution to the scalar Helmholtz equation, the Riccati (or Schelkunoff) spherical Bessel functions are present. The Riccati spherical Bessel functions relate to the spherical Bessel function and normal Bessel functions as follows:

$$\tilde{J}_n(kr) = [(kr) b_n(kr)] = \sqrt{\frac{\pi kr}{2}} B_{\left(n+\frac{1}{2}\right)}(kr). \quad (3.23)$$

Therefore, in the spherical core region, the solutions for  $A_r$  and  $F_r$  are of the form

$$\begin{Bmatrix} A_r \\ F_r \end{Bmatrix} = \sum_{m=0}^{\infty} \sum_{\substack{n=m \\ n \neq 0}}^{\infty} (c_{mn} \cos m\phi + d_{mn} \sin m\phi) P_n^m(\cos\theta) \hat{J}_n(kr) . \quad (3.24)$$

When expressed in terms of exponential Fourier series in  $\phi$ , the solutions are of the form

$$\begin{Bmatrix} A_r \\ F_r \end{Bmatrix} = \sum_{m=-\infty}^{\infty} \sum_{\substack{n=m \\ n \neq 0}}^{\infty} a_{mn} P_n^m(\cos\theta) \hat{J}_n(kr) e^{jm\phi} . \quad (3.25)$$

The coefficients within the two summations are determined by the solution of the scattering problem provided by EMRAD.

The spherical coordinate electric and magnetic field components can now be found for the TE and TM cases. For the TM case, where

$$\mathbf{H}_{TM} = \nabla \times (A_r \mathbf{r}) \quad (3.26)$$

and

$$\mathbf{E}_{TM} = \frac{1}{j\omega\epsilon} \nabla \times \nabla \times (A_r \mathbf{r}) , \quad (3.27)$$

the field components are

$$E_{rTM} = \frac{1}{j\omega\epsilon} \left( \frac{\partial^2}{\partial r^2} A_r + k^2 A_r \right) \quad (3.28)$$

$$E_{\theta TM} = \frac{1}{j\omega\epsilon} \frac{1}{r} \frac{\partial^2 A_r}{\partial r \partial \theta} \quad (3.29)$$

$$E_{\phi TM} = \frac{1}{j\omega\epsilon} \frac{1}{r \sin\theta} \frac{\partial^2 A_r}{\partial r \partial \phi} \quad (3.30)$$

$$H_{r_{TM}} = 0 \quad (3.31)$$

$$H_{\theta_{TM}} = \frac{1}{r \sin \theta} \frac{\partial A_r}{\partial \phi} \quad (3.32)$$

$$H_{\phi_{TM}} = -\frac{1}{r} \frac{\partial A_r}{\partial \theta} \quad (3.33)$$

For the TE case, where

$$\mathbf{H}_{TE} = -\nabla \times (\mathbf{F}_r \mathbf{r}) \quad (3.34)$$

and

$$\mathbf{E}_{TE} = \frac{1}{j\omega\epsilon} \nabla \times \nabla \times (\mathbf{F}_r \mathbf{r}), \quad (3.35)$$

the field components are

$$E_{r_{TE}} = 0 \quad (3.36)$$

$$E_{\theta_{TE}} = -\frac{1}{r \sin \theta} \frac{\partial F_r}{\partial \phi} \quad (3.37)$$

$$E_{\phi_{TE}} = \frac{1}{r} \frac{\partial F_r}{\partial \theta} \quad (3.38)$$

$$H_{r_{TE}} = \frac{1}{j\omega\mu} \left( \frac{\partial^2}{\partial r^2} F_r + k^2 F_r \right) \quad (3.39)$$

$$H_{\theta_{TE}} = \frac{1}{j\omega\mu} \frac{1}{r} \frac{\partial^2 F_r}{\partial r \partial \theta} \quad (3.40)$$

$$H_{\phi_{TE}} = \frac{1}{j\omega\mu} \frac{1}{r \sin \theta} \frac{\partial^2 F_r}{\partial r \partial \phi} \quad (3.41)$$

The total fields are the sum of the TE and TM parts

$$E_r = \frac{1}{j\omega\epsilon} \left( \frac{\partial^2}{\partial r^2} A_r + k^2 A_r \right) \quad (3.42)$$

$$E_\theta = -\frac{1}{r \sin\theta} \frac{\partial F_r}{\partial \phi} + \frac{1}{j\omega\epsilon} \frac{1}{r} \frac{\partial^2 A_r}{\partial r \partial \theta} \quad (3.43)$$

$$E_\phi = \frac{1}{r} \frac{\partial F_r}{\partial \theta} + \frac{1}{j\omega\epsilon} \frac{1}{r \sin\theta} \frac{\partial^2 A_r}{\partial r \partial \phi} \quad (3.44)$$

$$H_r = \frac{1}{j\omega\mu} \left( \frac{\partial^2}{\partial r^2} F_r + k^2 F_r \right) \quad (3.45)$$

$$H_\theta = \frac{1}{r \sin\theta} \frac{\partial A_r}{\partial \phi} + \frac{1}{j\omega\mu} \frac{1}{r} \frac{\partial^2 F_r}{\partial r \partial \theta} \quad (3.46)$$

$$H_\phi = -\frac{1}{r} \frac{\partial A_r}{\partial \theta} + \frac{1}{j\omega\mu} \frac{1}{r \sin\theta} \frac{\partial^2 F_r}{\partial r \partial \phi} \quad (3.47)$$

The solution for the coefficients in the  $A_r$  and  $F_r$  expansions is performed by the finite element and unimoment solution method explained in Appendix A. The finite element method is used by EMRAD and applied to Region II between the inner core and outer exterior region. In this finite element region there is the inhomogeneous axially symmetric structure of the radome.

EMRAD generates solutions for incident plane waves with Poynting vectors at incident angles specified by the program user, such that the Poynting vector's direction is specified by the unit propagation vector  $\mathbf{p} = \sin \alpha \mathbf{x} + \cos \alpha \mathbf{z}$ . As any plane wave can be decomposed into the sum of two orthogonal, linearly polarized plane waves, EMRAD evaluates two plane waves for each incident angle, a TM plane wave and a TE plane wave, as shown in Fig. 3.3. The TM

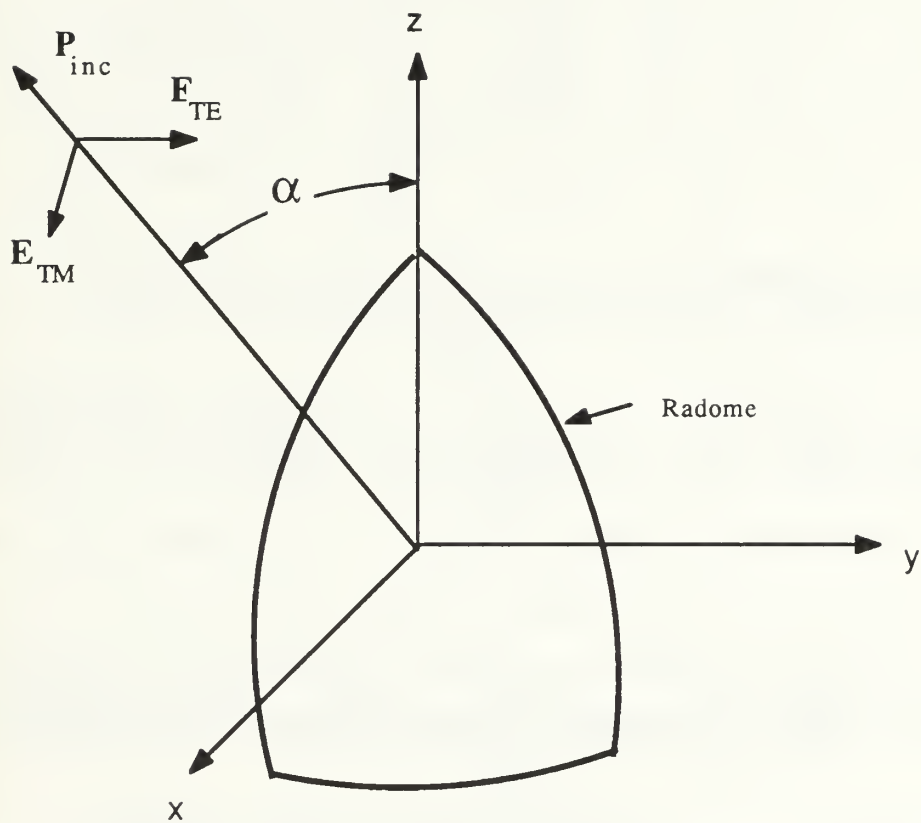


Figure 3.3 Incident Poynting vector with TE and TM plane waves

and TE plane waves are orthogonal to the Poynting vector and to each other. The TE plane wave is always in the y direction. The TM wave is in the x-z plane and directed as determined by the expression  $\cos \alpha x - \sin \alpha z$ . For incident plane waves specified in this manner, the solution for the component values of the E fields in the core of the radome can be determined from taylored equations for the TM and the TE incident plane waves. For the TM incident wave, the core E-field component values are determined as:

$$E_r(r, \theta, \phi) = \frac{-jE_o \sin \theta}{\sqrt{\epsilon_r} (k_o r)^2} \sum_{m=0}^M \tau_m \cos(m \phi) \sum_{\substack{n=m \\ n \neq 0}}^N \left[ b_n n (n+1) \hat{J}_n(k r) \frac{P_n^m(\cos \theta)}{\sin \theta} \right] \quad (3.48)$$

$$E_\theta(r, \theta, \phi) = \frac{-jE_o \sqrt{\mu_r}}{k_o r} \sum_{m=0}^M \tau_m \cos(m \phi) \sum_{\substack{n=m \\ n \neq 0}}^N \left[ a_n \hat{J}_n(k r) \frac{P_n^m(\cos \theta)}{\sin \theta} + b_n \hat{J}'_n(k r) \frac{d P_n^m}{d \theta} \right] \quad (3.49)$$

and

$$E_\phi(r, \theta, \phi) = \frac{jE_o \sqrt{\mu_r}}{k_o r} \sum_{m=0}^M \tau_m \sin(m \phi) \sum_{\substack{n=m \\ n \neq 0}}^N \left[ a_n \hat{J}_n(k r) \frac{d P_n^m}{d \theta} + b_n \hat{J}'_n(k r) \frac{P_n^m(\cos \theta)}{\sin \theta} \right]. \quad (3.50)$$

For the TE incident wave, the core E-field component values are determined as:

$$E_r(r, \theta, \phi) = \frac{E_o \sin \theta}{\sqrt{\epsilon_r} (k_o r)^2} \sum_{m=0}^M \tau_m \sin(m \phi) \sum_{\substack{n=m \\ n \neq 0}}^N \left[ b_n n (n+1) \hat{J}_n(k r) \frac{P_n^m(\cos \theta)}{\sin \theta} \right] \quad (3.51)$$

$$E_\theta(r, \theta, \phi) = \frac{E_o \sqrt{\mu_r}}{k_o r} \sum_{m=0}^M \tau_m \sin(m \phi) \sum_{\substack{n=m \\ n \neq 0}}^N \left[ a_n \hat{J}_n(k r) \frac{P_n^m(\cos \theta)}{\sin \theta} + b_n \hat{J}'_n(k r) \frac{d P_n^m}{d \theta} \right] \quad (3.52)$$

and

$$E_{\phi}(r, \theta, \phi) = \frac{E_0 \sqrt{\mu_r}}{k_0 r} \sum_{m=0}^M \tau_m \cos(m\phi) \sum_{\substack{n=m \\ n \neq 0}}^N \left[ a_n \hat{J}_n(kr) \frac{dP_n^m}{d\theta} + b_n \hat{J}_n(kr) \frac{P_n^m(\cos\theta)}{\sin\theta} \right]. \quad (3.53)$$

With the  $a_n$  and  $b_n$  coefficients supplied by EMRAD for each pair of plane waves, TM and TE, at each user-specified angle, CORFLD generates the interior phasor field components using the equations above. The total magnitude of the complex vector field at any point within the radome's core is expressed as the square root of the sum of the squares of the complex absolute values of the field components. This total magnitude is computed and displayed for each incident wave by CORFLD, using the  $a_n$  and  $b_n$  coefficients supplied by EMRAD.

In order to determine the perturbation of the electromagnetic field due to the presence of the radome, CORFLD generates the values of the incident plane wave, then compares this to the core region field components calculated by EMRAD and CORFLD. The formulas for the undisturbed incident TM and TE planes waves are

$$\mathbf{E}^{\text{TM}} = E_0 e^{-jk_0 \mathbf{p} \cdot \mathbf{r}} (\mathbf{x} \cos\alpha - \mathbf{z} \sin\alpha) \quad (3.54)$$

and

$$\mathbf{E}^{\text{TE}} = E_0 e^{-jk_0 \mathbf{p} \cdot \mathbf{r}} \mathbf{y} \quad (3.55)$$

The magnitude factor,  $E_0 = 1.0$ , is set by EMRAD for both TM and TE waves. The unit propagation vector,  $\mathbf{p}$ , includes the direction of propagation for the incident waves and is designated as

$$\mathbf{p} = (\mathbf{x} \sin\alpha + \mathbf{z} \cos\alpha) \quad (3.56)$$



This vector is dotted with the position vector,  $\mathbf{r}$ , for each point on the plane of interest, as defined as

$$\mathbf{r} = (xx + yy + zz) . \quad (3.57)$$

With the dot product evaluated in the exponential, the TM and TE waves are specified as

$$\mathbf{E}^{\text{TM}} = E_0 e^{-jk_0(x \sin \alpha + z \cos \alpha)} (\mathbf{x} \cos \alpha - \mathbf{z} \sin \alpha) \quad (3.58)$$

and

$$\mathbf{E}^{\text{TE}} = E_0 e^{-jk_0(x \sin \alpha + z \cos \alpha)} \mathbf{y} . \quad (3.59)$$

The relative magnitude and phase of the computed field in the direction of the theoretical field are calculated and displayed. This "scaled dot product" is defined as

$$E_{\text{dot}} = \frac{\mathbf{E} \cdot \mathbf{e}_i}{E_i} , \quad (3.60)$$

where  $\mathbf{E}$  is the computed field,  $\mathbf{e}_i$  is a unit vector pointing in the same direction as either the TM or TE incident field specified in Equations (3.58) and (3.59), and

$$E_i = E_0 e^{-jk_0(x \sin \alpha + z \cos \alpha)} . \quad (3.61)$$

The remaining field term that is computed and displayed by CORFLD is the error term. The error term is that portion of the computed field which is perpendicular to the incident field vector. In normalized form this becomes,

$$E_{\text{error}} = \left| \frac{\mathbf{E} - (\mathbf{E} \cdot \mathbf{e}_i) \mathbf{e}_i}{E_i} \right| . \quad (3.62)$$

The relative magnitude of the error term is calculated and displayed by CORFLD as a measure of electromagnetic disturbance caused by the presence of the radome. This built-in theoretical field comparison is used in Chapter V as a measure of modelling accuracy by comparing the generated theoretical fields to the fields computed and assembled by EMRAD and CORFLD for an ideal radome constructed of air ( $\epsilon_r = 1$ ).

### C. CANTING THE PLANAR ARRAY

The planar antenna within a radome can be canted in any direction allowed by the gimbal system that is used with the antenna. In order to evaluate the field components across a canted planar antenna within the radome core, the coordinates of each point on the antenna must be converted from the local planar coordinate system to the global radome core coordinate system. CORFLD uses a transformation from local planar to global core coordinates, assuming a two-axis gimbal system where the antenna is rotated about the original z-axis, as shown in Fig. 3.4, followed by a rotation about the new y-axis, as shown in Fig. 3.5.

The transformation matrix is formed by multiplying two matrices, one for each axis rotation [Ref. 12]. The transformation for the rotation about the z-axis is provided by the matrix

$$\begin{bmatrix} x \\ y \\ z \end{bmatrix} = \begin{bmatrix} +\cos\beta & -\sin\beta & 0.0 \\ \sin\beta & \cos\beta & 0.0 \\ 0.0 & 0.0 & 1.0 \end{bmatrix} \begin{bmatrix} x' \\ y' \\ z' \end{bmatrix}. \quad (3.63)$$

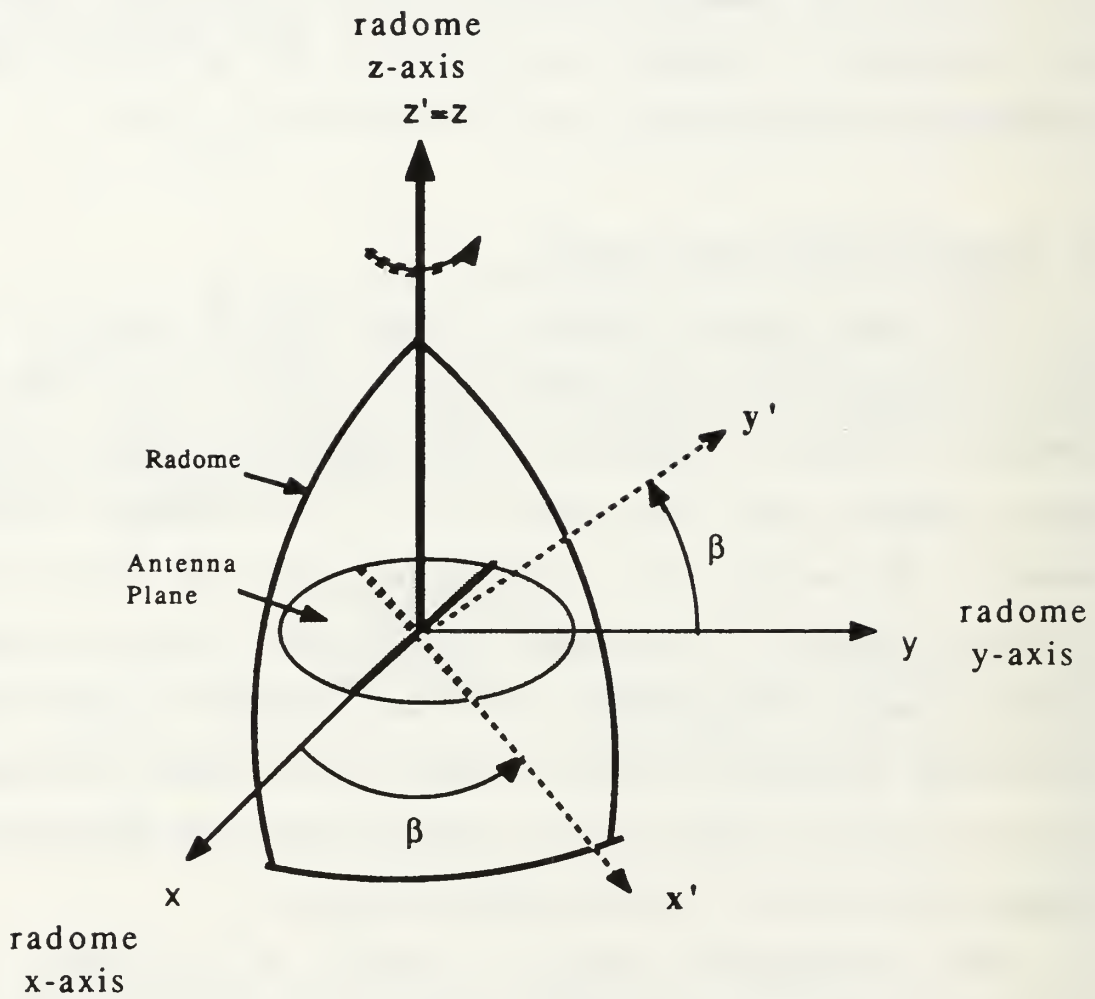


Figure 3.4 Rotation about the z-axis

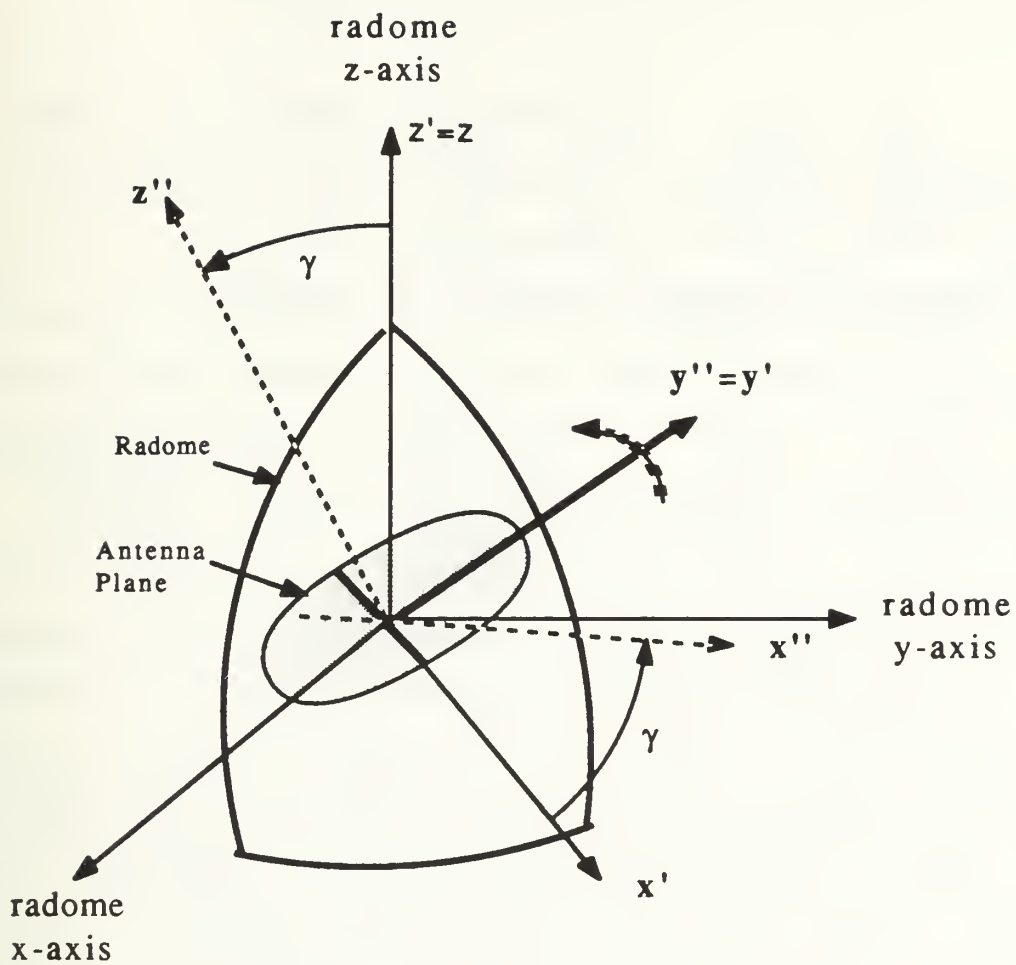


Figure 3.5 Rotation about the new y-axis

The transformation for the rotation about the y-axis is provided by the matrix

$$\begin{bmatrix} x' \\ y' \\ z' \end{bmatrix} = \begin{bmatrix} \cos\gamma & 0.0 & \sin\gamma \\ 0.0 & 1.0 & 0.0 \\ -\sin\gamma & 0.0 & \cos\gamma \end{bmatrix} \begin{bmatrix} x'' \\ y'' \\ z'' \end{bmatrix}. \quad (3.64)$$

The complete transformation is given by the product

$$\begin{aligned} \begin{bmatrix} x \\ y \\ z \end{bmatrix} &= \begin{bmatrix} +\cos\beta & -\sin\beta & 0.0 \\ \sin\beta & \cos\beta & 0.0 \\ 0.0 & 0.0 & 1.0 \end{bmatrix} \cdot \begin{bmatrix} \cos\gamma & 0.0 & \sin\gamma \\ 0.0 & 1.0 & 0.0 \\ -\sin\gamma & 0.0 & \cos\gamma \end{bmatrix} \begin{bmatrix} x'' \\ y'' \\ z'' \end{bmatrix} \\ &= \begin{bmatrix} \cos\gamma \cos\beta & -\sin\beta & \sin\gamma \cos\beta \\ \cos\gamma \sin\beta & \cos\beta & \sin\gamma \sin\beta \\ -\sin\gamma & 0.0 & \cos\gamma \end{bmatrix} \begin{bmatrix} x'' \\ y'' \\ z'' \end{bmatrix}. \quad (3.65) \end{aligned}$$

This transformation matrix is used by CORFLD to determine the global radome coordinates from the local antenna coordinates for a gimballed antenna rotated by  $\beta$  degrees about the z-axis, then  $\gamma$  degrees about the new y-axis. With this computational tool the fields that are received by an antenna within the core of the radome can be determined for any orientation of the antenna and for any computed incident field.

#### IV. PROGRAM EXECUTION AND DATA FLOW

##### A. THE RADOME MODEL DESIGN PROCESS

The design process developed by this thesis is represented by Fig. 4.1. The radome design procedure is an iterative process of selecting radome size and material parameters, radome shaping functions, and placement of the axis origin in order to allow for an optimal mesh formation by EMRAD.

The flow of data starts when RADSHIP is used to design the radome. RADSHIP generates a material file which is ready for use by EMRAD and a structure data file which is in the format required by CURVE DIGITIZER. CURVE DIGITIZER is used to visually check the radome structure as designed in RADSHIP. After verifying the structure data file, the program EMCADIN, developed by Connolly [Ref. 4], is used to translate the data file into the form required by EMRAD. After data translation, the program EMESH, developed by Morgan [Ref. 3], is used to check that the mesh to be generated in EMRAD is optimally placed. The placement of the origin in RADSHIP when generating the structure data file can be modified by a placement factor. With the material and structure files are prepared, EMRAD is executed to generate the interior coefficients of expansion for use by CORFLD. A sample annotated execution through the data flow follows.

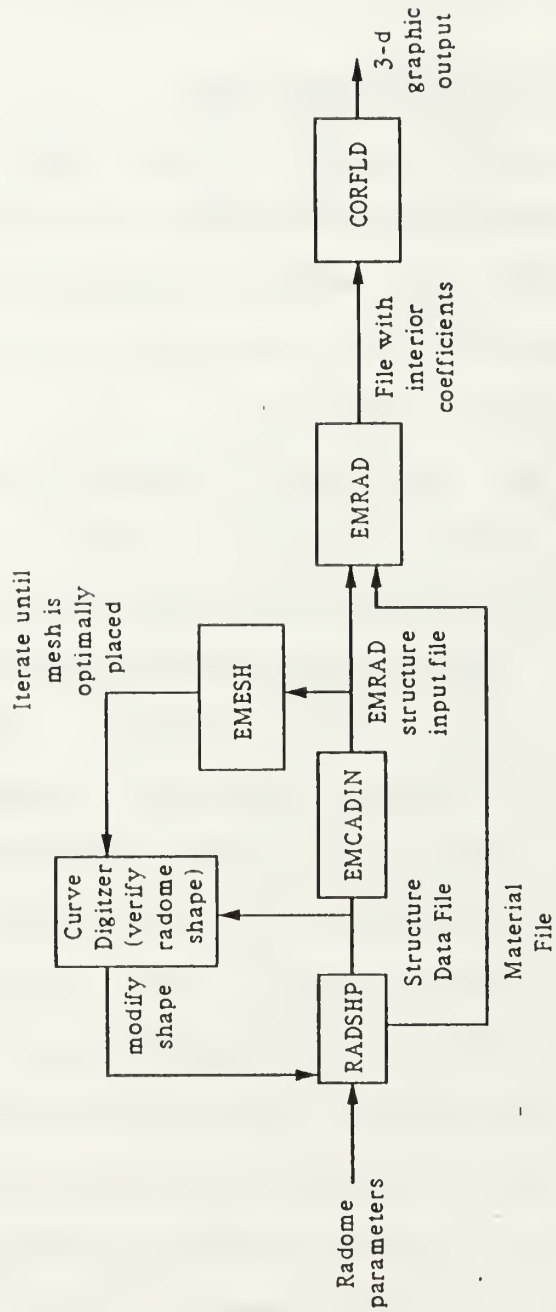


Figure 4.1 Radome model design process

## B. RADSHP EXECUTION

RADSHP is a menu-driven program that accepts data from the keyboard. When the executable version of RADSHP is available, RADSHP is invoked by typing

```
> RADSHP
```

at the DOS prompt. The program will load itself, then provide introductory information.

```
WELCOME TO RADSHP
```

```
THIS PROGRAM GENERATES RADOME MATERIAL AND SHAPE DATA  
FILES FOR USE WITH EMRAD, BASED ON USER INPUT.
```

RADSHP prompts for data file names for the material and structure output files. Sample keyboard inputs are provided. User inputs are preceded by "==>".

```
TWO FILES ARE REQUIRED TO HOLD PROGRAM OUTPUT DATA.
```

```
PLEASE ENTER THE NAME OF THE FILE TO BE USED TO  
HOLD THE PROGRAM MATERIAL PARAMETER DATA. THE EXTENSION  
.MAT WILL BE ADDED AUTOMATICALLY, I. E. YOURNAME.MAT
```

```
==> MATFIL
```

```
PLEASE ENTER THE NAME OF THE FILE TO BE USED
```



TO HOLD THE PROGRAM OUTPUT DATA. THE EXTENSION .DAT WILL  
WILL BE ADDED AUTOMATICALLY, I. E. YOURNAME.DAT

==> STRFIL

RADSHP will allow the construction of radomes with up to five layers  
of construction. At present, each of these layers must completely  
enclose the previous layered region.

ENTER THE NUMBER OF LAYERS (.LE. 5)

==> 2

RADSHP prompts for the parameters of each layer of construction.

Each layer of the radome will have material constants,  
an outer height of the radome layer, H,  
a outer base radius, R, and  
a shape function, & shape factor parameters (if appl.),

The first "layer" will be the inner core of the radome,  
normally filled with air.

Layer No: 1

This is the inner core of the radome

Please enter the radome layer height, H,  
and the outer base radius, R, for this layer.

==> 1.25,0.50

RADSHP provides a menu of the shaping functions available for radome construction. The curved parabola is not normally used for outer layers of the radome, but is included as an option for inner layer construction.

The following shaping functions are available,

1. General Ogive
2. Tangent Ogive
3. von Karman
4. Power Series
5. Parabola, curved
6. Parabola, capped by pointed apex

Indicate desired shaping function by entering a number

1,2, ... or 6

==> 2

Each shaping function requires input of their respective shaping factors. These are prompted for and then listed for each layer as the radome is constructed. The tangent ogive and the von Karman functions have shaping factors that are determined by the height and base radius of the radome layer; these factors are determined and listed. The factor designation follows the form adopted in the equation in Chapter II.

The tangent ogive shaping function determines two factors for the radome construction. These are calculated based on the height and radius of the radome layer.

These factors are  $F4 = 6.50$  and  $F5 = 6.38$

LAYER	SHAPE	HEIGHT	RADIUS	F1	F2	F3	F4	F5	F6	F7
1	TAN Ogive	1.25	.50	.00	.00	.00	6.50	6.38	.00	.00

Layer No: 2

This is the outer layer of the radome

Please enter the radome layer height, H,  
and the outer base radius, R, for this layer.

==> 1.30,0.55

The following shaping functions are available,

1. General Ogive
2. Tangent Ogive
3. von Karman
4. Power Series
5. Parabola, curved
6. Parabola, capped by pointed apex

Indicate desired shaping function by entering a number  
1,2, ... or 6

==> 2

The tangent ogive shaping function determines two factors for the radome construction. These are calculated based on the height and radius of the radome layer.

These factors are  $F4 = 6.42$  and  $F5 = 6.28$

LAYER	SHAPE	HEIGHT	RADIUS	F1	F2	F3	F4	F5	F6	F7
1	TAN Ogive	1.25	.50	.00	.00	.00	6.50	6.38	.00	.00
2	TAN Ogive	1.30	.55	.00	.00	.00	6.42	6.28	.00	.00

After all the structure forming data is entered, RADSHP prompts for the material relative permittivity parameter for each layer of construction. Layer 1 is the inner-most region and the permittivity will normally equal unity.

Layer No: 1

This is the inner core of the radome

Enter Er for this Layer:

==> 1.0

Layer No: 2

This is the outer layer of the radome

Enter Er for this Layer:

==> 4.0

With the structure and material parameters entered, RADSHP prompts for headers to identify the radome constructed. This header information is stored in the material data file and will follow the data files throughout the execution of the programs in this package.

THE HEADERS ALLOW THE USER TO IDENTIFY THIS SET OF DATA FROM ALL OTHER SETS.

PLEASE ENTER HEADER #1 (64 CHARACTERS MAX)

==> This is a test data set for RADSHF example

PLEASE ENTER HEADER #2 (64 CHARACTERS MAX)

==> Header info stays with data set throughout

With all the data input and calculations completed, RADSHF reports the generation of the material and structure files and terminates.

Computations and output are completed, the data file, MATFIL.MAT holds the material specifications for input to EMCAD.

The data file, STRFIL.DAT, holds the radome shape data for viewing in the CAD package, CURVE DIGITIZER.

The structure file required for input to EMCAD can be generated by the executing the program EMCADIN, using, STRFIL.DAT, as input to EMCADIN,

The output file from EMCADIN will be in proper format for input to EMCAD for the structure file.

Stop - Program terminated.

>

### C. RADOME CONSTRUCTION VERIFICATION.

The construction of the radome by RADSHP is verified by entering the CURVE DIGITIZER package and displaying the structure data file generated by RADSHP. Figure 4.2 is a copy of the CURVE DIGITIZER display of the radome shape created in the example execution above. Upon review and acceptance of the structure data file, EMCADIN is used to translate the data file into the form required by EMRAD. EMCADIN is invoked by typing

```
>EMCADIN
```

at the system prompt. The program will load itself and displays the greeting heading and prompts for the structure data file as input.

```
WELCOME TO EMCADIN
```

```
THIS PROGRAM ACCEPTS PROPERLY FORMATTED INPUT DATA  
FROM CURVE DIGITIZER AND CONVERTS IT TO A FORM  
WHICH CAN BE USED BY EMCAD.
```

```
PLEASE PRESS ENTER TO CONTINUE.
```

```
INPUT FILENAME
```

```
INPUTFN IS THE INPUT FILENAME OF THE FILE CONTAINING  
THE DATA OF INTEREST WHICH WILL BE INTERPOLATED ON AND  
CONVERTED TO A FORM WHICH CAN SUBSEQUENTLY BE USED BY  
EMCAD
```

```
PLEASE ENTER THE NAME OF THE INPUT FILE. THE EXTENSION
```

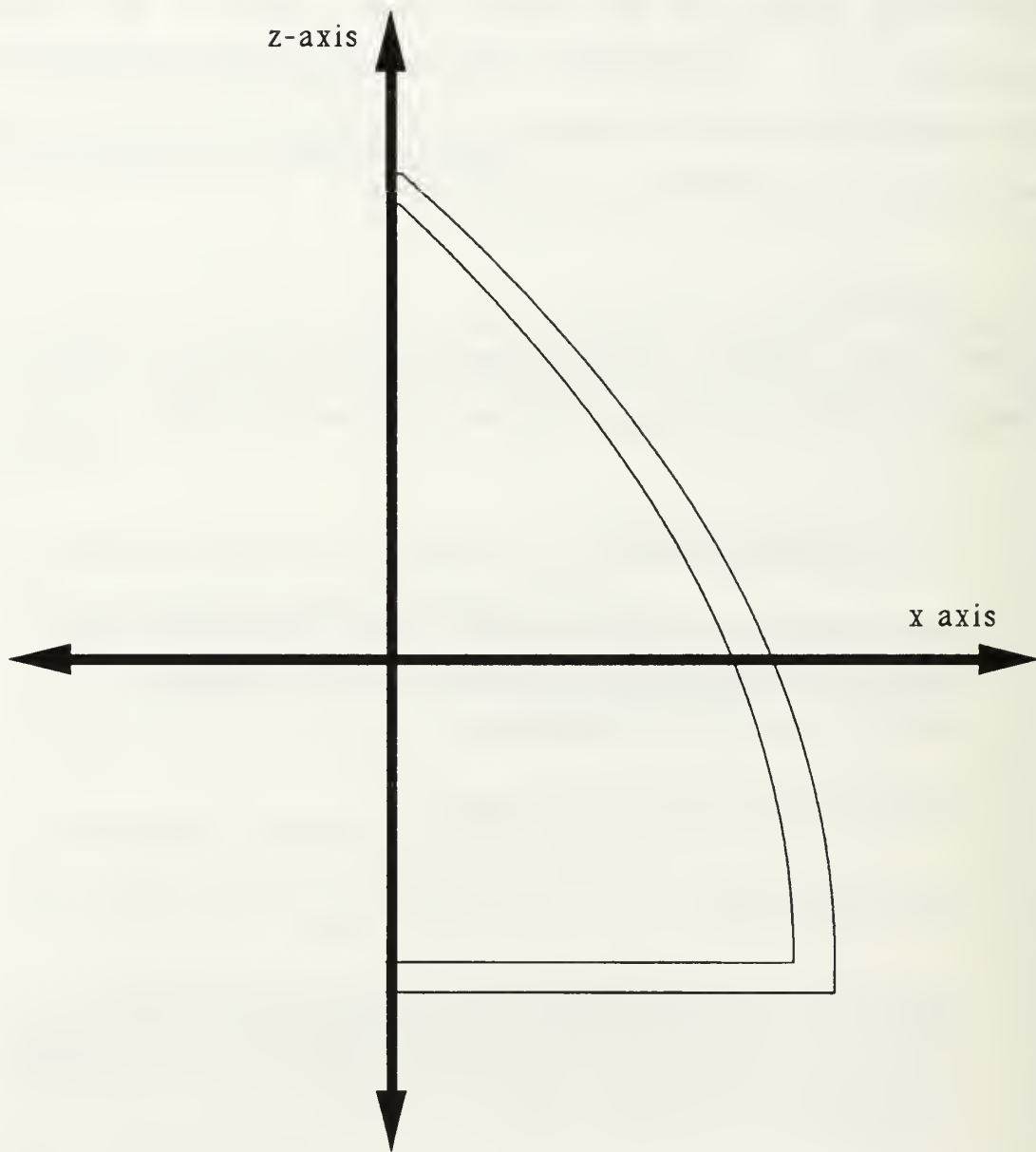


Figure 4.2 Tangent ogive created by RADFLD  
as displayed by CURVE DIGITIZER

OF THE FILENAME MUST BE .DAT, I.E. FILENAME.DAT

==> STRFIL.DAT

EMCADIN then prompts the user for the data file name to hold the structure file that is prepared for EMRAD execution.

OUTPUT FILENAME

OUTPUTFN IS THE OUTPUT FILENAME OF THE FILE CONTAINING THE DATA WHICH HAS BEEN INTERPOLATED AND CONVERTED TO A FORM WHICH WILL BE USED BY EMCAD.

PLEASE ENTER THE NAME OF THE OUTPUT FILE. THE EXTENSION OF THE FILENAME MUST BE INCLUDED I.E. FILENAME.DAT

==> STRFIL.STR

There are several data files used within these packages, the default file name extensions should be: ".MAT" for material data files, ".DAT" for structure data files suitable for CURVE DIGITIZER, and ".STR" for structure files suitable for EMRAD.

After receiving the data file names to work with, EMCADIN prompts for angular resolution requirements. EMCADIN uses linear interpolation to provide the capability to generate output data with better resolution than the input data. The default resolution of data generation by RADSHIP is one thousand points in the x-z plane, using 180 points of angular resolution in EMCADIN is sufficient for good results.



## RESOLUTION

DELTHE IS THE USER INPUT VALUE OF THE DESIRED THETA RESOLUTION IN DEGREES.

PLEASE ENTER THE DESIRED DELTA THETA VALUE IN DEGREES.

==> 180.

Upon completion of the data file translation by EMCADIN, the data files required for execution by EMRAD are complete and in the proper format. MATFIL.MAT is the example material file and STRFIL.STR is the example structure file. Before executing EMRAD, the efficiency of mesh generation to be expected during EMRAD can be previewed by using the program EMESH developed by Morgan. Figure 4.3 shows the mesh generated by EMESH for the example radome, as displayed by CURVE DIGITIZER.

## D. EMRADEXECUTION

With the data files generated and an optimal mesh solution, the data flow is ready to initiate EMRAD. EMRAD is a menu-driven program developed by Connolly and Morgan and has been slightly modified to provide the interior spherical coefficients of expansion for use by CORFLD. EMRAD can be invoked by typing

>EMCAD

at the DOS prompt. The program will load itself and provide

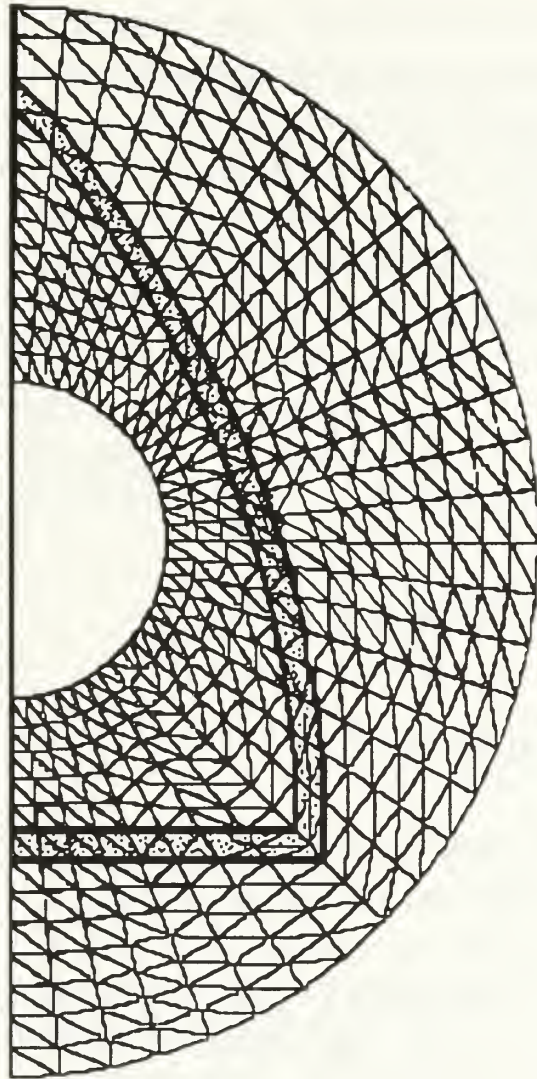


Figure 4.3 Tangential ogive with mesh generated by EMESH as displayed by CURVE DIGITIZER

introductory information.

\*\*\*\*\* WELCOME TO EMRAD \*\*\*\*\*

THIS PROGRAM COMPUTES EM FIELD SCATTERING FROM PENETRABLE BODIES OF REVOLUTION USING THE COUPLED AZIMUTHAL POTENTIAL (CAP) FORMULATION IN CONJUNCTION WITH A VARIATIONAL FINITE-ELEMENT TECHNIQUE AND A TRI-REGIONAL UNIMOMENT METHOD. THE NUMERICAL SOLUTION IS PERFORMED USING A TWO-SWEEP RICCATI TRANSFORM WITH CIRCUMFERENTIAL MARCHING.

UPDATED VERSION OF ORIGINAL U.C. BERKELEY CODE.

MODIFICATIONS BY	M.A. MORGAN	MAR 1987 - DEC 1989
	E.M. CONNOLLY	JUL 1987 - APR 1988
	R.J. VINCE	SEP 1989 - DEC 1989 .

PLEASE PRESS ANY KEY TO CONTINUE.

\*\*\*\*\* EMRAD INPUT \*\*\*\*\*

EMRAD ALLOWS A USER TO INPUT THE NECESSARY INFORMATION ACCORDING TO THE LEVEL OF HIS EXPERTISE.

1 NOVICE LEVEL - GIVES BRIEF EXPLANATIONS/DESCRIPTIONS OF INPUT VALUES. DESCRIBES THE REQUIRED FORMAT FOR THE INPUT VALUE. GIVES TYPICAL VALUES WHERE APPLICABLE.

2 EXPERT LEVEL - ASSUMES THE USER IS FAMILIAR WITH THE INPUT PARAMETERS AND FORMATS. SIMPLY PROMPTS FOR REQUIRED INPUTS.

3 EXIT EMRAD

PLEASE SELECT THE LEVEL OF EXPERTISE BY ENTERING 1, 2, OR 3.

==> 1

The names of the data files generated by RADSHIP and translated by EMCADIN are entered at the keyboard when prompted by EMRAD.

EMRAD REQUIRES DATA INPUT FROM TWO FILES PREPARED IN ACCORDANCE WITH THE USERS MANUAL. THESE FILES MUST CONTAIN MATERIAL PARAMETERS AND STRUCTURE PARAMETERS, RESPECTIVELY.

ENTER MATERIAL PARAMETER FILE (D:FILENAME.EXTENSION) :

==> MATFIL.MAT

ENTER STRUCTURE DATA FILE (D:FILENAME.EXTENSION):

==> STRFIL.STR

EMRAD opens both files and displays the header information which RADSHIP placed in the material file.

This is a test dataset for RADSHIP example  
Header will stay with dataset throughout

EMRAD creates several datafiles. The first will be the diary file for the execution of EMRAD. This file will have the ".OUT" extension. The second data file generated will have the same root name as the

diary file, this is the data file which holds the spherical coefficients of expansion for the core field generation. This second file will have the extension ".INT" and will be used as input to CORFLD.

THE OUTPUT DATA FILE IS THE FILE CONTAINING THE OUTPUT RESULTS OF ALL NUMERICAL CALCULATIONS CONDUCTED BY EMRAD. THE FORMAT FOR THIS INPUT IS FILENAME ONLY. NO EXTENSION IS REQUIRED OR DESIRED. EMRAD AUTOMATICALLY APPENDS AN EXTENSION OF .OUT TO YOUR FILENAME.

A SECOND OUTPUT DATA FILE WILL BE CREATED TO STORE THE COEFFICIENTS FOR THE INTERIOR CORE EXPANSION. EMRAD WILL APPEND AN EXTENSION OF .INT FOR THIS DATA FILE. PLEASE ENTER THE FILENAME OF THE OUTPUT DATA FILES.

==> INTFIL

EMRAD was developed by Morgan and Connolly to determine the scattered field and the radar cross section of the body of revolution under study. Four output data files are created for input to separate graphing routines.

THE OUTPUT GRAPHICS DATA FILE IS THE FILE CONTAINING THE OUTPUT DATA FROM EMRAD TO BE USED AS INPUT TO GRAPHING ROUTINES. THE FORMAT FOR THIS INPUT IS FILENAME ONLY. NO EXTENSION IS REQUIRED OR DESIRED. EMRAD AUTOMATICALLY APPENDS AN EXTENSION OF .TMT, .TMP, .TET, AND .TEP TO YOUR FILENAME AS IT PRODUCES FOUR OUTPUT FILES FOR GRAPHICS.

.TMT -----> TM INCIDENCE, F-THETA

.TMP -----> TM INCIDENCE, F-PHI

.TET -----> TE INCIDENCE, F-THETA

.TET -----> TE INCIDENCE, F-PHI

PLEASE ENTER THE FILE NAME OF THE OUTPUT DATA FILE.

==> SCATGRF

EMRAD prompts for a graphics caption to be included with the data set, this caption is passed along to CORFLD and is included with each plotted figure. This caption affords the user the ability to identify this data set from all other sets.

THE GRAPHICS CAPTION IS A PERSONALIZED CAPTION ALLOWING THE USER TO IDENTIFY THIS SET OF GRAPHS FROM ALL OTHER SETS.

THE MAXIMUM LENGTH OF THIS CAPTION IS 64 CHARACTERS.

NOTE: WHEN USED WITH THE GRAPHICS PACKAGE, THE PROGRAM IS ABLE TO DIFFERENTIATE BETWEEN UPPER CASE AND LOWER CASE CHARACTERS.

PLEASE ENTER ANY GRAPHICS CAPTION YOU DESIRE

==> Graphics caption

As discussed in Appendix A, EMRAD utilizes a semi-annular conformal mesh in order to conduct electromagnetic field calculations. EMRAD prompts the user for a minimum and maximum mesh density. EMRAD conducts the analysis of the radome structure using a linear variation of density from maximum density decreasing to minimum density.

DMIN AND DMAX ARE PARAMETERS OF MESH DENSITY IN TERMS OF

ELEMENTS/INTERIOR LAMBDA. INPUT VALUES ARE EXPECTED TO BE REAL, I.E. THE DECIMAL POINT MUST BE INCLUDED.  
TYPICAL VALUES ARE DMIN = 10. AND DMAX = 15.

PLEASE INPUT DMIN

==> 15

PLEASE INPUT DMAX

==> 18

EMRAD allows for analysis of up to five incident fields. EMRAD prompts for the number of incident angles, and then for the value of each angle, in degrees. EMRAD uses the poynting vector direction for the incident angle. This translates to an angle of 180 degrees for an angle incident at the radome's apex, 135 degrees for an angle incident 45 degrees off the apex, and 90 degrees for an incident angle off the beam of the radome.

THE NUMBER OF INCIDENT FIELD ANGLES IS THE TOTAL NUMBER OF INCIDENT FIELDS THAT IMPINGE ON THE OBJECT OF INTEREST. THIS PROGRAM ALLOWS A MAXIMUM OF FIVE INCIDENT FIELD ANGLES. WHEN ENTERING YOUR ANSWER PLEASE DO NOT INCLUDE A DECIMAL BECAUSE THE INPUT MUST BE IN INTEGER FORMAT, I.E.

NA = 3 , NA = 1

PLEASE INPUT THE NUMBER OF INCIDENT FIELD ANGLES.

==> 2

ENTER INC FLD ANGLE (DEG) FOR # 1

==> 180

ENTER INC FLD ANGLE (DEG) FOR # 2

==> 135

EMRAD performs scattering calculations by starting at  $\theta = 0$ , and progressing clockwise to  $\theta = 180$  in equal increments, the menu allows the user to determine the size of the increments.

THE NUMBER OF SCATTERING FIELD THETA POINTS DETERMINES THE SPACING BETWEEN THETA POINTS DURING EMRAD ITERATIONS AND CALCULATIONS.

DELTA THETA =  $180 / (\text{NUMBER THETA POINTS} - 1)$  SO...

NUMBER THETA POINTS = 37 -----> DELTA THETA = 5 DEGREES

NUMBER THETA POINTS = 19 -----> DELTA THETA = 10 DEGREES

WHEN ENTERING YOUR ANSWER, PLEASE DO NOT INCLUDE A DECIMAL BECAUSE THE INPUT MUST BE IN INTEGER FORMAT. I.E. NT = 19

PLEASE INPUT THE NUMBER OF SCATTERING FIELD THETA POINTS

==> 19

As part of the scattering analysis, EMRAD allows for eight angles of user observation.



THE NUMBER OF PHI ANGLES IS THE TOTAL NUMBER OF PHI ANGLES.  
THIS PROGRAM ALLOWS A MAXIMUM OF THREE PHI ANGLES. WHEN  
ENTERING YOUR ANSWER PLEASE DO NOT INCLUDE A DECIMAL  
BECAUSE THE INPUT MUST BE IN INTEGER FORMAT. I.E.

NP = 3 , NP = 1

PLEASE INPUT THE NUMBER OF PHI ANGLES.

==> 0

EMRAD truncates the modal analysis of the electromagnetic field infinite fourier expansions for the incident plane waves and the interior core as well as the exterior scattered fields. Mathematical estimates of truncations are provided and the user is prompted for truncation limits. Higher truncations may increase the modelling accuracy.

ENTER MSTOP (.LE. 13)

ESTIMATED "MINIMUM" VALUE IS: 4

==> 5

Modal truncations for the number of spherical harmonic modes in the spherical radome core and external scattering region are estimated. The user is prompted for truncation limits for the spherical harmonics.

ENTERING NO. OF INTERNAL AND EXTERNAL EXPANSION MODES

ESTIMATED (KI\*RMIN) "MINIMUM" INTERNAL N1 = 4

ENTER N1 (.GE. MSTOP):

==> 5

ESTIMATED (KO\*RMIN) "MINIMUM" EXTERNAL N2 = 9

ENTER N2 (.GE. MSTOP):

==> 9

Check that N1+N2 is .LE. 35 .... Otherwise Abort

==> [RETURN]

When executing the numerical solution, EMRAD requires a large amount of temporary disk storage space. The amount of storage required is estimated and provided to the user. The user must select a disk drive that has adequate memory available for usage. The use of a ram drive configuration can increase the speed of execution by EMRAD.

\*\*\*\*\* Temporary Storage of Riccati Matrices \*\*\*\*\*

Estimated Disk Space Needed in MegaBytes: 1.930000E+00

ENTER Hard Drive or RAM Disk Letter ( C, D, E ... ):

==> E

With all of the data and parameters specified, EMRAD begins the numerical analysis of the electromagnetic interaction of the radome structure and the specified incident plane waves. Execution is monitored by reports to the terminal screen.

#### INDEXING PROGRAM THROUGH VALUES OF M

```
M-LOOP .... M = 0
CALL MESH
ENTER I-LOOP; NO STEPS TO COMPLETE: 38
I= 1 NO STEPS TO GO: 37
CALL LODER
CALL MARCH
I= 2 NO STEPS TO GO: 36
.
EX M-LOOP, DATOUT
```

```
***** EMRAD COMPLETED *****
```

Stop - Program terminated.

Upon termination of the program EMRAD, the coefficients for analysis of the radome core fields have been stored in the data file, ready for CORFLD execution.

#### E. CORFLD EXECUTION

CORFLD is a menu driven program that accepts data from the data file created by EMRAD and from the keyboard. When the

executable version of CORFLD is available, CORFLD is invoked by typing

```
> CORFLD
```

at the DOS prompt. The program will load itself, then provide introductory information.

```
WELCOME TO CORFLD
```

```
CORFLD ASSEMBLES THE FIELD ON THE INTERIOR OF A RADOME  
WITH THE COEFFICIENTS SUPPLIED BY AN EMRAD OUTPUT FILE.
```

CORFLD prompts for the name of the data file generated by EMRAD. Only the root file name is required, CORFLD attaches the ".INT" to the root file name.

```
THE OUTPUT DATA FILE IS THE FILE CONTAINING THE OUTPUT  
RESULTS OF INTERIOR FIELD CALCULATIONS CONDUCTED BY EMRAD.  
THE FORMAT FOR THIS INPUT IS FILENAME ONLY.  
NO EXTENSION IS REQUIRED OR DESIRED.  
CORFLD AUTOMATICALLY APPENDS AN EXTENSION OF .INT TO YOUR  
FILENAME.
```

```
PLEASE ENTER THE FILENAME OF THE OUTPUT DATA FILE.
```

```
==> INTFIL
```

Header information that has followed the data flow is obtained from the ".INT" data file by CORFLD and displayed on the screen. Notice

that the graphics caption entered during EMRAD execution as well as the headers entered during RADSHF execution are displayed.

#### TEST DATA FOR USER EXAMPLE

THIS HEADING FOLLOWS THE DATA THROUGHOUT

Graphics caption

CORFLD reads the material parameters stored in the ".INT" file and displays them on the screen.

SRE= (1.000000,-5.000000E-07)

SRU= (1.000000,-5.000000E-07)

KR = (1.000000,-1.000000E-06)

CORFLD reads the number of incident angles evaluated by EMRAD and displays each angle as the poynting vector angle of incidence and also as the angle of incidence to the radome exterior. The radome incident angle is displayed so that the user can use the angle as a reference when canting the planar antenna.

Incoming Inc. Angle # 1

EMRAD Poynting angle of incidence = 180.000000

Radome incident angle = 0.000000E+00

Incoming Inc. Angle # 2

EMRAD Poynting angle of incidence = 135.000000

Radome incident angle = 45.000000

After displaying the angles of incidence available for consideration, EMRAD prompts the user for the angle of interest. Only one angle

may be selected for each execution of CORFLD. In order to consider other angles, CORFLD must be re-executed by the user.

Select Angle of Interest By Number

==> 1

The angle of consideration is angle # 1 = 0.000000E+00 degrees

After an angle is selected for analysis, the user may enable a rotation of the planar array.

The planar array is set by default to lie in the x-y plane, with boresight in the z-direction.

Do you want to change the array boresight ?  
( "Y" or "N" )

==> N

CORFLD reads the data from the ".INT" file and assembles the interior field components.

MSTART= 0 MSTOP= 5  
Reading Coefficients and Constructing  
Fields for Each Azimuthal "m" Mode

Terminating M-Loop at m=1 for +/- Z-Axis Incidence

Azimuthal Mode "m" = 0

Reading Coefficients

Azimuthal Mode "m" = 1

Reading Coefficients

Generate Fields Across Array

SPHERICAL FIELDS COMPUTED

When the interior fields have been computed, the user may check for the field component values for any point on the planar array.

Check Values of Coordinates and E-Field ? (Y/N):

==> Y

Enter Array Triple Index to Check (J,L,I)

J= x-point 1,2,... 50

L= y-point 1,2,... 50

I= 1 for TM, 2 for TE

XP,YP,ZP: -5.115592E-02 -5.115592E-02 0.000000E+00

XC,YC,ZC: -5.115592E-02 -5.115592E-02 0.000000E+00

|E-RAD| = 5.023160E-01

|E-TH| = 1.391270E-02

|E-PHI| = 5.022836E-01

|E-TOT| = 7.104954E-01

Look at Another Point ? (Y/N):

==> N

The user is supplied with the selection menu to allow access to any component representation of the interior fields across the planar

antenna which is oriented as specified by the user. Component phase and magnitudes of the interior fields as well as the total field magnitudes are available,

CORFLD OUTPUT GRAPHICS PRESENTATION  
CORE FIELD REPRESENTATION SELECTION MENU

Please select the type of field representation of interest  
CORE will display the following field representations:

1. TM INCIDENT FIELD, E-THETA
2. TM INCIDENT FIELD, E-PHI
3. TM INCIDENT FIELD, E-RADIAL
4. TM INCIDENT FIELD, E-TOTAL FIELD MAGNITUDE
  
5. TE INCIDENT FIELD, E-THETA
6. TE INCIDENT FIELD, E-PHI
7. TE INCIDENT FIELD, E-RADIAL
8. TE INCIDENT FIELD, E-TOTAL FIELD MAGNITUDE
  
9. COMPARE COMPUTED FIELD TO INCIDENT FIELD
  
10. CHANGE ASPECT RATIO
  
0. FINISHED WITH THIS ANGLE OF INCIDENCE

Indicate your selection entering "1","2",..., "10", or "0"

==> 4

When the user has made a selection from the menu, the three dimensional (3-D) plotting routine is called and the user is allowed to



adjust the view angle for best observation of the 3-D plot, see Fig. 4.4,

#### CALL PLOTTING ROUTINE

A black and white 'stick' representation as well as a color 3-D fill representation are available to the user. The 'stick' representation generates the clearest output for printing and is used for all the data presented here.

Enter 0 for 3D-stick or 1 for 3D-fill option

==> 0

(\*\* SEE FIGURE 4.4 \*\*)

Default view angles are:  $\phi=-45^\circ$ ,  $\theta=70^\circ$ .

ENTER NEW ANGLES PHI & THETA (DEG) OR (9,9) WHEN DONE

==> 9,9

When the user is finished with an electric field component, the new view angle "9,9" is entered and the user is returned to the core field selection menu.

#### CORE FIELD REPRESENTATION SELECTION MENU

.  
. .  
. .

#### 9. COMPARE COMPUTED FIELD TO INCIDENT FIELD

Indicate your selection entering "1", "2", ..., "10", or "0"

The datafile used to generate fields is intfil.INT  
TEST DATA FOR USER EXAMPLE  
THIS HEADING FOLLOWS THE DATA THROUGHOUT  
Graphics caption

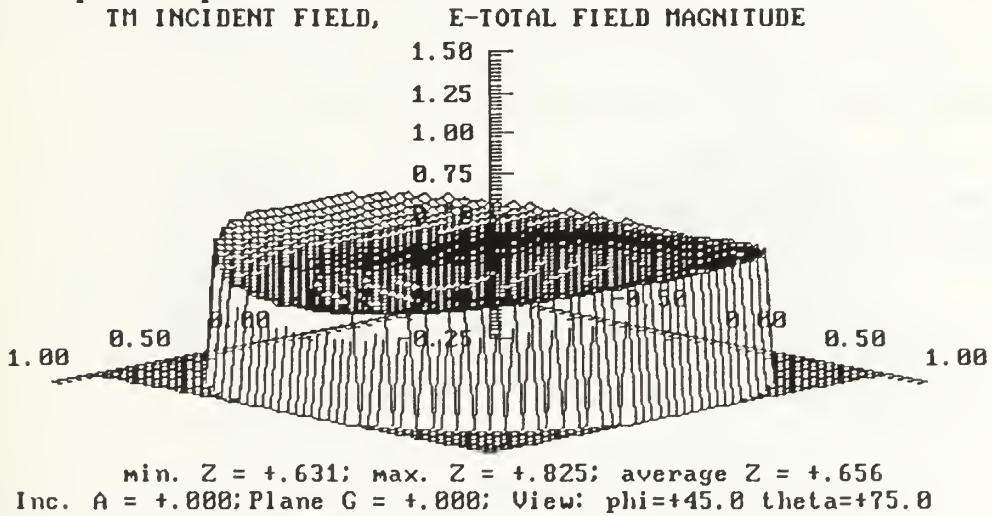


Figure 4.4 3-D plot of E-total field magnitude for example ogive radome

When the user wishes to see the amount of perturbation caused to the incident plane wave by the radome, selection "9" is entered,

==> 9

Selection "9" sends the user into Menu 2, for core field comparison to the ideal theoretical plane wave which would be incident on the antenna without the radome present.

#### CORE FIELD REPRESENTATION SELECTION MENU 2

Please select the type of field representation of interest  
CORE will display the following field representations:

1. TM INCIDENT FIELD, Computed Field dot Ideal Field
2. TM INCIDENT FIELD, Scaled Error component
3. TE INCIDENT FIELD, Computed Field dot Ideal Field
4. TE INCIDENT FIELD, Scaled Error component

Indicate your selection entering "1","2","3", or "4"

==> 2

CALL PLOTTING ROUTINE

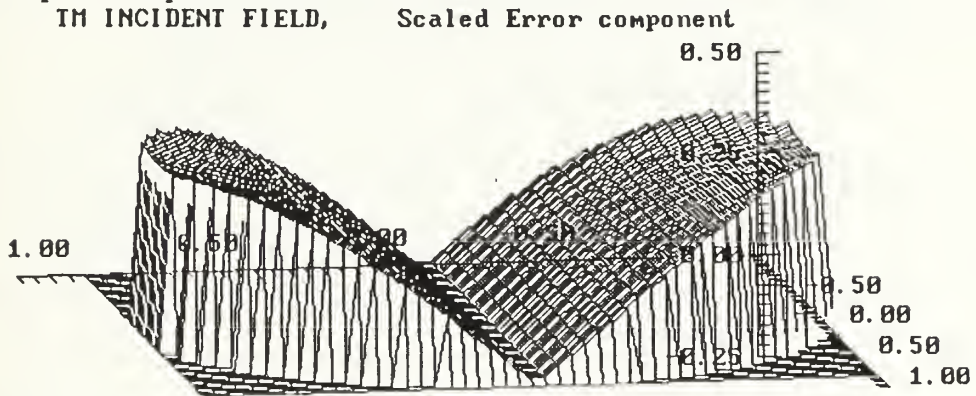
Enter 0 for 3D-stick or 1 for 3D-fill option

==> 0

Default view angles are:  $\phi=-45^\circ$ ,  $\theta=70^\circ$ .

(\*\* SEE FIGURE 4.5 \*\*)

The datafile used to generate fields is intfil.INT  
TEST DATA FOR USER EXAMPLE  
THIS HEADING FOLLOWS THE DATA THROUGHOUT  
Graphics caption



min. Z = +.013; max. Z = +.436; average Z = +.227  
Inc. A = +.000; Plane G = +.000; View: phi=+80.0 theta=+70.0

Figure 4.5 3-D plot of scaled error component for example ogive radome

ENTER NEW ANGLES PHI & THETA (DEG) OR (9,9) WHEN DONE

==> 9,9

CORFLD OUTPUT GRAPHICS PRESENTATION

CORE FIELD REPRESENTATION SELECTION MENU

.  
. .  
. .

0. FINISHED WITH THIS ANGLE OF INCIDENCE

Indicate your selection entering "1","2",...,"10",or "0"

==>0

\*\*\*\*\* CORE ANALYSIS COMPLETED \*\*\*\*\*

Stop - Program terminated.

When the user is finished with the angle of incidence selected, "0" is selected at the selection menu and the program execution is terminated.

## V. PROGRAM VALIDATION AND RESULTS

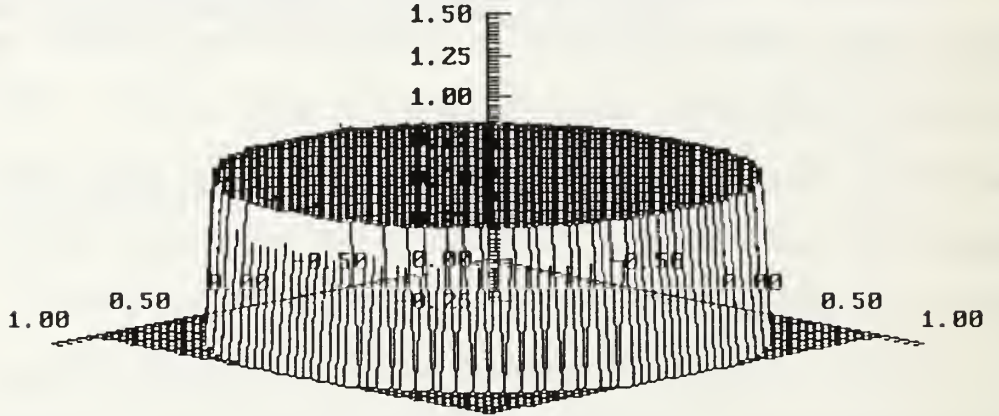
In order to validate the execution of EMRAD and CORFLD, the tangent ogive radome generated in Chapter IV was modified to have a relative permittivity equal to that of air,  $\epsilon_r=1.0$ . The field coefficients were generated by EMRAD and the core fields were computed by CORFLD and compared to the unperturbed incident field as listed in Chapter III.

Figures 5.1 and 5.2 show the magnitude and phase of the scaled dot product, as defined in Chapter III, between the computed and theoretical values for the TM and TE incident fields, respectively, for a "nose-on" incident angle. Each comparison shows a 94.9% magnitude matching with an almost constant  $2.59^\circ$  phase differential across the array. Figure 5.3 exhibits the scaled error component for the TM and TE incident fields, with an average magnitude of error component of 0.4%. The comparisons for this "nose-on" angle of incidence show that there is good agreement between the theoretical and calculated field components. It is observed that the TM and TE components displayed are  $90^\circ$  out of phase with each other. This is expected for "nose-on" incidence since the TM wave has its direction component in the -x direction, while the TE wave's direction component is in the y direction.

Figure 5.4 shows the magnitude and phase of the scaled dot product between the computed and theoretical values for the TM

The datafile used to generate fields is airfil.INI  
 Shaping function = TAN ogive  
 Material of formation is air, Er = 1

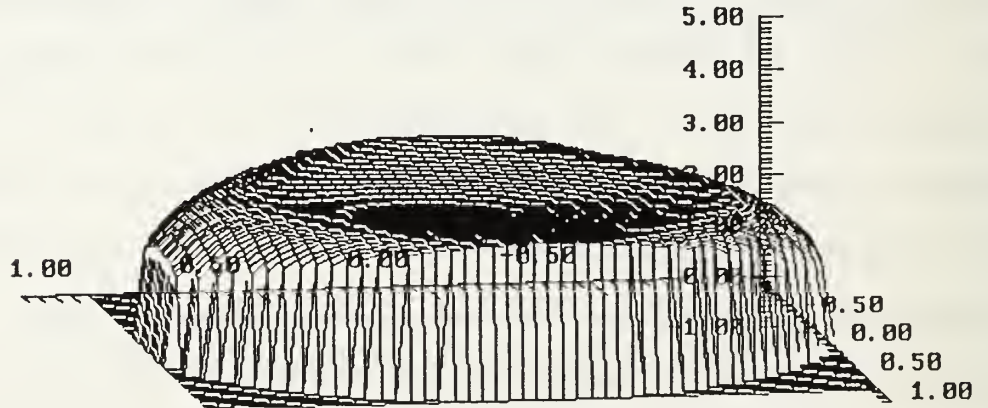
TM INCIDENT FIELD, Computed Field dot Ideal Field, MAGN.



min. Z = +.982; max. Z = +.996; average Z = +.949  
 Inc. A = +.000; Plane G = +.000; View: phi=+45.0 theta=+75.0

The datafile used to generate fields is airfil.INI  
 Shaping function = TAN ogive  
 Material of formation is air, Er = 1

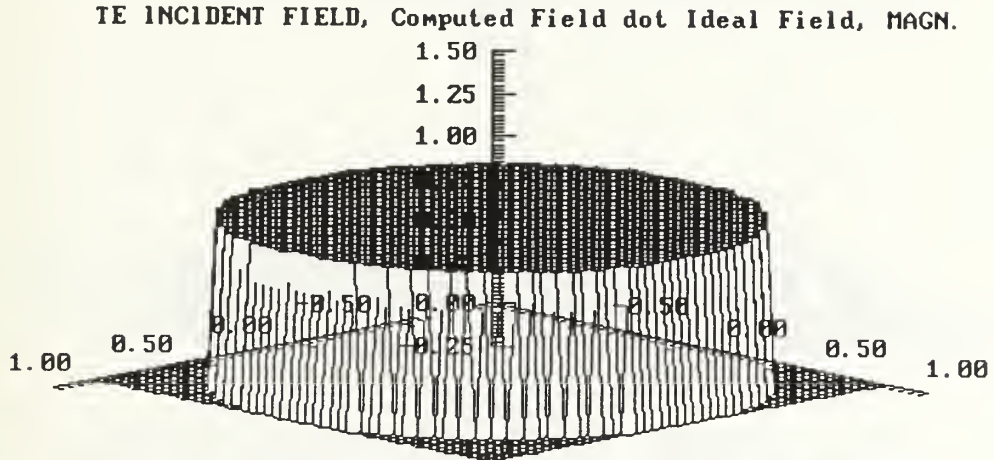
TM INCIDENT FIELD, Computed Field dot Ideal Field, PHASE



min. Z = +1.73; max. Z = +2.95; average Z = +2.59  
 Inc. A = +.000; Plane G = +.000; View: phi=+80.0 theta=+75.0

Figure 5.1 Dot product magnitude and phase for TM computed fields determined for radome composed of air compared with theoretical plane waves

The datafile used to generate fields is airfil.INT  
 Shaping function = TAN ogive  
 Material of formation is air,  $\epsilon_r = 1$



The datafile used to generate fields is airfil.INT  
 Shaping function = TAN ogive  
 Material of formation is air,  $\epsilon_r = 1$

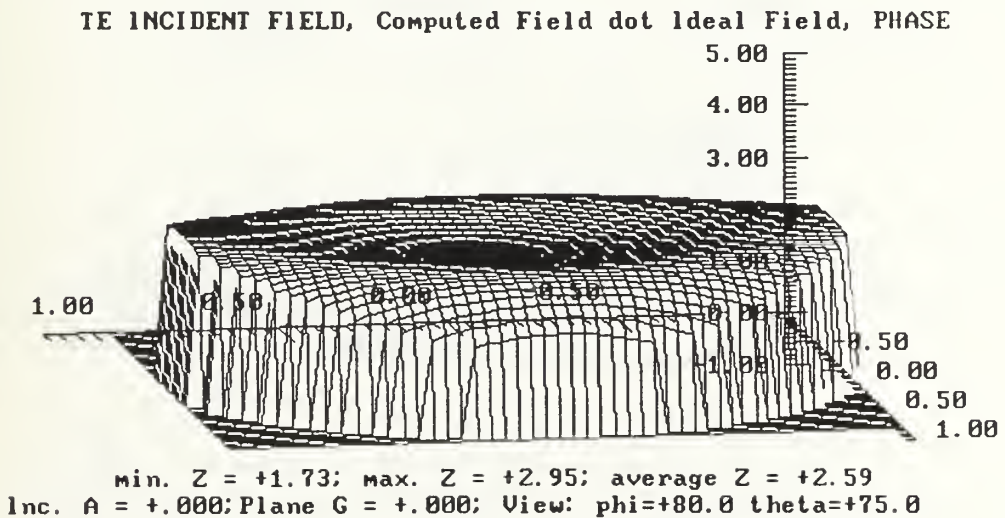
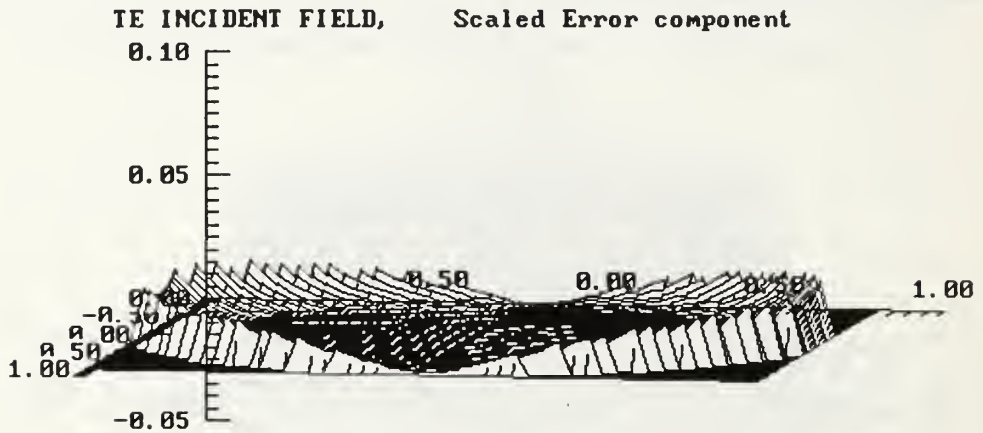


Figure 5.2 Dot product magnitude and phase for TE computed fields determined for radome composed of air compared with theoretical plane waves

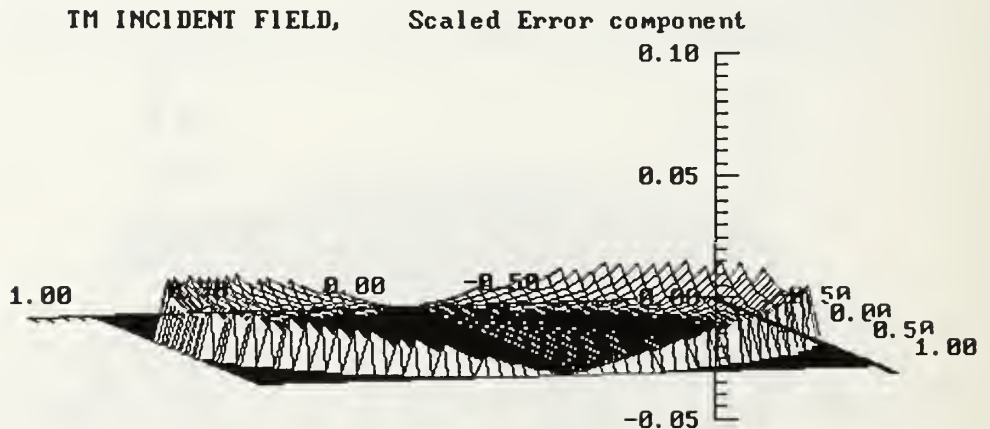


The datafile used to generate fields is airfil.INT  
 Shaping function = TAN ogive  
 Material of formation is air,  $\epsilon_r = 1$



min.  $Z = +.000$ ; max.  $Z = +.023$ ; average  $Z = +.004$   
 Inc.  $A = +.000$ ; Plane  $G = +.000$ ; View:  $\phi = +10.0$   $\theta = +80.0$

The datafile used to generate fields is airfil.INT  
 Shaping function = TAN ogive  
 Material of formation is air,  $\epsilon_r = 1$

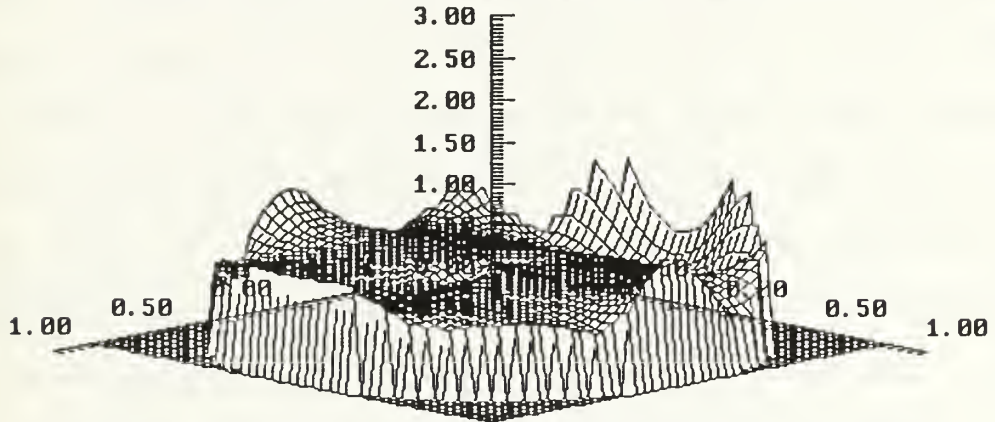


min.  $Z = +.000$ ; max.  $Z = +.023$ ; average  $Z = +.004$   
 Inc.  $A = +.000$ ; Plane  $G = +.000$ ; View:  $\phi = +75.0$   $\theta = +80.0$

Figure 5.3 Scaled error component for TM and TE computed fields determined for radome composed of air compared with theoretical plane waves

The datafile used to generate fields is airfil.INT  
 Shaping function = TAN ogive  
 Material of formation is air,  $\epsilon_r = 1$

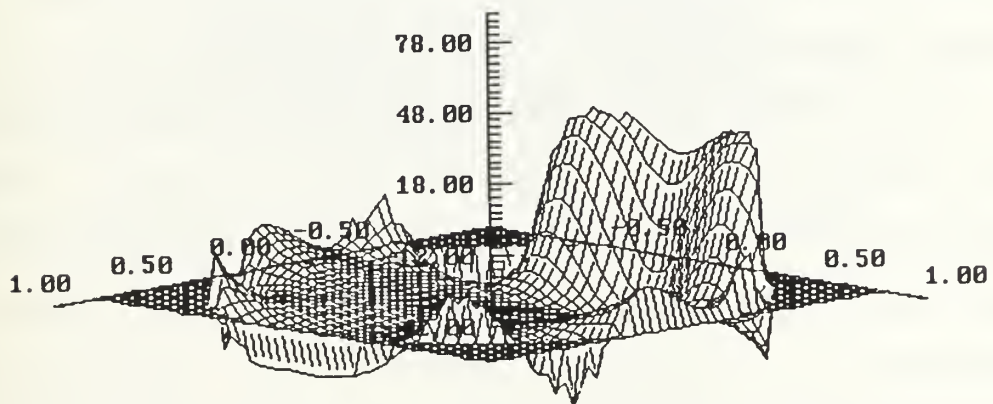
TM INCIDENT FIELD, Computed Field dot Ideal Field, MAGN.



min.  $Z = +.540$ ; max.  $Z = +1.66$ ; average  $Z = +.874$   
 Inc.  $A = +60.0$ ; Plane  $G = +60.0$ ; View:  $\phi = +45.0$   $\theta = +75.0$

The datafile used to generate fields is airfil.INT  
 Shaping function = TAN ogive  
 Material of formation is air,  $\epsilon_r = 1$

TM INCIDENT FIELD, Computed Field dot Ideal Field, PHASE



min.  $Z = -27.9$ ; max.  $Z = +60.1$ ; average  $Z = -2.84$   
 Inc.  $A = +60.0$ ; Plane  $G = +60.0$ ; View:  $\phi = +45.0$   $\theta = +75.0$

Figure 5.4 Dot product magnitude and phase for TM computed fields determined for radome composed of air compared with theoretical plane waves for incident angle of 60 degrees

incident field, for an incident angle  $60^\circ$  from the "nose-on" aspect. The magnitude of the scaled dot product between the computed and theoretical TM incident wave shows modal variation around the antenna plane. The magnitude of the computed value in the direction of the theoretical plane wave varies between 54.0% and 166%, with an average magnitude of 87.4%. The phase component of the dot product varies across the plane from  $-27.9^\circ$  to  $+60.1^\circ$ , with an average phase of  $-2.84^\circ$ . The maximum phase differential occurs at the edge of the antenna plane closest to the point of wave incidence, as the incident wave is defined as arriving in the  $-x - z$  axis. This variation seen in the magnitude and phase of the scaled dot product in the direction of the theoretical, undisturbed plane wave is confirmed in the scaled error component of Fig. 5.5 with an amplitude variation from 8.4% to 88.6%, averaging at 23.6% of the computed field evaluated as an error term perpendicular to the theoretical fields expected.

Figures 5.6 and 5.7 exhibit the behavior of the calculated TE  $60^\circ$  incident plane wave, which is similar, but less in magnitude compared to the calculated TM wave. Less modal variation is seen along the exhibited plane of the antenna. The scaled error component has a symmetry about the x-axis. The scaled error amplitude varies from 0.3% to 33.1%, with an average of 12.5%.

The form of the error components as analyzed for this radome constructed of air identifies a phase error in the determination of the computed fields. The data computations of the EMRAD subroutines have been previously validated by Morgan. These validations

The datafile used to generate fields is airfil.INT  
Shaping function = TAN ogive  
Material of formation is air, Er = 1

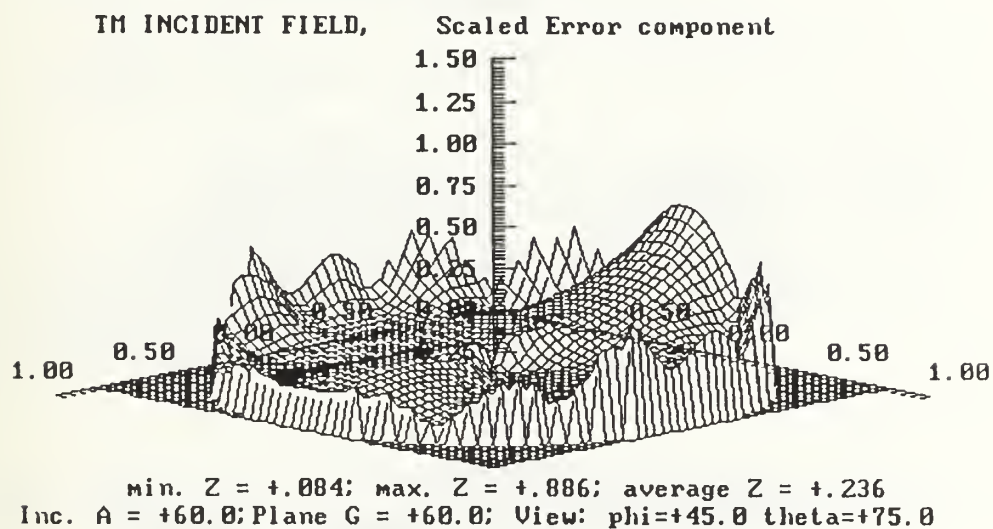
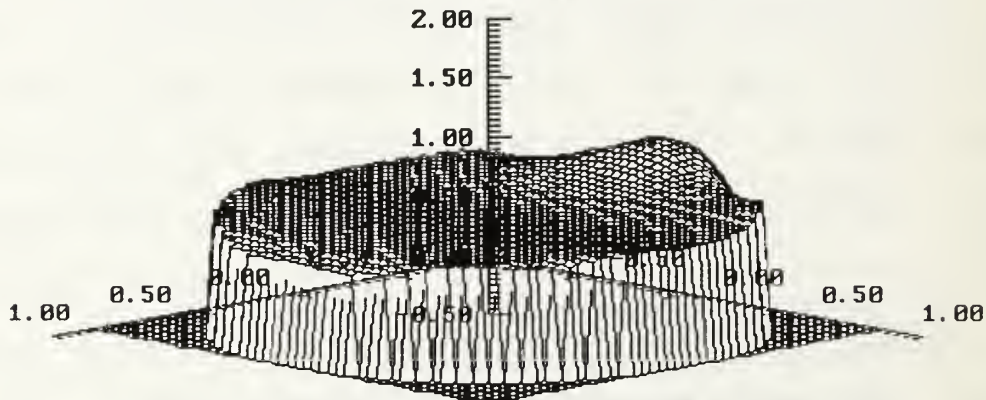


Figure 5.5 Scaled error component for TM computed fields determined for radome composed of air compared with theoretical plane waves for incident angle of 60 degrees

The datafile used to generate fields is airfil.INT  
 Shaping function = TAN ogive  
 Material of formation is air,  $\epsilon_r = 1$

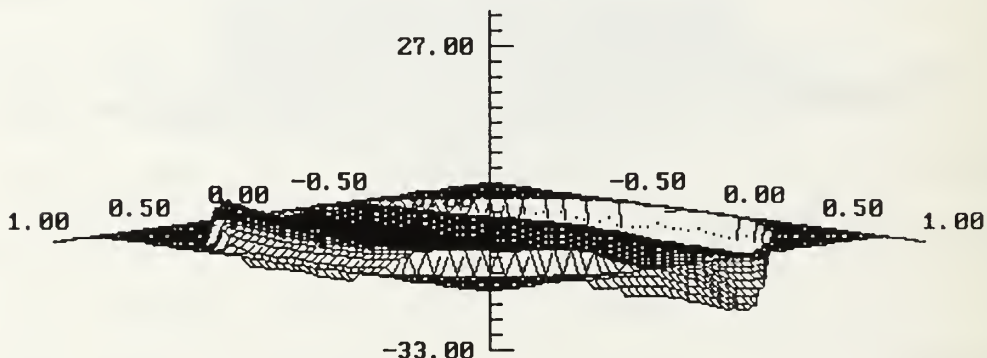
TE INCIDENT FIELD, Computed Field dot Ideal Field, MAGN.



min. Z = +.860; max. Z = +1.34; average Z = +.981  
 Inc. A = +60.0; Plane G = +60.0; View: phi=+45.0 theta=+75.0

The datafile used to generate fields is airfil.INT  
 Shaping function = TAN ogive  
 Material of formation is air,  $\epsilon_r = 1$

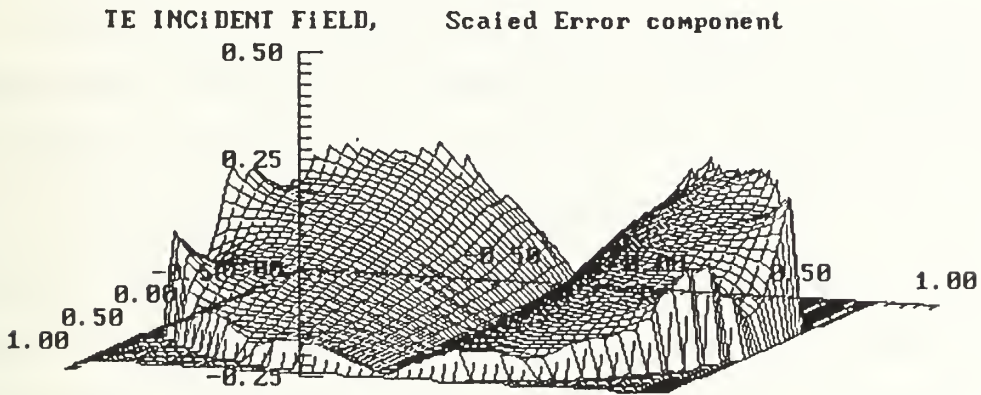
TE INCIDENT FIELD, Computed Field dot Ideal Field, PHASE



min. Z = -18.2; max. Z = +4.96; average Z = -.430  
 Inc. A = +60.0; Plane G = +60.0; View: phi=+45.0 theta=+75.0

Figure 5.6 Dot product magnitude and phase for TE computed fields determined for radome composed of air compared with theoretical plane waves for incident angle of 60 degrees

The datafile used to generate fields is airfii.INI  
Shaping function = TAN ogive  
Material of formation is air,  $\epsilon_r = 1$



min. Z = +.003; max. Z = +.331; average Z = +.125  
Inc. A = +60.0; Plane C = +60.0; View: phi=+20.0 theta=+75.0

Figure 5.7 Scaled error component for TM computed fields determined for radome composed of air compared with theoretical plane waves for incident angle of 60 degrees

considered the magnitude and phase of the scattered fields [Refs. 3 and 4], and the magnitude of the core fields [Ref. 10] along the main coordinate axes. This work is the first to plot both the phase and magnitude variations across the entire two-dimensional plane and identifies the possible need for increased computational accuracy in the numerical routines of EMRAD. There is also the possibility of unresolved programming errors in CORFLD which should be further investigated.

## B. COMPUTATION RESULTS FOR VARIOUS RADOME MATERIALS

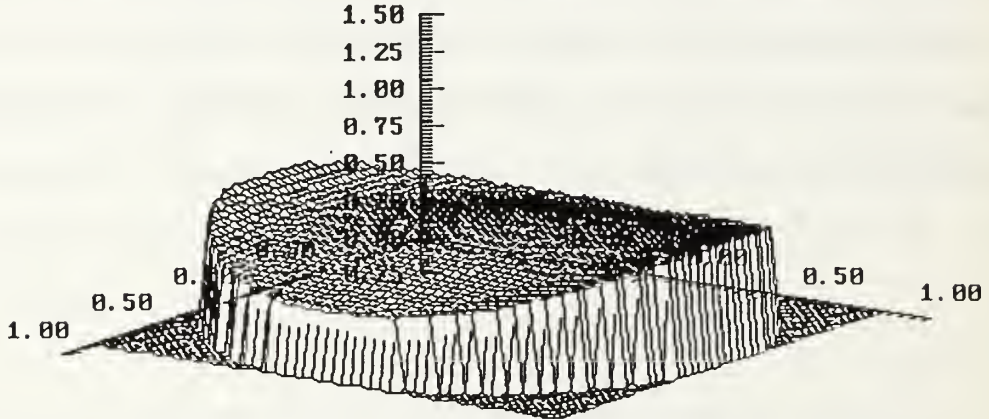
EMRAD and CORFLD executions for the tangent ogive standard established in Chapter IV were run for varying material permittivity according to the material properties listed in Table 2.1. The comparisons of the computed fields to the unperturbed theoretical incident plane waves are included only for the "nose-on" incident angle which has good results for the ideal "air" construction. Fiber-reinforced glass, with  $\epsilon_r=4.0$ ; glass ceramic, with  $\epsilon_r=5.5$ ; and refractory oxide, with  $\epsilon_r=8.0$ , are included. The form of field comparisons are similar in shape for each radome considered, only the magnitude of the plots varies. As expected from the discussion in Chapter II, the attenuation of the incident plane wave, received at the plane of the antenna in the core, increases with increasing relative permittivity. When the radome was constructed of air, the computed magnitude of each incident wave was 94.9%. When fiber-reinforced glass construction is considered, Figures 5.8, 5.9, and

5.10, the average magnitude of the computed wave is 60.1% and the average scaled error component is 22.7%. For the radome constructed of glass ceramic, Figures 5.11, 5.12, and 5.13, the average magnitude is 66.9% and the average scaled error component is 13.3%. For the refractory oxide radome, Figures 5.14, 5.15, and 5.16, the average magnitude of received field is 87.6% and the average scaled error component is 20.6%.



The datafile used to generate fields is P4FIL.INT  
 Shaping function = IAN ogive  
 Material of formation is fiber-reinforced glass

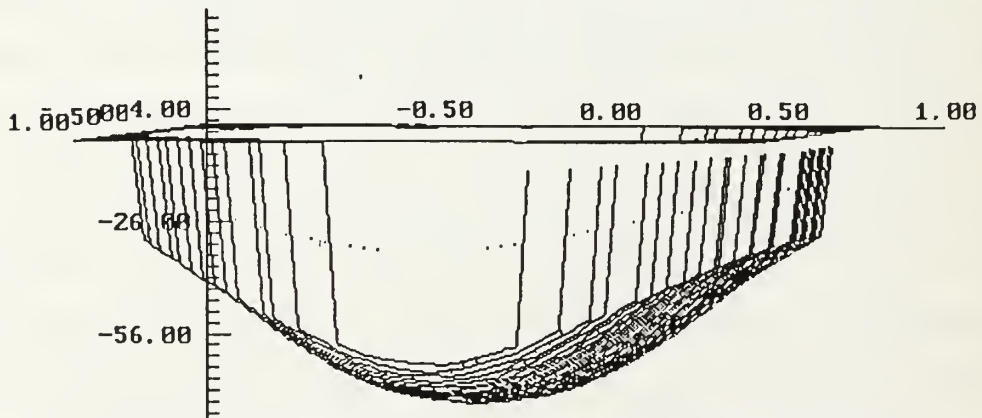
TM INCIDENT FIELD, Computed Field dot Ideal Field, MAGN.



min. Z = +.475; max. Z = +.811; average Z = +.601  
 Inc. A = +.000; Plane G = +.000; View: phi=+35.0 theta=+70.0

The datafile used to generate fields is p4fil.INT  
 Shaping function = IAN ogive  
 Material of formation is fiber-reinforced glass

TM INCIDENT FIELD, Computed Field dot Ideal Field, PHASE

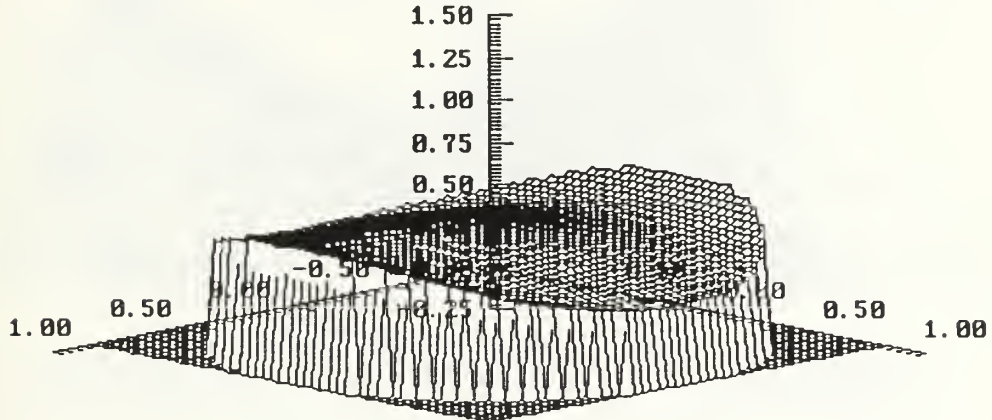


min. Z = -71.1; max. Z = -27.4; average Z = -51.8  
 Inc. A = +.000; Plane G = +.000; View: phi=+10.0 theta=+85.0

Figure 5.8 Dot product magnitude and phase for TM computed fields determined for radome composed of fiber-reinforced glass compared with theoretical plane waves for incident angle of 0 degrees

The datafile used to generate fields is p4fil.INT  
 Shaping function = TAN ogive  
 Material of formation is fiber-reinforced glass

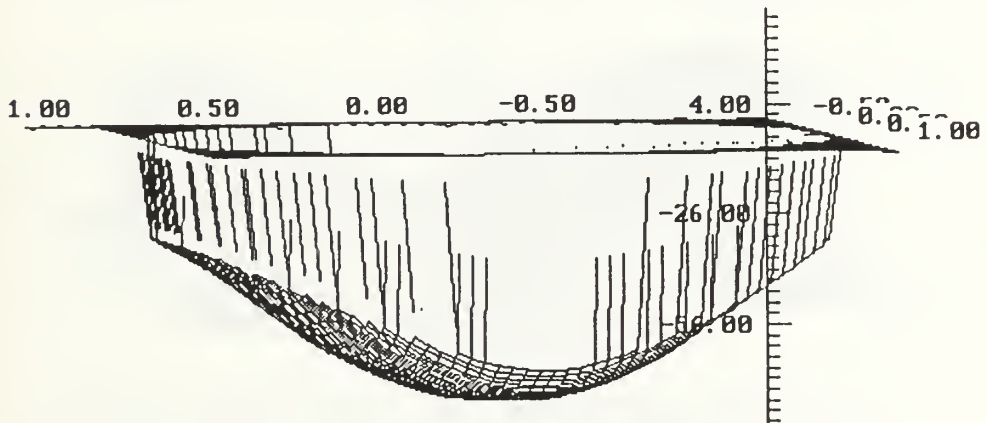
TE INCIDENT FIELD, Computed Field dot Ideal Field, MAGN.



min. Z = +.475; max. Z = +.811; average Z = +.601  
 Inc. A = +.000; Plane G = +.000; View: phi=+45.0 theta=+75.0

The datafile used to generate fields is p4fil.INT  
 Shaping function = TAN ogive  
 Material of formation is fiber-reinforced glass

TE INCIDENT FIELD, Computed Field dot Ideal Field, PHASE

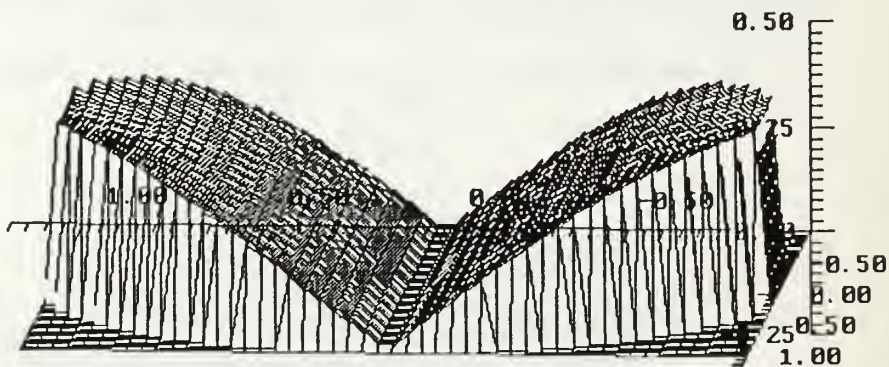


min. Z = -71.1; max. Z = -27.4; average Z = -51.8  
 Inc. A = +.000; Plane G = +.000; View: phi=+80.0 theta=+80.0

Figure 5.9 Dot product magnitude and phase for TE computed fields determined for radome composed of fiber-reinforced glass compared with theoretical plane waves for incident angle of 0 degrees

The datafile used to generate fields is p4fil.INT  
 Shaping function = TAN ogive  
 Material of formation is fiber-reinforced glass

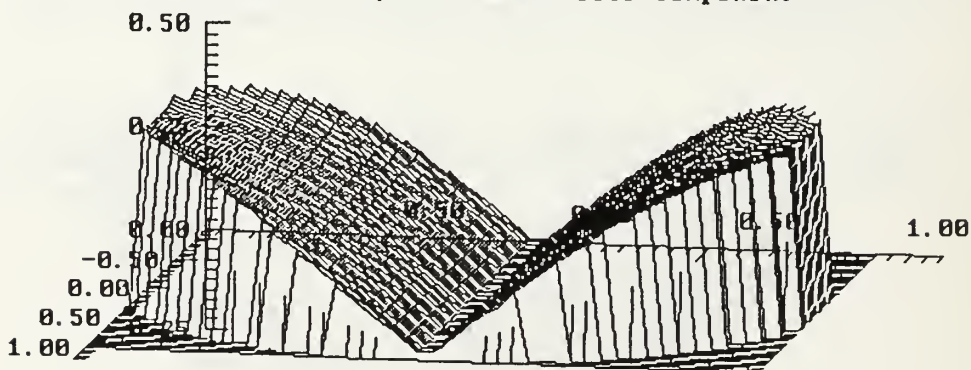
TM INCIDENT FIELD, Scaled Error component



min.  $Z = +.013$ ; max.  $Z = +.436$ ; average  $Z = +.227$   
 Inc.  $A = +.000$ ; Plane  $G = +.000$ ; View:  $\phi = +95.0$   $\theta = +70.0$

The datafile used to generate fields is p4fil.INT  
 Shaping function = TAN ogive  
 Material of formation is fiber-reinforced glass

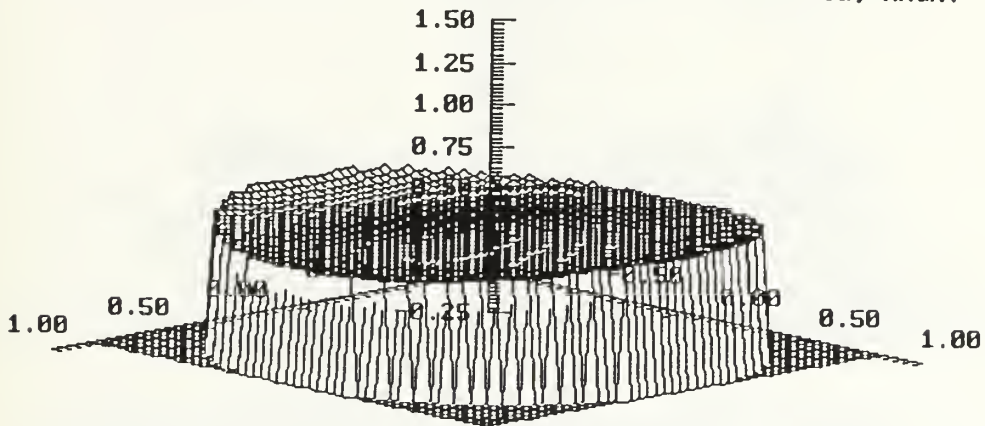
TE INCIDENT FIELD, Scaled Error component



min.  $Z = +.013$ ; max.  $Z = +.436$ ; average  $Z = +.227$   
 Inc.  $A = +.000$ ; Plane  $G = +.000$ ; View:  $\phi = +10.0$   $\theta = +70.0$

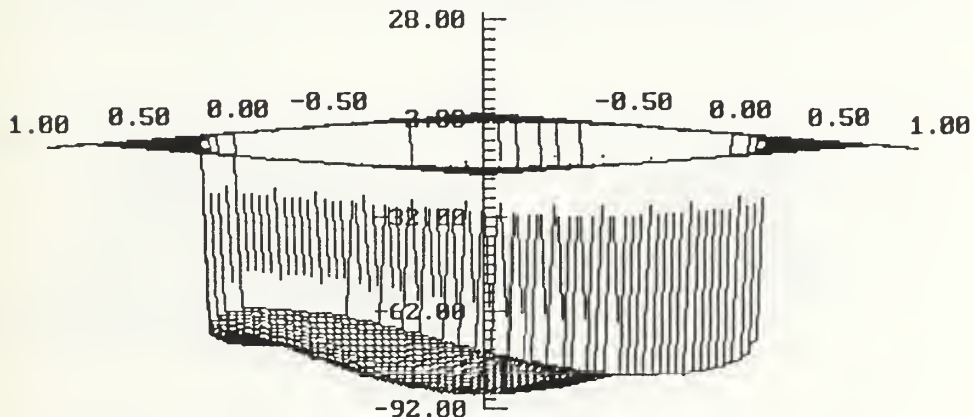
Figure 5.10 Scaled error component for TM and TE computed fields determined for radome composed of fiber-reinforced glass compared with theoretical plane waves for incident angle of 0 degrees

The datafile used to generate fields is c55fil.INT  
 TEST DATA FOR THESIS  
 Radome is tangential ogive,  
 constructed of ceramic,  $\epsilon_r = 5.5$   
 TM INCIDENT FIELD, Computed Field dot Ideal Field, MAGN.



min. Z = +.668; max. Z = +.803; average Z = +.669  
 Inc. A = +.000; Plane G = +.000; View: phi=+45.0 theta=+75.0

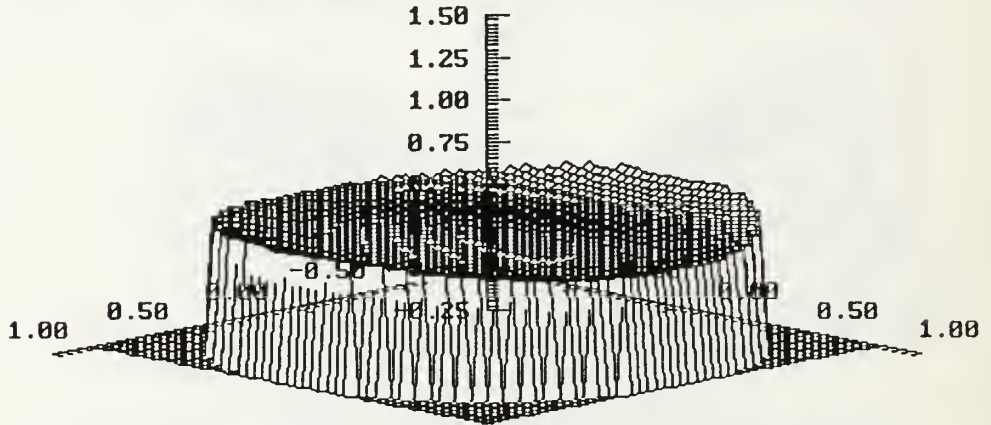
The datafile used to generate fields is c55fil.INT  
 TEST DATA FOR THESIS  
 Radome is tangential ogive,  
 constructed of ceramic,  $\epsilon_r = 5.5$   
 TM INCIDENT FIELD, Computed Field dot Ideal Field, PHASE



min. Z = -77.5; max. Z = -47.5; average Z = -61.9  
 Inc. A = +.000; Plane G = +.000; View: phi=+45.0 theta=+75.0

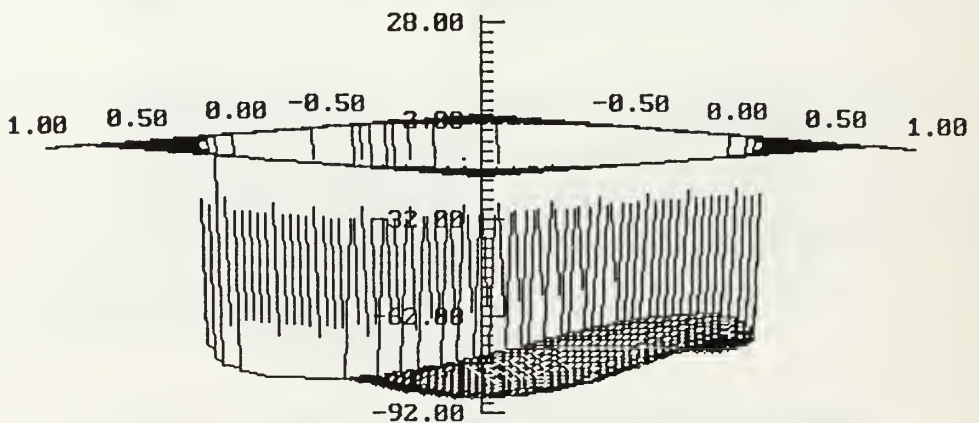
Figure 5.11 Dot product magnitude and phase for TM computed fields determined for radome composed of glass ceramic compared with theoretical plane waves for incident angle of 0 degrees

The datafile used to generate fields is c55fil.INT  
 TEST DATA FOR THESIS  
 Radome is tangential ogive,  
 constructed of ceramic,  $\epsilon_r = 5.5$   
 TE INCIDENT FIELD, Computed Field dot Ideal Field, MAGN.



min. Z = +.668; max. Z = +.803; average Z = +.669  
 Inc. A = +.000; Plane G = +.000; View: phi=+45.0 theta=+75.0

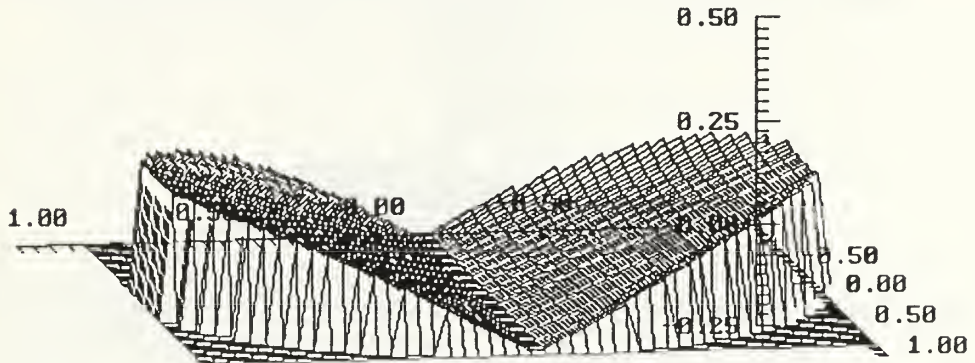
The datafile used to generate fields is c55fil.INT  
 TEST DATA FOR THESIS  
 Radome is tangential ogive,  
 constructed of ceramic,  $\epsilon_r = 5.5$   
 TE INCIDENT FIELD, Computed Field dot Ideal Field, PHASE



min. Z = -77.5; max. Z = -47.5; average Z = -61.9  
 Inc. A = +.000; Plane G = +.000; View: phi=+45.0 theta=+75.0

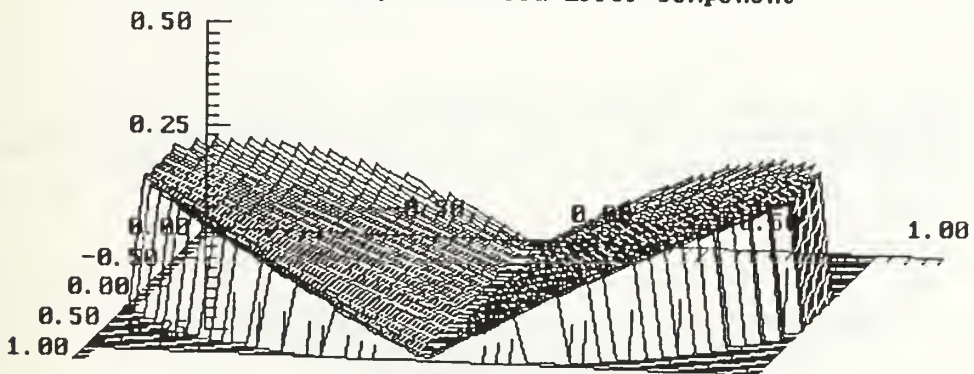
Figure 5.12 Dot product magnitude and phase for TE computed fields determined for radome composed of glass ceramic compared with theoretical plane waves for incident angle of 0 degrees

The datafile used to generate fields is c55fil.INT  
 TEST DATA FOR THESIS  
 Radome is tangential ogive,  
 constructed of ceramic,  $\epsilon_r = 5.5$   
 TM INCIDENT FIELD, Scaled Error component



min. Z = +.005; max. Z = +.312; average Z = +.133  
 Inc. A = +.000; Plane G = +.000; View: phi=+80.0 theta=+70.0

The datafile used to generate fields is c55fil.INT  
 TEST DATA FOR THESIS  
 Radome is tangential ogive,  
 constructed of ceramic,  $\epsilon_r = 5.5$   
 TE INCIDENT FIELD, Scaled Error component

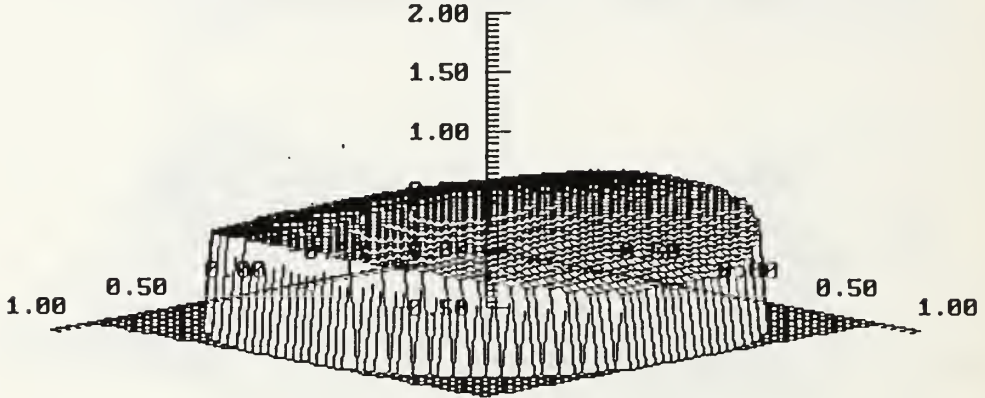


min. Z = +.005; max. Z = +.312; average Z = +.133  
 Inc. A = +.000; Plane G = +.000; View: phi=+10.0 theta=+70.0

Figure 5.13 Scaled error component for TM and TE computed fields determined for radome composed of glass ceramic compared with theoretical plane waves for incident angle of 0 degrees

The datafile used to generate fields is OX8FIL.INT  
 Shaping function = TAN ogive  
 Material of formation is refractory oxide, Er = 8

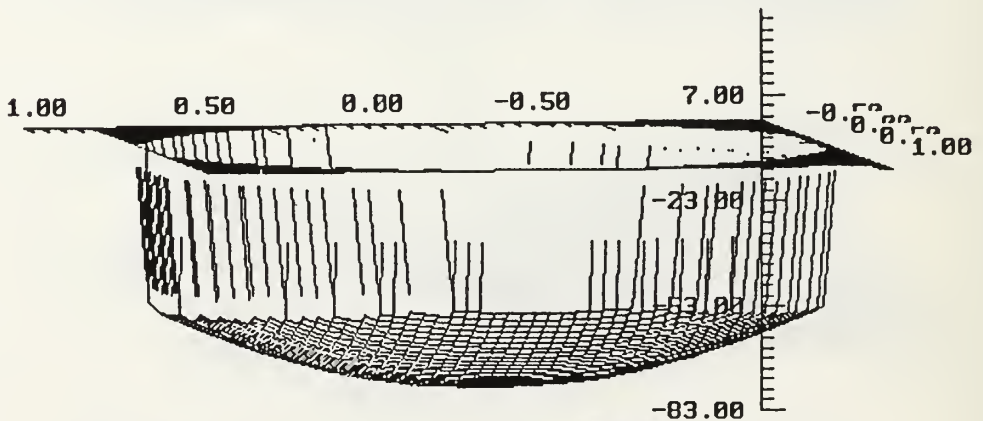
TM INCIDENT FIELD, Computed Field dot Ideal Field, MAGN.



min. Z = +.634; max. Z = +1.00; average Z = +.876  
 Inc. A = +.000; Plane G = +.000; View: phi=+45.0 theta=+75.0

The datafile used to generate fields is OX8FIL.INT  
 Shaping function = TAN ogive  
 Material of formation is refractory oxide, Er = 8

TM INCIDENT FIELD, Computed Field dot Ideal Field, PHASE

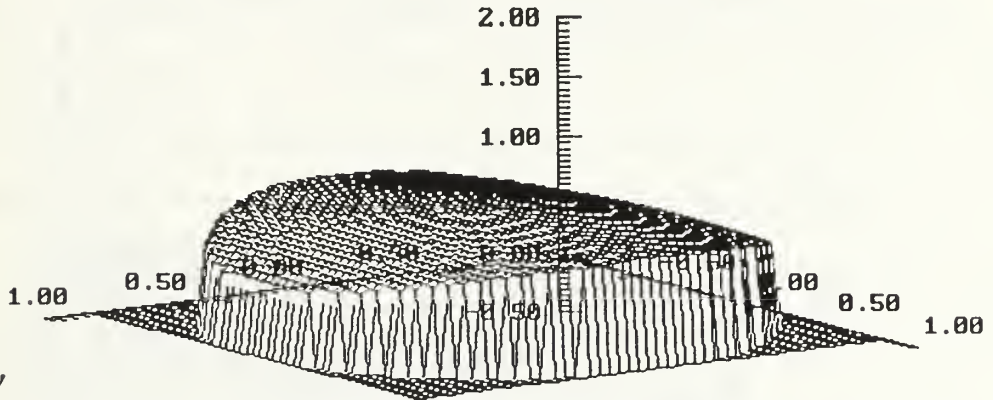


min. Z = -68.3; max. Z = -39.4; average Z = -52.4  
 Inc. A = +.000; Plane G = +.000; View: phi=+00.0 theta=+75.0

Figure 5.14 Dot product magnitude and phase for TM computed fields determined for radome composed of refractory oxide compared with theoretical plane waves for incident angle of 0 degrees

The datafile used to generate fields is OX8FIL.INT  
 Shaping function = TAN ogive  
 Material of formation is refractory oxide,  $\epsilon_r = 8$

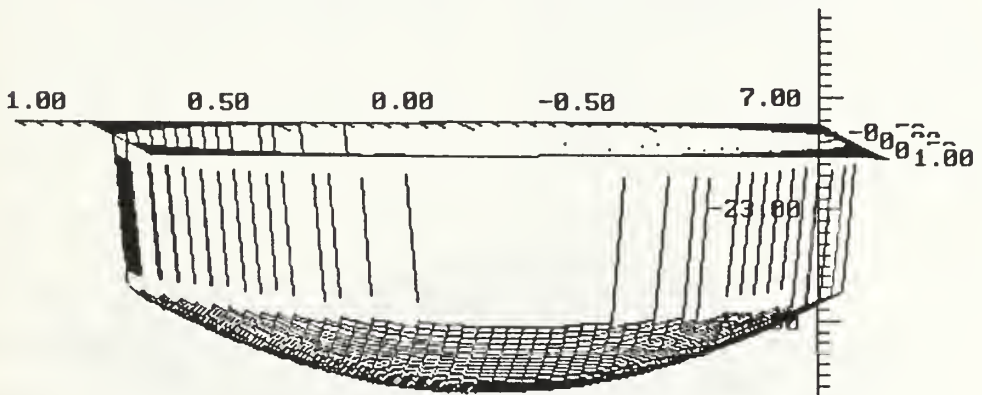
TE INCIDENT FIELD, Computed Field dot Ideal Field, MAGN.



min.  $Z = +.634$ ; max.  $Z = +1.00$ ; average  $Z = +.876$   
 Inc.  $A = +.000$ ; Plane  $G = +.000$ ; View:  $\phi = +55.0$   $\theta = +75.0$

The datafile used to generate fields is OX8FIL.INT  
 Shaping function = TAN ogive  
 Material of formation is refractory oxide,  $\epsilon_r = 8$

TE INCIDENT FIELD, Computed Field dot Ideal Field, PHASE



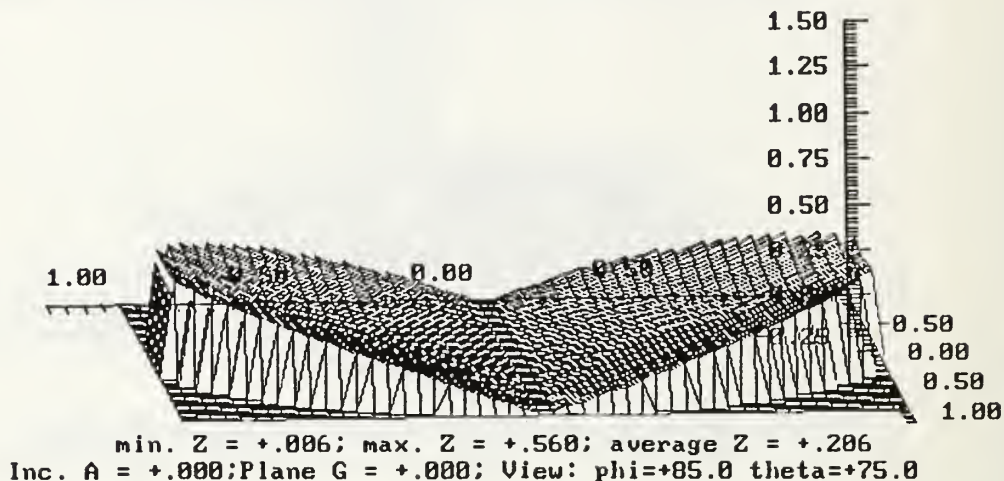
min.  $Z = -68.3$ ; max.  $Z = -39.4$ ; average  $Z = -52.4$   
 Inc.  $A = +.000$ ; Plane  $G = +.000$ ; View:  $\phi = +85.0$   $\theta = +80.0$

Figure 5.15 Dot product magnitude and phase for TE computed fields determined for radome composed of refractory oxide compared with theoretical plane waves for incident angle of 0 degrees



The datafile used to generate fields is OX8FIL.INT  
 Shaping function = TAN ogive  
 Material of formation is refractory oxide,  $\epsilon_r = 8$

TM INCIDENT FIELD, Scaled Error component



The datafile used to generate fields is OX8FIL.INT  
 Shaping function = TAN ogive  
 Material of formation is refractory oxide,  $\epsilon_r = 8$

TE INCIDENT FIELD, Scaled Error component

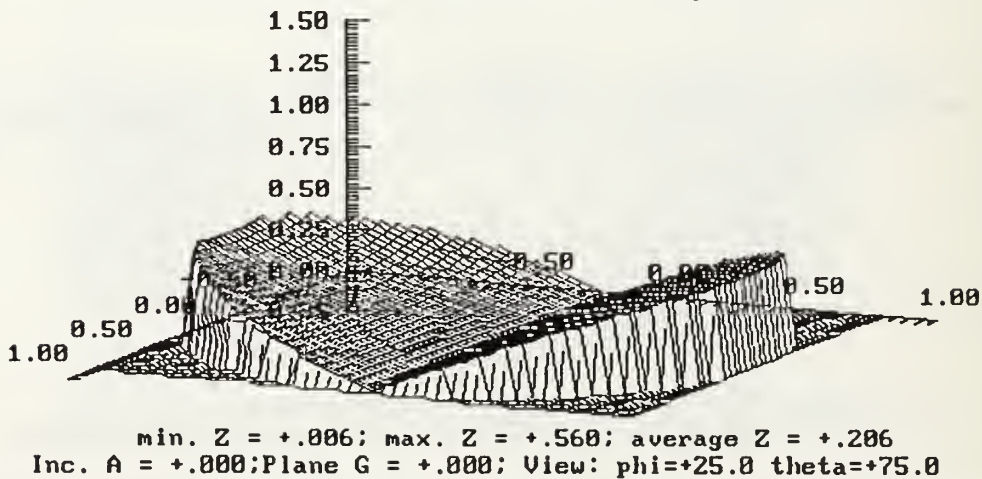


Figure 5.16 Scaled error component for TM and TE computed fields determined for radome composed of refractory oxide compared with theoretical plane waves for incident angle of 0 degrees

## VI. CONCLUSIONS

This thesis has presented a useful set of programs to numerically model a radome, designed of specified shape, construction, and material, and to evaluate the perturbation of the electromagnetic field as it passes through the modelled radome to the antenna within the radome structure. The radome design methodology was discussed in Chapter II, along with the radome shaping functions, wall construction, and choice of materials for radome construction. The program RADSHIP is introduced and the shaping function, as well as the shaping factors for each function are explained. Chapter III developed the electromagnetic theory required to assemble the field components within the interior radome core, using the coefficients provided by the EMRAD program. The theory required for transforming the coordinates of the canted antenna plane to the core coordinates for an assumed two-axis gimbal was also discussed. Chapter IV explained the data flow for the radome model design process by using an example of the program executions for the design of a monolithic tangent ogive, with computational analysis by EMRAD and field component generation by CORFLD. The verification of the radome design and optimal placing of the core origin by the use of CURVE DIGITIZER software is also discussed. Chapter V discussed the computational errors discovered in the 3-D plotting of the field components. The scaled magnitude of

the computed perturbed plane waves for the "nose-on" incident angle agreed within 95% of the theoretical value and the phase of the computed field was an almost constant  $2.59^\circ$  out of phase with the theoretical incident plane wave. The errors increase when the angle of incidence is off the "nose-on" aspect, with modal amplitude variations from 54% to 166% of the theoretical plane wave. Further diagnostics are required to determine the source of this error.

This is only the first stage in the development of a mathematical model for the interaction between the radome and the antenna system that the radome is designed to enclose. The model, in its present form, does not consider the presence of the antenna structure within the radome core. Further work is needed to determine the effect of the antenna structure and its interaction with the radome. When such a model is developed the predicted data can be compared to data collected by a physical antenna system. The culmination of this effort could be the analytic development of corrective lenses, as referred to in Chapter II, to correct or minimize the perturbation of the incident electromagnetic field caused by the radome structure.

## Appendix A

### EMRAD FIELD THEORY

The program EMRAD uses the unimoment method mentioned in Chapter II, as developed by Morgan and Mei [Ref. 5] to decouple the interior and exterior spherical solutions. The expansion coefficients for the electromagnetic fields within the radome structure are generated as part of the scattering solution. CORFLD uses these coefficients for construction of the interior fields. The theory required by CORFLD to formulate the electromagnetic fields within the radome is discussed in Chapter II.

The code developed by Morgan for EMRAD uses an optimized variational finite-element algorithm, in conjunction with a tri-regional unimoment method, to provide scattering solutions for each of multiple incident fields impinging on the specified structure. EMRAD represent a significant improvement in computational speed and versatility over computer codes which find the solution to the electromagnetic scattering and penetration problem by use of surface current integral equation formulations. This advantage results because of the highly sparse matrices embodied in the finite element solution vis-a-vis full matrices found using an integral equation formulation. An overview of the finite element scattering algorithm, along with the concept of coupled azimuthal potentials and the unimoment method are included in this appendix. Further information is available in references 3, 4, 5, 6, and 7.

## A. COUPLED AZIMUTHAL POTENTIALS

In the radome construction the material constitutive parameters,  $\epsilon(\mathbf{r})$  and  $\mu(\mathbf{r})$ , are invariant to the azimuthal coordinate  $\phi$  due to the axial symmetry of the radome. This axisymmetry allows implementation of vector field generation via coupled azimuthal potentials, as developed by Morgan, Chang and Mei [Ref. 7].

For ease of solution and representation, a normalized cylindrical coordinate system is adopted, as defined by  $(R, Z, \phi) = (k_0 \rho, k_0 z, \phi)$  where  $(\rho, z, \phi)$  are standard circular cylindrical coordinates and  $k_0 = 2\pi/\lambda_0$  is the free-space wavenumber of the time-harmonic field. The equations in this form are related to the standard spherical coordinates  $(r, \theta, \phi)$  as shown in Fig. A.1 using the substitutions

$$R = k_0 r \sin\theta \quad (\text{A.1})$$

and

$$Z = k_0 r \cos\theta . \quad (\text{A.2})$$

The total electromagnetic fields are decomposed into azimuthal modes by an exponential Fourier series in the  $\phi$ -coordinate such that

$$\mathbf{E}(R,Z,\phi) = \sum_{m=-\infty}^{\infty} \mathbf{e}_m(R,Z) e^{jm\phi} \quad (\text{A.3})$$

and

$$\eta_0 \mathbf{H}(R,Z,\phi) = \sum_{m=-\infty}^{\infty} \mathbf{h}_m(R,Z) e^{jm\phi} , \quad (\text{A.4})$$

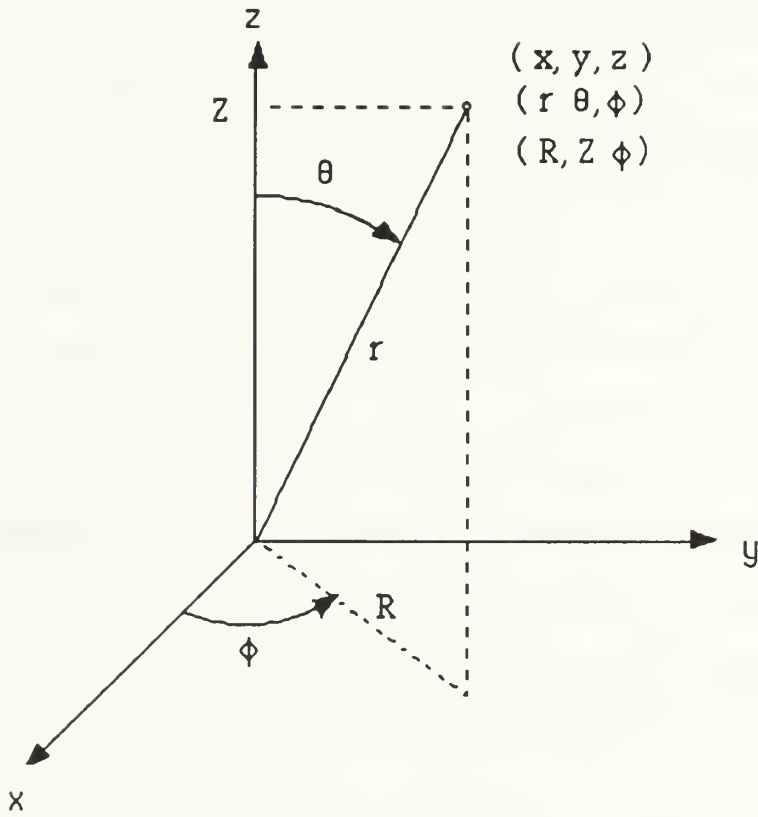


Figure A.1 Rectangular  $(x, y, z)$ , spherical  $(r, \theta, \phi)$ , and normalized cylindrical  $(R, Z, \theta)$  coordinate systems

where  $\eta_0 = 120 \pi \Omega$  is used to normalize the magnetic fields, so that  $\mathbf{h} = \eta_0 \mathbf{H}$ .

Using the axial symmetry of the radome construction, the modal fields decouple when the field expansions are substituted into Maxwell's equations, yielding [Ref. 7], after judicious cross substitutions the following modal field generating equations in terms of two scalar potentials,  $\Gamma_1( R,Z,m )$  and  $\Gamma_2( R,Z,m )$ :

$$\boldsymbol{\phi} \times \mathbf{e}_m = j f_m ( m \boldsymbol{\phi} \times \nabla \Gamma_1 - R \mu_r \nabla \Gamma_2 ) \quad (\text{A.5})$$

$$\boldsymbol{\phi} \cdot \mathbf{e}_m = \frac{\Gamma_1}{R} \quad (\text{A.6})$$

$$\boldsymbol{\phi} \times \mathbf{h}_m = j f_m ( m \boldsymbol{\phi} \times \nabla \Gamma_2 + R \epsilon_r \nabla \Gamma_1 ) \quad (\text{A.7})$$

$$\boldsymbol{\phi} \cdot \mathbf{h}_m = \frac{\Gamma_2}{R} \quad (\text{A.8})$$

where the two dimensional gradient operator is defined as

$$\nabla = [ \mathbf{R} (\partial/\partial r) + \mathbf{Z} (\partial/\partial Z) ] \quad (\text{A.9})$$

and  $f_m$  is a multiplicative function given by

$$f_m(R,Z) = [ \mu_r(R,Z) \epsilon_r(R,Z) R^2 - m^2 ]^{-1} . \quad (\text{A.10})$$

Note that the potentials,  $\Gamma_1$  and  $\Gamma_2$ , are proportional to the azimuthal components of the electric and magnetic fields,  $\mathbf{e}_m$  and  $\mathbf{h}_m$ . These potential functions are continuous everywhere, including at dielectric and magnetic interfaces. This property of uniform continuity in the field is used to obtain a numerical solution of the fields.

The total fields may be described in term of the uniformly continuous scalar potentials  $\Gamma_1( R,Z,m )$  and  $\Gamma_2( R,Z,m )$  such that

$$\mathbf{e}_m(R,Z) = j f_m ( m \nabla \Gamma_1 - R \mu_r \phi \times \nabla \Gamma_2 ) + \phi \frac{\Gamma_1}{R} \quad (\text{A.1 1})$$

and

$$\mathbf{h}_m(R,Z) = j f_m ( m \nabla \Gamma_2 + R \epsilon_r \phi \times \nabla \Gamma_1 ) + \phi \frac{\Gamma_2}{R} . \quad (\text{A.1 2})$$

This method of expanding the electromagnetic fields into modal components is named the Coupled Azimuthal Potential (CAP) method due to the fact that the scalar potentials  $\Gamma_1(R, Z, m)$  and  $\Gamma_2(R, Z, m)$  are coupled in these field equations and are not separable.

Due to the symmetry in the azimuthal coordinate,  $\phi$ , in radome design, an arbitrary meridional cross section of the radome construction may be represented in an  $(R, Z)$ -plane such that there exists a two-dimensional solution domain  $S$ , with a boundary curve forming the surface of revolution  $\delta S$ . It has been shown by Morgan, Chang and Mei [Ref. 7] that in this solution domain the potentials,  $\Gamma_1$  and  $\Gamma_2$ , satisfy the following formally self-adjoint pair of partial differential equations (PDE's),

$$\nabla \cdot ( f_m R \epsilon_r \nabla \Gamma_1 ) + \frac{\epsilon_r}{R} \Gamma_1 + m \nabla \cdot ( f_m \phi \times \nabla \Gamma_2 ) = 0 \quad (\text{A.1 3})$$

and

$$-m \nabla \cdot ( f_m \phi \times \nabla \Gamma_1 ) + \nabla \cdot ( f_m R \mu_r \nabla \Gamma_2 ) + \frac{\mu_r}{R} \Gamma_2 = 0 , \quad (\text{A.1 4})$$

with Dirichlet boundary conditions (BC) for  $\Gamma_1$  and  $\Gamma_2$  specified on  $\delta S$  .



In addition to this PDE formulation there is an easily managed variational principle [Ref. 7] established using either an Euler-Lagrange approach or a stationary-theorem approach. The variational principle is based upon the existence of a stationary functional of the potentials,  $\Gamma_1$  and  $\Gamma_2$ , and their gradients such that

$$SF = \iint_S L(R, Z, \Gamma_1, \Gamma_2, \nabla\Gamma_1, \nabla\Gamma_2) dRdZ, \quad (A.15)$$

where the Lagrangian operator,  $L$ , is unique within an arbitrary constant multiplier and arbitrary independent additive function. The Lagrangian operator has the quadratic form

$$\begin{aligned} L = & f_m \nabla\Gamma_1 \cdot (R\epsilon_r \nabla\Gamma_1 + m\phi \times \nabla\Gamma_2) \\ & + f_m \nabla\Gamma_2 \cdot (R\mu_r \nabla\Gamma_2 - m\phi \times \nabla\Gamma_1) \\ & - \frac{1}{R} \left( \epsilon_r \Gamma_1^2 + \mu_r \Gamma_2^2 \right). \end{aligned} \quad (A.16)$$

With this analytical approach to the solution of the electromagnetic field's behavior through the axially symmetric radome structure, the determination of the field on a point-to-point basis is accomplished through a numerical finite-element algorithm.

## B. FINITE ELEMENT ALGORITHM

The numerical solution of the electromagnetic field problem involving scattering by, and penetration of, the radome is accomplished by the development of a finite-element algorithm using the mesh geometry in Fig A.2. This configuration in the meridional  $(R, Z)$ -plane uses linear triangular elements which are

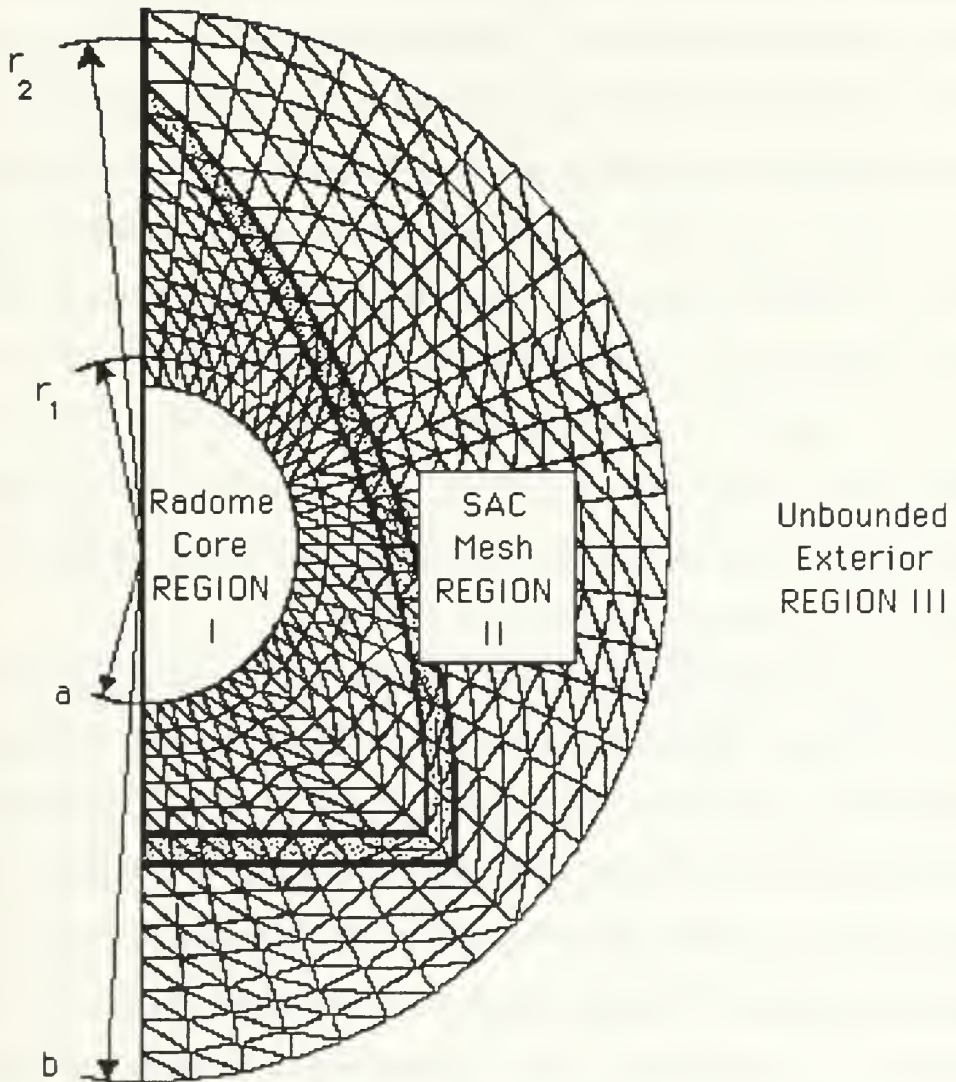


Figure A.2 Finite Element Mesh Geometry

arranged by the EMRAD program to conform to the surfaces of the axisymmetric radome. The selection of surface conformation simplifies numerical analysis of the normal derivative discontinuities at the surface boundaries. The two-dimensional mesh configuration that is developed is named the semiannular conformal (SAC) mesh.

Figure A.2 graphically represents the separate spatial regions which are of interest. The homogeneous inner spherical core of the radome occupies Region I. The inhomogeneous axisymmetric radome wall construction cross-section is in Region II. The unbounded exterior region exists exterior to the outer sphere in the homogeneous free-space of Region III. Note that the surfaces of the inner sphere, Region I, and the exterior Region III, bound the area of interest for numerical analysis in Region II.

The electromagnetic fields within the homogeneous inner core of the radome (Region I) and the unbounded exterior (Region III) are defined in terms of the appropriate spherical harmonic modal expansions of the radial TE and TM field components. At the surfaces,  $r = a$  and  $r = b$ , the modal elements in these fields are applied as sets of Dirichlet boundary conditions. Then, the numerical solution for the fields in the finite-element domain of Region II is generated for each boundary condition. Finally, the unknown modal expansion coefficients for the core and exterior scattered fields are obtained by enforcing continuity of the electromagnetic fields at the interfaces along  $r = r_1$  and  $r = r_2$ . This approach to numerical solution of the fields is the basis of the unimoment method. In the implementation of the variational principle using the finite-element

method, the azimuthal modal field components are selected as the fundamental unknowns.

In Region II of Fig. A.2, the SAC mesh is composed of numerous interior nodes. Each of these interior nodes is surrounded by six triangular regions known as "elements". The azimuthal field components within the mesh are represented as basis function expansions,

$$\phi \cdot \mathbf{e}_m(\mathbf{R}, \mathbf{Z}) = \sum_{n=1}^N \mathbf{e}_m(n) u_n(\mathbf{R}, \mathbf{Z}) \quad (\text{A.17})$$

and

$$\phi \cdot \mathbf{h}_m(\mathbf{R}, \mathbf{Z}) = \sum_{n=1}^N \mathbf{h}_m(n) u_n(\mathbf{R}, \mathbf{Z}) . \quad (\text{A.18})$$

Each of the respective sets of  $\mathbf{e}_m(n)$  and  $\mathbf{h}_m(n)$  represent one of the  $N$  complex nodal values found in the azimuthal fields. The finite element basis functions  $u_n(\mathbf{R}, \mathbf{Z})$  are area coordinate linear pyramid functions which each assume a value of unity at their associated node,  $n$ , and zero at each of the neighboring nodes. There is an assumption of linear variation within each of the triangular elements in the surrounding group such that

$$u_n(\mathbf{R}, \mathbf{Z}) = a_{n,\ell} R + b_{n,\ell} Z + c_{n,\ell} . \quad (\text{A.19})$$

The real constants ( $a$ ,  $b$ ,  $c$ ) corresponding to each node,  $n$ , in element  $\ell$  is found in terms of the nodal ( $\mathbf{R}$ ,  $\mathbf{Z}$ )-coordinates of the element.

The variational finite-element technique is initiated by substituting the linear shape-function expansions in Equations (A.17) and (A.18) into the stationary Euler-Lagrange functional,  $SF$ , as

described in Equation (A.15). The stationary point of SF is then computed by imposing the null derivative condition with respect to each of the unknown coordinates representing the interior nodal fields, while constraining the "known" boundary nodal fields. The resulting linear system describing the nodal fields is

$$\sum_{i=1}^N \{e_m(i) \iint_{S_n} [f_m R \epsilon_r \nabla(Ru_n) \cdot \nabla(Ru_i) - R \epsilon_r u_n u_i] dRdZ + h_m(i) \iint_{S_n} [mf_m \nabla(Ru_n) \cdot \phi \times \nabla(Ru_i)] dRdZ\} = 0 \quad (A.20)$$

and

$$\sum_{i=1}^N \{h_m(i) \iint_{S_n} [f_m R \mu_r \nabla(Ru_n) \cdot \nabla(Ru_i) - R \mu_r u_n u_i] dRdZ - e_m(i) \iint_{S_n} [mf_m \nabla(Ru_n) \cdot \phi \times \nabla(Ru_i)] dRdZ\} = 0 \quad (A.21)$$

for each value of the internal nodes,  $n$ , where  $i$  spans all nodes, including boundary nodes. As these above equations are enforced for each internal node, they involve integrations over only the elements connected to this node,  $S_n$ , and therefore relate the value of  $e_m(n)$  and  $h_m(n)$  only to adjacent nodal values,  $e_m(i)$  and  $h_m(i)$ . Then, in the SAC mesh implementation, in the case of each internal node and the six adjacent nodes, the above equation will relate 14 adjacent node azimuthal field values, some of which may be specified at the boundary.

The computation for each nodal value, as indicated by Equations (A.20) and (A.21), results in a sparse global system matrix which contains generally complex elements. At each node the mean values of the spatially variable  $\epsilon_r(R, Z)$  and  $\mu_r(R, Z)$  are used as the material constants in that triangular element. Applying the Dirichlet boundary conditions to the SAC mesh shown in Fig. A.2, Morgan and Mei [Ref. 5] found the numerical finite-element solution for the electromagnetic fields in Region II using a two-sweep block-by-block matrix inversion algorithm related to the Riccati transform for difference equations. At each constant colatitude,  $\theta = \theta_k$ , a vector of internal nodal azimuthal field values along the ray from  $r_1$  to  $r_2$  is defined by  $\beta_k$ . The resultant global system matrix defined by Equations (A.20) and (A.21) has a diagonal tri-block submatrix structure, which can be represented locally by relationships between adjacent radial node vectors in the mesh,

$$A_k \beta_{k-1} + B_k \beta_k + C_k \beta_{k+1} = \alpha_k, \quad (\text{A.22})$$

such that  $A_k$ ,  $B_k$ , and  $C_k$  are sparse submatrices. These form the tri-block diagonal structure of the global system matrix while  $\alpha_k$ , the local driving function, is generated from Equations (A.20) and (A.21) using the known Dirichlet BC's at  $r=a$  and  $r=b$ .

The system solution in the two-dimensional meridional (R, Z) plane is performed in a step-wise manner beginning at the positive Z-axis ( $\theta_k = \theta_1 = 0$ ) and proceeding in equal marching increments of  $\Delta\theta$ . At each  $\theta_k$ , the SAC mesh is constructed using a minimum distortion scheme to conform to the approximate piecewise smooth

surfaces. At each  $\theta_k$  increment, as the mesh is constructed in this sequential circumferential manner, the three block matrices are generated which relate adjacent radial node vectors.

During the incremental marching of  $\theta_k$ , the block-by-block Riccati matrix inversion is implemented. The Riccati matrix,  $\mathbf{R}_k$ , and the associated vector,  $\mathbf{S}_k$ , are related to the vector,  $\boldsymbol{\beta}_k$ , by the transformation

$$\boldsymbol{\beta}_{k-1} = \mathbf{R}_k \boldsymbol{\beta}_k + \mathbf{S}_k . \quad (\text{A.23})$$

Substituting this Riccati relation into Equation (A.22), solving for  $\boldsymbol{\beta}_k$  and returning to the form of the Riccati transform yields the recurrence relations

$$\mathbf{R}_{k+1} = -(\mathbf{B}_k + \mathbf{A}_k \cdot \mathbf{R}_k)^{-1} \cdot \mathbf{C}_k \quad (\text{A.24})$$

and

$$\mathbf{S}_{k+1} = (\mathbf{B}_k + \mathbf{A}_k \cdot \mathbf{R}_k)^{-1} \cdot (\boldsymbol{\beta}_k - \mathbf{A}_k \cdot \mathbf{S}_k) . \quad (\text{A.25})$$

Using these relations, the Riccati transform sweeps forward from initial conditions, using the equations of step-wise evolution in Equations (A.24) and (A.25) to sequentially generate and store the  $\mathbf{R}_k$  matrices and the  $\mathbf{S}_k$  vectors. This is called the "first sweep". The solution vectors  $\boldsymbol{\beta}_k$  are then obtained by using the transform in Equation (A.23) to perform a "backsweep" with calculations using the stored Riccati arrays. This sequentially localized technique for handling the Dirichlet boundary value problem blends easily with

the unimoment method which is used to solve the electromagnetic field in Regions I and III of Fig. A.2.

### C. UNIMOMENT METHOD

The unimoment method is a computational procedure which provides for the numerical solution of the incident, scattered and spherical core electromagnetic field expansions when dealing with the constructed SAC finite-element mesh of Fig. A.2. The numerical solution is generated by representing the core ( $r \leq r_1$ ) and the exterior scattered ( $r \geq r_2$ ) fields in terms of radial TE and TM spherical harmonic expansions, each with unknown core and scattered modal field coefficients. In order to solve for these unknown coefficients, the core expansion of Region I is applied as a boundary condition along  $r = a$ , while the boundary condition at  $r = b$  is determined as the addition of the incident field and the scattered field expansion in Region III.

Superposition is then applied to the boundary conditions, composed of the core field expansion and the exterior field expansion in order to find a complete solution. The complete field solution is found from the addition of the partial field solutions generated from two sets of applied BC's. The first set of boundary conditions applied is composed of the modal spherical harmonic core fields along  $r = a$  with zero fields along  $r = b$ . The second set of boundary conditions contains the spherical harmonic exterior scattered and incident fields at  $r = b$  with null fields at  $r = a$ . These multiple boundary conditions generate multiple solutions at the nodes along both boundaries,



$r = r_1$  and  $r = r_2$ . The unknown core and scattered modal field coefficients are obtained by setting the weighted superposition of interior solutions equal to the original field expansions. This equality is enforced along the boundaries at  $r = r_1$  and  $r = r_2$ , utilizing least squares.

The success of the unimoment method is contingent upon the capability to analytically represent the electromagnetic fields everywhere outside of the finite element mesh region. These representations, as developed for Regions I and III, are given as infinite series of spherical harmonics which must be truncated to facilitate numerical calculations. The plane-wave fields that are incident on the radome are decomposed in spherical coordinates into azimuthal modes as

$$E_{\phi}^i(r, \theta, \phi) \cong \sum_{m=0}^M e_{m, \phi}^i(r, \theta) \begin{bmatrix} j \sin(m \phi) \\ \cos(m \phi) \end{bmatrix} \quad (\text{A.26})$$

and

$$\eta_0 H_{\phi}^i(r, \theta, \phi) \cong \sum_{m=0}^M h_{m, \phi}^i(r, \theta) \begin{bmatrix} \cos(m \phi) \\ j \sin(m \phi) \end{bmatrix}, \quad (\text{A.27})$$

where  $M$  is the mathematical truncation index of the series representation. The bracketed sinusoids represent the polarization convention used for TE and TM modes, respectively.

During computations, the numerical solution of the unknown core and scattered modal field coefficients is run concurrently with the sequential Riccati transform finite-element solution in Region II.

On the forward sweep, boundary conditions for both the incident and the modal fields are generated only at the local node row being considered in that particular sweep step. On the backsweep the nodal values for each applied boundary condition are obtained along the  $r = r_1$  and  $r = r_2$  contours. The corresponding incident field and spherical harmonic field at each node are generated, and then the nodal residual fields are formed. During the backsweep, inner products integrations are accumulated and their contributions are added to a field moment matrix and the incident-field driving vector, which corresponds to each incident field. The field expansion coefficients for each incident field are obtained by multiplying the inverse of the field moment matrix with that field's driving vector. With the field expansion coefficients calculated and collected, the electromagnetic field within the radome core can be determined on a point-to-point basis as developed in Chapter II .

## Appendix B

### RADSHP PROGRAM CODE

#### PROGRAM RADSHP

```
C
C *****
C
C GENERATING THE MATERIAL FILE AND DATA STRUCTURE FILE
C FOR A LAYERED DIELECTRIC RADOME
C MATERIAL FILE PREPARED FOR EMRAD
C DATAFILE PREPARED FOR CURVE DIGITIZER
C USE EMCADIN TO GENERATE STRUCTURE FILE FOR EMRAD
C Written by R.J.Vince Nov-Dec 89
C
C *****
C VARIABLE DECLARATIONS
C *****
      REAL X(5,1001), Z(5,1001), PI, DELTHETA, DEGTORAD
      REAL THETA,C(5),R(5),H(5),DELZ(5),SHFT,FACTOR,F(5,7)
      INTEGER IBIG, I, L, SEPRATN, NSHAPE, NLMAX, RESOLV, RESPTS
      COMPLEX ER(5),UR(5)
      CHARACTER*10 SHAPE(6)
      CHARACTER*64 HDR1,HDR2
      CHARACTER*8 YNAME
      CHARACTER*12 MATFIL,DATFIL
      CHARACTER*1 YN

$LARGE

C
C *****
C INITIAL VALUES
C *****
```

```
PI=3.1415927
DEGTORAD = PI/180.
SEPRATN = 999990
RESOLV=1000
RESPTS=RESOLV+1
NLMAX = 5
```

```
C INITIALIZE SHAPE FUNCTION FACTOR ARRAY
```

```
C
```

```
DO 67 I=1,NLMAX
DO 65 J=1,6
F(I,J)=0.0
```

```
65 CONTINUE
```

```
67 CONTINUE
```

```
C
```

```
C
```

```
C *****
```

```
C INPUT NECESSARY DATA
```

```
C *****
```

```
C
```

```
C PROMPT FOR OUTPUT FILENAMES
```

```
C
```

```
WRITE(*,110)
```

```
110 FORMAT(/9X,'WELCOME TO RADSHP',
```

```
1 //9X,'THIS PROGRAM GENERATES RADOME MATERIAL AND SHAPE DATA',
```

```
2 //7X,'FILES FOR USE WITH EMRAD, BASED ON USER INPUT.',
```

```
3 ///9X,'TWO FILES ARE REQUIRED TO HOLD PROGRAM OUPUT DATA.',
```

```
4 //9X,' PLEASE ENTER THE NAME OF THE FILE TO BE USED TO ',
```

```
5 /7X,'HOLD THE PROGRAM MATERIAL PARAMETER DATA. THE EXTENSION',
```

```
6 /7X,'.MAT WILL BE ADDED AUTOMATICALLY, I. E. YOURNAME.MAT',/)
```

```
READ(*,100) YNAME
```

```
NCHAR = INDEX(YNAME,' ') -1
```

```
MATFIL = YNAME(1:NCHAR) // '.MAT'
```

```
OPEN(1,FILE=MATFIL,STATUS='UNKNOWN',ACCESS='SEQUENTIAL',
```

```

1  FORM='FORMATTED')
  WRITE(*,111)
111  FORMAT(//9X,'PLEASE ENTER THE NAME OF THE FILE TO BE USED ',
1    /7X,'TO HOLD THE PROGRAM OUTPUT DATA. THE EXTENSION .DAT WILL',
2    /7X,'WILL BE ADDED AUTOMATICALLY, I. E. YOURNAME.DAT',/7X)
  READ(*,100) YNAME
  NCHAR = INDEX(YNAME,' ') -1
  DATFIL = YNAME(1:NCHAR) // '.DAT'
  OPEN(2,FILE=DATFIL,STATUS='UNKNOWN',ACCESS='SEQUENTIAL',
1  FORM='FORMATTED')

```

C

C PROMPT FOR # OF LAYERS WITHIN THE RADOME

C

```

5  WRITE(*,114)NLMAX
114  FORMAT(/7X,'ENTER THE NUMBER OF LAYERS (.LE. ',I2,')',/7X)
  READ(*,*) NL

  IF ( (NL .LT. 1) .OR. (NL .GT. NLMAX) ) THEN
    WRITE(*,115)NLMAX+1
115  FORMAT(/7X,'NUMBER OF LAYERS IS OUT OF RANGE,(0<#<',I2,')',/7X)
  GOTO 5
  ENDIF

```

C

C LOOP TO INPUT LAYER INFORMATION

C

```

  WRITE(*,7)
7  FORMAT(/8X,'Each layer of the radome will have material consts,',
1  /10X,'an outer height of the radome layer,H,',
2  /10X,'a outer base radius,R, and',
3  /10X,'a shape function, & shape factor parameters (if appl.)',
4  //10X,'The first "layer" will be the inner core of the radome, ',
5  /10X,'normally filled with air.')

```

```

DO 12 L=1,NL
39 CONTINUE
WRITE(*,9) L
9 FORMAT(/,1 Layer No: ',I3)

IF (L.EQ.1) THEN
WRITE(*,*) ' This is the inner core of the radome'
ELSEIF (L.EQ.NL) THEN
WRITE(*,*) ' This is the outer layer of the radome'
ENDIF

```

C Prompt for Height and Radius of this layer

C

```

WRITE(*,*)
WRITE(*,43)
43 FORMAT(/8X,'Please enter the radome layer height,H,'
1 /8X,' and the outer base radius,R, for this layer.')
READ(*,*) H(L),R(L)

```

C Prompt for shaping function, to determine equations to be used

C to generate this layer of the radome

C

```

WRITE(*,*)
WRITE(*,10)
10 FORMAT(/8X,'The following shaping functions are available, '
1 /8X,' 1. General Ogive'
2 /8X,' 2. Tangent Ogive'
3 /8X,' 3. von Karman'
4 /8X,' 4. Power Series'
5 /8X,' 5. Parabola, curved'
6 /8X,' 6. Parabola, capped by pointed apex'
7 //8X,' Indicate desired shaping function by entering a number'
8 /10X,' 1,2, ... or 6 ')

```

```

READ(*,*) NSHAPE

      IF (NSHAPE.EQ.1) THEN
C   Ogive
      SHAPE(L) = 'Gen. Ogive'
      CALL OGIVE(L,X,Z,H,R,F,RESOLV,RESPTS,NLMAX)

      ELSEIF (NSHAPE.EQ.2) THEN
C   Tangent Ogive
      SHAPE(L) = 'TAN Ogive '
      CALL TANOGIVE(L,X,Z,H,R,F,RESOLV,RESPTS,NLMAX)

      ELSEIF (NSHAPE.EQ.3) THEN
C   von Karman
      SHAPE(L) = 'von Karman'
      CALL VONKRMN(L,X,Z,H,R,RESOLV,RESPTS,NLMAX)

      ELSEIF (NSHAPE.EQ.4) THEN
C   Power Series
      SHAPE(L) = 'Pwr Series'
      CALL POWER(L,X,Z,H,R,F,RESOLV,RESPTS,NLMAX)

      ELSEIF (NSHAPE.EQ.5) THEN
C   Parabola (curved)
      SHAPE(L) = 'Para Curve'
      CALL PARACRV(L,X,Z,H,R,F,RESOLV,RESPTS,NLMAX)

      ELSEIF (NSHAPE.EQ.6) THEN
C   Parabola with apex
      SHAPE(L) = 'Para APEX'
      CALL APEX(L,X,Z,H,R,F,RESOLV,RESPTS,NLMAX)

      ELSE
C   Selection out of limits
      WRITE (*,*) 'Selection is not available, try again.'
      WRITE (*,*)

```

```
GOTO 39
ENDIF
```

```
C Provide listing of inner layer parameters
```

```
C
```

```
WRITE(*,554)
DO 11 I=1,L
WRITE (*,555) I,SHAPE(I),H(I),R(I),(F(I,J),J=1,7)
```

```
11 CONTINUE
```

```
WRITE(*,*)
```

```
12 CONTINUE
```

```
C
```

```
C SHIFT RADOME SO THAT ORIGIN IS NEAR THE CENTER OF INNER LAYER
```

```
C NOTE: FACTOR is adjusted for optimal placement of origin for
```

```
C mesh construction by EMRAD
```

```
C
```

```
FACTOR=0.4
```

```
C Max inner height = Z(NL,RESPTS)
```

```
C
```

```
SHFT=Z(1,RESPTS)*(FACTOR)
```

```
DO 88 L=1,NL
```

```
DO 77 I=1,RESPTS
```

```
Z(L,I)=Z(L,I)-SHFT
```

```
77 CONTINUE
```

```
88 CONTINUE
```

```
C
```

```
C *****
```

```
C OUTPUT
```

```
C *****
```



```

        DO 330 L=1,NL
C   OUTPUT LAYER X,Z POINTS FROM TIP TO X-Z PLANE
        DO 220 I=RESPTS,1,-1
            WRITE(2,*) X(L,I),Z(L,I)
220    CONTINUE

C   CLOSE LAYER BELOW SHIFTED X-Y PLANE
C   AT Z=[ -1*[SUM OF (LAYER THICKNESS)] - SHFT ]
C
C
C   DETERMINE LAYER THICKNESS, INNER LAYER HAS NO SHIFT FOR THICKNESS
C   OTHER LAYERS HAVE BOTTOM THICKNESS DETERMINED BY RADIAL THICKNESS
C   NOTE - THE SHIFT PERFORMED FOR THICKNESS IS ADDITIVE FOR LAYERS
C
        IF (L.EQ.1) THEN
            THICK = 0
        ELSE
            THICK = THICK + R(L)-R(L-1)
        ENDIF
C
        BOTTM = (-1.0 * THICK) - SHFT
        WRITE(2,*) R(L), BOTTM
        WRITE(2,*) 0.0, BOTTM
        WRITE(2,*) SEPRATN,SEPRATN
330    CONTINUE

C   SIGNAL TERMINATION OF DATA SET
        WRITE(2,100) 'END, END'

C   Put summary of data to screen
C
        WRITE(*,554)
        DO 440 I=1,NL
            WRITE (*,555) I,SHAPE(I),H(I),R(I),(F(I,J),J=1,7)

```

440 CONTINUE

```
C
C  PROMPT FOR HEADER INFORMATION
C
  WRITE(*,112)
112 FORMAT(/7X,'THE HEADERS ALLOW THE USER TO IDENTIFY THIS',/7X,
1'SET OF DATA FROM ALL OTHER SETS.',
2//7X,'PLEASE ENTER HEADER #1 (64 CHARACTERS MAX)',/7X)
  READ(*,100) HDR1
  WRITE(*,113)
113 FORMAT(/7X,'PLEASE ENTER HEADER #2 (64 CHARACTERS MAX)',/7X)
  READ(*,100) HDR2

C
C  WRITE HEADER INFORMATION INTO MATERIAL OUTPUT DATA FILE
C
  WRITE(1,105) HDR1
  WRITE(1,105) HDR2

C
C  WRITE LAYER INFORMATION INTO MATERIAL OUTPUT DATA FILE
C
  WRITE(1,106) NL

C  Prompt for material Er for each layer of construction
C
DO 812 L=1,NL
  WRITE(*,9) L

  IF (L.EQ.1) THEN
    WRITE(*,*) '  This is the inner core of the radome'
  ELSEIF (L.EQ.NL) THEN
    WRITE(*,*) '  This is the outer layer of the radome'
  ENDIF
```

C Prompt for material constants

C

```
WRITE(*,*) 'Enter Er for this Layer: '
```

```
READ(*,*) ERR
```

C Ensure that Imag Er is < 0

C

```
ERI = -0.000001
```

```
ER(L)=CMPLX(ERR,ERI)
```

```
UR(L)=CMPLX(1.0,-1.E-6)
```

```
WRITE(1,102) ER(L),UR(L)
```

```
812 CONTINUE
```

C PLACE COPY OF CONSTRUCTION AT BOTTOM OF MATERIAL FILE

C

```
WRITE(1,554)
```

```
DO 660 I=1,NL
```

```
WRITE (1,555) I,SHAPE(I),H(I),R(I),(F(I,J),J=1,7)
```

```
660 CONTINUE
```

C --- FINAL OUTPUT TO SCREEN

```
WRITE(*,999) MATFIL,DATFIL,DATFIL
```

```
999 FORMAT(/,8X,
```

```
1' Computations and output are completed,the datafile ',A,
```

```
2/,8X,' holds the material specifications for input to EMCAD.'
```

```
3//,8X,' The datafile, 'A,', holds the radome shape data for'
```

```
4/,8X,' viewing in the CAD package, CURVE DIGITIZER. '
```

```
5//,8X,' The structure file required for input to EMCAD can be'
```

```
6/,8X,' generated by the executing the program EMCADIN, '
```

```
7/,8X,' using, 'A,', as input to EMCADIN, '
```

```
8//,8X,' The output file from EMCADIN will be in proper format'
```

9/,8X,' for input to EMCAD for the structure file.')

WRITE(\*,\*)

C

C \*\*\*\*\*

100 FORMAT(A)

101 FORMAT(I5)

102 FORMAT(4(E14.6))

103 FORMAT(I5,5(E14.6))

104 FORMAT(2(I5))

105 FORMAT(' ',A)

106 FORMAT(I5)

554 FORMAT (/#####)

1 //1X,'LAYER',2X,' SHAPE ',2X,'HEIGHT',2X,'RADIUS',

1 2X,' F1 ',2X,' F2 ',2X,' F3 ',2X,' F4 ',2X,' F5 ',

2 2X,' F6 ',2X,' F7 '/1X,'-----',2X,'-----',2X,'-----',

3 2X,'-----',2X,'----',2X,'----',2X,'----',2X,'----',

4 2X,'----',2X,'----',2X,'----')

555 FORMAT (1X,I5,2X,A10,2X,F6.2,2X,F6.2,7(F6.2))

9999 CONTINUE

C

C END PROGRAM RADOME

C

CLOSE(1)

CLOSE(2)

STOP

END

\*\*\*\*\*

C OGIVE SHAPING FUNCTION SUBROUTINE

SUBROUTINE OGIVE(L,X,Z,H,R,F,RESOLV,RESPTS,NLMAX)

INTEGER IBIG, I, L, SEPRATN, NSHAPE, NLMAX, RESPTS, RESOLV

REAL X(NLMAX,RESPTS), Z(NLMAX,RESPTS), PI, DELTHETA, DEGTORAD

REAL THETA,C(5),R(5),H(5),DELZ(5),SHFT,FACTOR

REAL ALPHA1(5), ALPHA(5), B, M, RL,GAMMA, F(NLMAX,7)

COMPLEX ER,UR

CHARACTER\*1 YN

C SET CONSTANTS

C

PI=3.1415927

DEGTORAD = PI/180.

C

C DEFINE START AND END POINT OF EACH RADOME LAYER

C

Z(L,1)=0.0

X(L,1)=R(L)

Z(L,RESPTS)=H(L)

X(L,RESPTS)=0.0

C ..... DEFINE RADOME LAYER BY OGIVE EQUATIONS ....

DELZ(L)=H(L)/RESOLV

C Prompt for Shaping factors for this ogive layer

C

WRITE(\*,\*)

WRITE(\*,43)

43 FORMAT(8X,'The ogive shaping function requires three shaping',

1/8X,'factors for determining the radome construction.'

1//8X,'The first factor, F1, determine the arc of curvature',

1/8X,'of the radome surface. Please enter F1:')

READ(\*,\*)F(L,1)

WRITE(\*,\*)

WRITE(\*,45)

45 FORMAT(8X,' Two other shaping factors are used to determine the',

1/8X,'relative position of the center of the ogive shaping',

1/8X,'arc, relative to the radome apex.',

1//8X,' The first of these factors, F2, determines the perp. ',

1/8X,'distance from the z-axis to the center of the arc.',

1//8X,' The second positioning factor, F3, determines the',  
 1//8X,'the distance from the center of the arc to the apex',  
 1//8X,'of the radome, along the z-axis.',  
 1//8X,'Please enter the position factors for the center of the',  
 1//8X,' curvature arc, F2 and F3.)

READ(\*,\*)F(L,2),F(L,3)

DO 33 I=2,RESPTS-1

Z(L,I)=Z(L,I-1)+DELZ(L)

C EQUATION OF RADOME IS  $x = \sqrt{F1^2 - (F2 - (H - z))^2} - F3$

C

$X(L,I) = \sqrt{F(L,1)^2 - (F(L,2) - (H(L) - Z(L,I)))^2} - F(L,3)$

33 CONTINUE

C ..... END OF RADOME LAYER ....

RETURN

END

\*\*\*\*\*END OF OGIVE

\*\*\*\*\*

C TANGENT OGIVE SHAPING FUNCTION SUBROUTINE

SUBROUTINE TANOGIVE(L,X,Z,H,R,F,RESOLV,RESPTS,NLMAX)

INTEGER IBIG, I, L, SEPRATN, NSHAPE, NLMAX, RESPTS, RESOLV

REAL X(NLMAX,RESPTS), Z(NLMAX,RESPTS), PI, DELTHETA, DEGTORAD

REAL THETA,C(5),R(5),H(5),DELZ(5),SHFT,FACTOR

REAL ALPHA1(5), ALPHA(5), B, M, RL,GAMMA, F(NLMAX,7)

COMPLEX ER,UR

CHARACTER\*1 YN

C SET CONSTANTS

C

PI=3.1415927

DEGTORAD = PI/180.

```

C
C DEFINE START AND END POINT OF EACH RADOME LAYER
C
  Z(L,1)=0.0
  X(L,1)=R(L)
  Z(L,RESPTS)=H(L)
  X(L,RESPTS)=0.0

C ..... DEFINE RADOME LAYER BY TANGENT OGIVE EQUATIONS ....

```

```

  DELZ(L)=H(L)/RESOLV

```

```

C Determine Shaping factors for this ogive layer

```

```

C
  F(L,4) = R(L)/2.0 + 2.0*( H(L)**2.0 )/R(L)
  F(L,5) = F(L,4) - R(L)/4.0

```

```

  WRITE(*,*)

```

```

  WRITE(*,43)F(L,4),F(L,5)

```

```

43 FORMAT(8X,'The tangent ogive shaping function determines two',

```

```

  1/8X,'factors for the radome construction. These are calculated'

```

```

  1/8X,'based on the height and radius of the radome layer.',

```

```

  1/8X,'These factors are F4 = ',F6.2,'and F5 = ',F6.2)

```

```

  DO 33 I=2,RESPTS-1

```

```

    Z(L,I)=Z(L,I-1)+DELZ(L)

```

```

C EQUATION OF RADOME IS  $x=\sqrt{F4^{**2} - z^{**2}} - F5$ 

```

```

C
  X(L,I) = 4.0* (SQRT( F(L,4)**2- Z(L,I)**2 ) - F(L,5))

```

```

33 CONTINUE

```

```

C ..... END OF RADOME LAYER ....

```

RETURN

END

\*\*\*\*\*END OF TAN OGIVE

\*\*\*\*\*

C von Karman SHAPING FUNCTION SUBROUTINE

SUBROUTINE VONKRMN(L,X,Z,H,R,RESOLV,RESPTS,NLMAX)

INTEGER IBIG, I, L, SEPRATN, NSHAPL, NLMAX, RESPTS, RESOLV

REAL X(NLMAX,RESPTS), Z(NLMAX,RESPTS), PI, DELTHETA, DEGTORAD

REAL THETA,C(5),R(5),H(5),DELZ(5),SHFT,FACTOR,SQP,ZF

REAL ALPHA1(5), ALPHA(5), B, M, RL,GAMMA

COMPLEX ER,UR

CHARACTER\*1 YN

C SET CONSTANTS

C

PI=3.1415927

SQP=SQRT(PI)

DEGTORAD = PI/180.

C

C DEFINE START AND END POINT OF EACH RADOME LAYER

C

Z(L,1)=0.0

X(L,1)=R(L)

Z(L,RESPTS)=H(L)

X(L,RESPTS)=0.0

C ..... DEFINE RADOME LAYER BY VON KARMAN EQUATIONS ....

DELZ(L)=H(L)/RESOLV

DO 33 I=2,RESPTS-1

Z(L,I)=Z(L,I-1)+DELZ(L)

C EQUATION OF RADOME IS

C  $x = (R / (\text{SQRT}(\text{PI}))) * \text{SQRT}(FZ - \text{SIN}(2 * FZ) / 2)$



```

C      for FZ = ACOS( 1 - 2 * (H-z)/H )
      FZ  = ACOS( 1.0 - 2.0 * ( H(L)-Z(L,I) ) / H(L) )
      X(L,I) = R(L)/SQP * SQRT( FZ - 0.5*SIN(2*FZ) )

```

33 CONTINUE

C ..... END OF RADOME LAYER ....

RETURN

END

\*\*\*\*\*END OF VON KARMAN

\*\*\*\*\*

C POWER SERIES SHAPING FUNCTION SUBROUTINE

SUBROUTINE POWER(L,X,Z,H,R,F,RESOLV,RESPTS,NLMAX)

INTEGER IBIG, I, L, SEPRATN, NSHAPE, NLMAX, RESPTS, RESOLV

REAL X(NLMAX,RESPTS), Z(NLMAX,RESPTS), PI, DELTHETA, DEGTORAD

REAL THETA,C(5),R(5),H(5),DELZ(5),SHFT,FACTOR

REAL ALPHA1(5), ALPHA(5), B, M, RL,GAMMA, F(NLMAX,7)

COMPLEX ER,UR

CHARACTER\*1 YN

C SET CONSTANTS

C

PI=3.1415927

DEGTORAD = PI/180.

C

C DEFINE START AND END POINT OF EACH RADOME LAYER

C

Z(L,1)=0.0

X(L,1)=R(L)

Z(L,RESPTS)=H(L)

X(L,RESPTS)=0.0

C ..... DEFINE RADOME LAYER BY OGIVE EQUATIONS ....

DELZ(L)=H(L)/RESOLV

C Prompt for Shaping factor for this power series layer

C

WRITE(\*,\*)

WRITE(\*,43)

43 FORMAT(8X,' The power series shaping function requires a',

1/8X,'shaping factor, F6, to be used in the exponential in',

1/8X,'order to determine the radome construction.',

1//8X,' When F6 = 1.0 the radome shape is conical',

1/8X,' For F6 = 0.75 the radome shape approximates the ',

1/8X,'Newtonian contour (minimizes drag). Please enter F6:')

READ(\*,\*) F(L,6)

DO 33 I=2,RESPTS-1

Z(L,I)=Z(L,I-1)+DELZ(L)

C EQUATION OF RADOME IS  $x=R * ((H-z)/H)**F6$

C

X(L,I) = R(L) \* ((H(L)-Z(L,I)) / H(L))\*\*F(L,6)

33 CONTINUE

C ..... END OF RADOME LAYER ....

RETURN

END

\*\*\*\*\*END OF POWER SERIES

\*\*\*\*\*

C PARABOLIC SHAPING FUNCTION SUBROUTINE

SUBROUTINE PARACRV(L,X,Z,H,R,F,RESOLV,RESPTS,NLMAX)

INTEGER IBIG, I, L, SEPRATN, NSHAPE, NLMAX, RESPTS, RESOLV

REAL X(NLMAX,RESPTS), Z(NLMAX,RESPTS), PI, DELTHETA, DEGTORAD

REAL THETA,C(5),R(5),H(5),DELZ(5),SHFT,FACTOR

REAL ALPHA1(5), ALPHA(5), B, M, RL,GAMMA, F(NLMAX,7)

COMPLEX ER,UR  
CHARACTER\*1 YN

C SET CONSTANTS

C

PI=3.1415927

DEGTORAD = PI/180.

C

C DEFINE START AND END POINT OF EACH RADOME LAYER

C

Z(L,1)=0.0

X(L,1)=R(L)

Z(L,RESPTS)=H(L)

X(L,RESPTS)=0.0

C ..... DEFINE RADOME LAYER BY PARABOLIC EQUATION ....

C Prompt for Shaping factor for this parabolic layer

C

WRITE(\*,\*)

WRITE(\*,43)

43 FORMAT(8X,' The parabolic shaping function requires a',

1/8X,'shaping factor, F7, to determine the curvature of,

1/8X,'the parabolic arc for the radome construction.'

1//8X,'Please enter F7:')

READ(\*,\*)F(L,7)

C ..... FOR ROUNDED PARABOLIC RADOME LAYER ....

C ... RADOME IS SCALED TO A HEIGHT = SCALE FUNCTION,C

DELZ(L)=F(L,7)/RESOLV

DO 33 I=2,RESPTS-1

Z(L,I)=Z(L,I-1)+DELZ(L)

C RECALL EQUATION OF RADOME IS  $X^2=F7-Z$ ,  $X=\text{SQRT}(F7-Z)$   
X(L,I)=SQRT( F(L,7)-Z(L,I) )

33 CONTINUE

C  
C SCALE POINTS TO RADOME DIMENSIONS

C  
DO 44 I=2,RESPTS-1  
X(L,I)=X(L,I)\*R(L)/SQRT( F(L,7) )  
Z(L,I)=Z(L,I)\*H(L)/F(L,7)

44 CONTINUE

C ..... END OF ROUNDED RADOME LAYER ....

C ..... END OF RADOME LAYER ....

RETURN

END

\*\*\*\*\*END OF PARA CURVE

\*\*\*\*\*

C POINTED PARABOLIC SHAPING FUNCTION SUBROUTINE

SUBROUTINE APEX(L,X,Z,H,R,F,RESOLV,RESPTS,NLMAX)

INTEGER IBIG, I, L, SEPRATN, NSHAPE, NLMAX, RESPTS, RESOLV

REAL X(NLMAX,RESPTS), Z(NLMAX,RESPTS), PI, DELTHETA, DEGTORAD

REAL THETA,C(5),R(5),H(5),DELZ(5),SHFT,FACTOR

REAL ALPHA1(5), ALPHA(5), B, M, RL,GAMMA, F(NLMAX,7)

COMPLEX ER,UR

CHARACTER\*1 YN

C SET CONSTANTS

C

PI=3.1415927

DEGTORAD = PI/180.

C

C DEFINE START AND END POINT OF EACH RADOME LAYER

C

Z(L,1)=0.0

X(L,1)=R(L)

Z(L,RESPTS)=H(L)

X(L,RESPTS)=0.0

C ..... DEFINE RADOME LAYER BY POINTED PARABOLIC EQUATION ...

C Prompt for Shaping factor for this parabolic layer

C

WRITE(\*,\*)

WRITE(\*,43)

43 FORMAT(8X,' The APEX parabolic shaping function requires a',

1/8X,'shaping factor, F7, to determine the curvature of',

1/8X,'the parabolic arc for the radome construction and the',

1/8X,'percent of the radome that is the pointed apex.',

1//8X,'Please enter F7:')

READ(\*,\*)F(L,7)

C ..... FOR POINTED RADOME LAYER .....

C ... RADOME IS SCALED TO A HEIGHT = MODIFIED SCALE FUNCTION,F7+1

DELZ(L)=( F(L,7)+1.0 )/RESOLV

DO 55 I=2,RESPTS-1

Z(L,I)=Z(L,I-1)+DELZ(L)

C

IF( Z(L,I).LE.( F(L,7) - 1 ) ) THEN

C RECALL EQUATION OF CONE IS  $X^2=F7-Z$ ,  $X=\text{SQRT}(F7-Z)$

```
      X(L,I)=SQRT( F(L,7)-Z(L,I) )
    ELSE
C     STRAIGHT LINE FORMULA FOR POINTED END
      X(L,I)=( ( F(L,7) +1 )-Z(L,I) )/2.0
    ENDIF
```

```
55  CONTINUE
```

```
C
C     SCALE POINTS TO RADOME DIMENSIONS
C
```

```
DO 66 I=2,RESPTS-1
  X(L,I)=X(L,I)*R(L)/SQRT( F(L,7) )
  Z(L,I)=Z(L,I)*H(L)/( F(L,7)+1.0 )
```

```
66  CONTINUE
```

```
C ..... END OF POINTED RADOME LAYER ....
```

```
C ..... END OF RADOME LAYER ....
```

```
  RETURN
```

```
  END
```

```
*****END OF PARA APEX
```

## Appendix C

### CORFLD PROGRAM CODE

#### PROGRAM CORFLD

```
C   Program Created by LT R.J. Vince (Aug-Dec 89)
C   Modifications by M.A. Morgan (Nov-Dec 89)

C   Computing core E-field at each point along a 50x50 radome grid
C   in the radome's field coordinate system.
C
INTEGER BELL,FF,NPTS,L,J,K,K1,NA,NINC
INTEGER MSTART,MSTOP,N1,NM1,M,MF,MD,M1,M2,MM
INTEGER I,ITE,ITM,KN,CA,CB,NJN,NLP,SELECT,SELCT1
REAL ALPHA(13),DALPHA(13),ANGINC(13)
REAL THETA,PHI,PI,DTR,RMIN,RCORE
REAL XP,YP,ZP,R,COST,SINT,COSP,SINP,S,C,CMP,SMP,SA,SAMX
REAL R1,R2,RSQ,EM,TH,FI,RPTS,L1,J1,PLOT(50,50),A(3,3)
REAL P(40),DP(40),TP(6),PP(6)
REAL EOTM,EOTE,EI(8),EDTERR(50,50,2),EDTER1,EDTER2
COMPLEX EXP1,E(8),EDOT(50,50,2),EDOT1,EDOT2
COMPLEX EP1,EP2,ET1,ET2,ER1,ER2,JAY,RK,SRE,SRU,KR
COMPLEX ERAD(50,50,2),ETH(50,50,2),EPI(50,50,2)
COMPLEX ER(16),UR(16),COEF(70,80),CJ(40),DCJ(40),CPLOT
CHARACTER*1 YN
CHARACTER*8 PRDAT
CHARACTER*12 PRD1,PRD2,PRD3
CHARACTER*64 GRFLAB,HDR1,HDR2,TITLE1,TITLE2,DUM

$LARGE
C
C   Setting constants
    BELL=CHAR(7)
    FF = CHAR(12)
    PI = 3.14159265359
    DTR= PI/180.
    JAY= (0.0,1.0)

C   Set default angle of rotation of planar antenna array away from z axis

C   Set default aspect ratio for plotting
    ASPECT = 1.35

C   Set number of points of resolution across array
    NPTS=50
    RPTS=( FLOAT(NPTS) - 1. )/2.

C**Initialize arrays
C   Initialize the E-field matrices
```

```

C
  DO 1 L=1,NPTS
    DO 1 J=1,NPTS
      DO 1 K=1,2
        ERAD(J,L,K)=(0.,0.)
        ETH(J,L,K)=(0.,0.)
        EPHI(J,L,K)=(0.,0.)
1 CONTINUE

C Prompt for input data filename without extension
C
  WRITE(*,14)
  READ(*,101) PRDAT
  NCHAR=INDEX(PRDAT,' ') -1
  PRD1 = PRDAT(1:NCHAR) // '.INT'
  OPEN(14,FILE=PRD1)

C
  TITLE1='The datafile used to generate fields is '
  TITLE1=TITLE1(1:40) // PRD1

C
  PRD2= PRDAT(1:NCHAR) // '.DAT'
  OPEN(15,FILE=PRD2)

C Write header from structure data file
C
  READ(14,101) HDR1
  READ(14,101) HDR2
  READ(14,101) GRFLAB
  WRITE(15,101) HDR1
  WRITE(15,101) HDR2
  WRITE(15,101) GRFLAB
  WRITE(*,101) HDR1
  WRITE(*,101) HDR2
  WRITE(*,101) GRFLAB

C Read interior core Er,Ur
C
  READ(14,507) ER(1),DUM
  READ(14,507) UR(1),DUM
  SRE=CSQRT(ER(1))
  SRU=CSQRT(UR(1))
  KR=SRE*SRU
  WRITE(*,*)
  WRITE(*,*)'SRE= ',SRE
  WRITE(*,*)'SRU= ',SRU
  WRITE(*,*)'KR = ',KR
  WRITE(15,*)' SRE=',SRE,', SRU=',SRU,', KR = ',KR

C Read minimum diameter of missile radome core expansion
C Assuming in Ko*r Wavenumber Units

```



```

C
  READ(14,503) RMIN,DUM
  RCORE=RMIN

C Read number of incident field angles (.LE. 5)
C
  READ(14,500) NA,DUM
  NINC=2*NA

C Read incident angles
C
  IPZ=0
  IMZ=0
  DO 11 I=1,NA

    READ(14,511) DANGLE

C    Checking for +/- Z-Axis Incident Fields
C
  IF(DANGLE.EQ.0.0) IPZ=I
  IF(DANGLE.EQ.180.0) IMZ=I

  DALPHA(I)= DANGLE

C  EMRAD uses Poynting vector angle with Z-axis reference
C  ANGLE of incidence = 180 - DALPHA from EMRAD
C
  ANGINC(I)= 180- DANGLE

C
  WRITE(*,*) '    Incoming Inc. Angle #',I
  WRITE(*,*) ' EMRAD Poynting angle of incidence = ',DALPHA(I)
  WRITE(*,*) '    Radome incident angle = ',ANGINC(I)
  WRITE(*,*)
  WRITE(15,*) ' Incoming Inc. Angle #',I,' = ',DALPHA(I)

C Set-up array of angles in radian measure
C
  ALPHA(I)=DTR*DALPHA(I)
11 CONTINUE
  NAI=1
  IF (NA.EQ.1) GO TO 13

C
C Determine angle of interest
C
12 CONTINUE
  WRITE(*,*) ' Select Angle of Interest By Number '
  WRITE(*,*)
  READ(*,*) NAI
  IF ((NAI.GE.1).OR.(NAI.LE.NA)) GO TO 13
  WRITE(*,*) ' That Number is Not Available ... Try Again'
  WRITE(*,*)

```

GO TO 12  
13 CONTINUE

C

C Checking if Selected Field is +/- Z-Axis Incident

IM1=0

IF((NAI.EQ.IPZ).OR.(NAI.EQ.IMZ)) IM1=1

WRITE(\*,\*)

WRITE(\*,\*) ' The angle of consideration is angle #',NAI

1 ,'= ',ANGINC(NAI),' degrees'

WRITE(\*,\*)

WRITE(15,\*) ' The angle of consideration is angle #',NAI

1 ,'= ',ANGINC(NAI),' degrees'

WRITE(15,\*)

C Transformation of coordinates to gimble mounted planar array

C

WRITE(\*,\*) ' The planar array is set by default to lie in the'

WRITE(\*,\*) ' x-y plane, with boresight in the z-direction.'

WRITE(\*,\*)

WRITE(\*,\*) ' Do you want to change the array boresight ?'

WRITE(\*,\*) ' ("Y" or "N" )'

IFLG=0

DTH=0.0

READ(\*,101) YN

IF(YN.EQ.'Y'.OR.YN.EQ.'y') THEN

WRITE(\*,\*)

WRITE(\*,\*) 'Enter Boresight Theta Angle (in degrees)'

READ(\*,\*) DTH

TH = DTH \* DTR

WRITE(\*,\*)

WRITE(\*,\*) 'Enter Boresight Phi Angle (in degrees)'

READ(\*,\*) DFI

FI = DFI \* DTR

IFLG=1

C Loading Transformation Matrix from Array to Core Coordinates

C

CT=COS(TH)

ST=SIN(TH)

CP=COS(FI)

SP=SIN(FI)

A(1,1)=CT\*CP\*\*2.0+SP\*\*2.0

A(1,2)=CP\*SP\*(CT-1.0)

A(1,3)=ST\*CP

A(2,1)=CP\*SP\*(CT-1.0)

A(2,2)=CT\*SP\*\*2.0+CP\*\*2.0

A(2,3)=ST\*SP

A(3,1)=-ST\*CP

```
A(3,2)=-ST*SP
A(3,3)=CT
```

```
ENDIF
```

```
C Get modal information
```

```
C
```

```
READ(14,505) MSTART,MSTOP,DUM
WRITE(*,*) 'MSTART=',MSTART,' MSTOP=',MSTOP
WRITE(15,*) 'MSTART=',MSTART,' MSTOP=',MSTOP
```

```
C Loop modals to read modal coefficients
```

```
C
```

```
WRITE(*,*) 'Reading Coefficients and Constructing'
WRITE(*,*) 'Fields for Each Azimuthal "m" Mode'
WRITE(*,*)
```

```
C
```

```
IF((MSTART.EQ.0).AND.(IM1.EQ.1)) THEN
WRITE(*,*) 'Terminating M-Loop at m=1 for +/- Z-Axis Incidence'
WRITE(*,*)
      MSTOP=1
ENDIF
```

```
DO 777 MD=MSTART,MSTOP
```

```
    READ(14,500) M,DUM
    WRITE(15,*) 'M= ',M
    IF(M.EQ.MD) GO TO 220
    WRITE(*,*) 'Error in Reading "m" - Check Data File'
    STOP
```

```
220 CONTINUE
```

```
    WRITE(*,*)
    WRITE(*,*) 'Azimuthal Mode "m" = ',M
    WRITE(*,*)
    IF(M.EQ.0)THEN
      EM = 1.0
      MF = 1
    ELSE
      EM = 2.0
      MF = 0
    ENDIF
```

```
    WRITE(*,*) 'Reading Coefficients'
    READ(14,500) NM1,DUM
    DO 665 ID=1,NA
      READ(14,500) I,DUM
      IF(ID.EQ.I) GO TO 221
      WRITE(*,*) 'Inc Angle Index Read Error - Check Data File'
      STOP
```

```
221 CONTINUE
```

```
    WRITE(15,*) 'I= ',I
    ITM=I
```

```

DO 222 KN=1,NM1
  CA=KN
  CB=CA+NM1
  READ(14,555) COEF(CA,ITM),COEF(CB,ITM),DUM
  WRITE(15,*) KN,COEF(CA,ITM),COEF(CB,ITM),DUM
222  CONTINUE
  ITE=I+NA
DO 333 KN=1,NM1
  CA=KN
  CB=CA+NM1
  READ(14,555) COEF(CA,ITE),COEF(CB,ITE),DUM
  WRITE(15,*) KN,COEF(CA,ITE),COEF(CB,ITE),DUM
333  CONTINUE
665  CONTINUE

C   Skipping Field Generation for m=0 if +/- Z-Axis Incidence
    IF((M.EQ.0).AND.(IM1.EQ.1)) GO TO 777

    WRITE(*,*) 'Generate Fields Across Array'

    DX=RCORE/RPTS
    DY=DX

    DO 55 J=1,NPTS
    DO 33 L=1,NPTS

C   Determine local planar array coordinates
C
    J1=FLOAT(J-1)-RPTS
    L1=FLOAT(L-1)-RPTS
    XP=J1*DX
    YP=L1*DY
    ZP=0.0

C   If Array Tilted Then Transform Coordinates
C   From local Planar array coordinates
C       to global Core coordinates....
C
    IF(IFLG.EQ.1) THEN
      XC=A(1,1)*XP+A(1,2)*YP+A(1,3)*ZP
      YC=A(2,1)*XP+A(2,2)*YP+A(2,3)*ZP
      ZC=A(3,1)*XP+A(3,2)*YP+A(3,3)*ZP
    ELSE
      XC=XP
      YC=YP
      ZC=ZP
    ENDIF

C   Determine if R <= RCORE, Else Skip Field Computation
C
    RSQ=XC*XC+YC*YC+ZC*ZC
    R=SQRT(RSQ)

```

IF (R.GT.RCORE) GO TO 32

C Determine spherical Bessel function scaled radius argument

C

RK=KR\*R

C Determine Complex Spherical Bessel function and Derivative

C

NJN=M+NM1+MF

CALL CSBSL(RK,NJN,CJ,DCJ)

C Compute Core Coordinates and Functions

C

THETA=ACOS(ZC/R)

PHI=ARCTAN2(YC,XC)

C=COS(THETA)

S=SIN(THETA)

CMP=EM\*COS(M\*PHI)

SMP=EM\*SIN(M\*PHI)

C Determine Legendre Polynomial and Derivative

C

NLP=NM1+MF

CALL LPAD(M,NLP,C,P,DP)

C Consider only the incident angle of interest

C

I=NAI

ITM=I

ITE=ITM+NA

C Initialize additive KN-sum fields to zero

C

EP1=(0.,0.)

EP2=(0.,0.)

ET1=(0.,0.)

ET2=(0.,0.)

ER1=(0.,0.)

ER2=(0.,0.)

\* . . . . .

DO 22 KN=1,NM1

N=KN+M+MF-1

NJ=N+1

NL=KN+MF

CA=KN

CB=CA+NM1

ET1=ET1+COEF(CA,ITM)\*M\*CJ(NJ)\*P(NL)

+COEF(CB,ITM)\*DCJ(NJ)\*DP(NL)

1

EP1=EP1+COEF(CA,ITM)\*CJ(NJ)\*DP(NL)

```

1      +COEF(CB,ITM)*M*DCJ(NJ)*P(NL)
      ER1=ER1+COEF(CB,ITM)*N*(N+1)*CJ(NJ)*P(NL)

      ET2=ET2+COEF(CA,ITE)*M*CJ(NJ)*P(NL)
1      +COEF(CB,ITE)*DCJ(NJ)*DP(NL)
      EP2=EP2+COEF(CA,ITE)*CJ(NJ)*DP(NL)
1      +COEF(CB,ITE)*M*DCJ(NJ)*P(NL)
      ER2=ER2+COEF(CB,ITE)*N*(N+1)*CJ(NJ)*P(NL)

22     CONTINUE
*     . . . . .

      ETH(J,L,1)=ETH(J,L,1)-JAY*SRU*CMP*ET1/R
      EPHI(J,L,1)=EPHI(J,L,1)+JAY*SRU*SMP*EP1/R
      ERAD(J,L,1)=ERAD(J,L,1)-JAY*S*CMP*ER1/(SRE*RSQ)

      ETH(J,L,2)=ETH(J,L,2)+SRU*SMP*ET2/R
      EPHI(J,L,2)=EPHI(J,L,2)+SRU*CMP*EP2/R
      ERAD(J,L,2)=ERAD(J,L,2)+S*SMP*ER2/(SRE*RSQ)

32     CONTINUE
33     CONTINUE
*     .....
55     CONTINUE
C
C== End of loops across antenna plane =====

777 CONTINUE
C
C** End of modal loop for field analysis

C*****
C Determine magnitude and phase of Computed field in the direction
C of the theoretical field vector, and the magnitude of the error.
C

      SINA=SIN(ALPHA(NAI))
      COSA=COS(ALPHA(NAI))

C Loop through array to determine field components
C
      DO 634 J=1,NPTS
      DO 633 L=1,NPTS

C Determine local planar array coordinates
C
      J1=FLOAT(J-1)-RPTS
      L1=FLOAT(L-1)-RPTS
      XP=J1*DX
      YP=L1*DY
      ZP=0.0

```

```

C   If Array Tilted Then Transform Coordinates
C   From Array to Core ....
C
IF(IFLG.EQ.1) THEN
  XC=A(1,1)*XP+A(1,2)*YP+A(1,3)*ZP
  YC=A(2,1)*XP+A(2,2)*YP+A(2,3)*ZP
  ZC=A(3,1)*XP+A(3,2)*YP+A(3,3)*ZP
ELSE
  XC=XP
  YC=YP
  ZC=ZP
ENDIF
RSQ=XC*XC+YC*YC+ZC*ZC
R=SQRT(RSQ)

C   Determine if R <= RCORE, Else Zero Fields
C
IF (R.LE.RCORE) THEN

C   Compute Core Coordinates and Functions
C
  THETA=ACOS(ZC/R)
  PHI=ARCTAN2(YC,XC)
  CT=COS(THETA)
  ST=SIN(THETA)
  CP=COS(PHI)
  SP=SIN(PHI)

C   NOTE: R IS GIVEN IN TERMS OF KO*R
C   == KO IS INCLUDED IN R, DEFINE KO=1.0
C
  KO=1.0

C   TM and TE Plane waves are of unit magnitude
C
  EOTE=1.0
  EOTM=1.0

C   Complex incident field is exponential(-j*ko*p.r)
C   use field direction for incident angle 180 to 90 degrees
C
  EXP1= CEXP( -JAY*KO*( XC*SINA+ZC*COXA ) )

C   Compute plane wave field unit vectors and components
C
C   E TM = cos(alpha)Ux - sin(alpha)Uz
C
C   E TMT

```

```

      EI(1) = COSA*CT*CP - SINA*(-ST)
      E(1) = EOTM*EXP1*EI(1)
C   E T M P
      EI(2) = COSA*(-SP)
      E(2) = EOTM*EXP1*EI(2)
C   E T M R
      EI(3) = COSA*ST*CP - SINA*(CT)
      E(3) = EOTM*EXP1*EI(3)
C   E T M T O T
      E(4)=SQRT(CABS(E(1))**2.0+CABS(E(2))**2.0+CABS(E(3))**2.0)

C   E T E = U y
C
C   E T E T
      EI(5) = CT*SP
      E(5) = EOTE*EXP1*EI(5)
C   E T E P
      EI(6) = CP
      E(6) = EOTE*EXP1*EI(6)
C   E T E R
      EI(7) = ST*SP
      E(7) = EOTE*EXP1*EI(7)
C   E T E T O T
      E(8)=SQRT(CABS(E(5))**2.0+CABS(E(6))**2.0+CABS(E(7))**2.0)

```

\*\*\*\*\*

```

C   Find magnitude and phase of Computed field in the direction
C   of the theoretical field vector
C   E . ei / Ei = ( eth*ETH+ephi*EPHI+erad*ERAD )/EO*EXP1
C
      EDOT1=EI(1)*ETH(J,L,1)+EI(2)*EPHI(J,L,1)+EI(3)*ERAD(J,L,1)
      EDOT(J,L,1)=EDOT1/(EOTM*EXP1)

      EDOT2=EI(5)*ETH(J,L,2)+EI(6)*EPHI(J,L,2)+EI(7)*ERAD(J,L,2)
      EDOT(J,L,2)=EDOT2/(EOTE*EXP1)

C   Find rel. magnitude of Computed field perpendicular to the direction
C   of the theoretical field vector, the error component in the
C   Computed field.
C
C   Rel error = | E - (E.ei) ei | / E0
C
C   = sqrt{ |Eth - (E.ei)*eth|**2 + |Erad - (E.ei)*erad|**2
C     + |Ephi - (E.ei)*ephi|**2 } / E0
C
C   Field error magnitude is computed
C
      EDTER1= CABS(ETH(J,L,1) -EDOT1*EI(1))**2.0
1     + CABS(EPHI(J,L,1)-EDOT1*EI(2))**2.0
1     + CABS(ERAD(J,L,1)-EDOT1*EI(3))**2.0

```



```
EDTERR(J,L,1)=SQRT(EDTER1)/(EOTM)
```

```
EDTER2= CABS(ETH(J,L,2) -EDOT2*EI(5))**2.0
```

```
1 + CABS(EPHI(J,L,2)-EDOT2*EI(6))**2.0
```

```
1 + CABS(ERAD(J,L,2)-EDOT2*EI(7))**2.0
```

```
EDTERR(J,L,2)=SQRT(EDTER2)/(EOTE)
```

```
ELSE
```

```
C R > RCORE , Set field components to zero
```

```
C
```

```
EDOT(J,L,1)=0.0
```

```
EDOT(J,L,2)=0.0
```

```
EDTERR(J,L,1)=0.0
```

```
EDTERR(J,L,2)=0.0
```

```
ENDIF
```

```
633 CONTINUE
```

```
634 CONTINUE
```

```
C*****
```

```
WRITE(*,*) 'SPHERICAL FIELDS COMPUTED'
```

```
WRITE(*,*)
```

```
C Optional Listing of Coordinates and E-Fields
```

```
C
```

```
WRITE(*,*) 'Check Values of Coordinates and E-Field ? (Y/N):'
```

```
READ(*,101) YN
```

```
IF((YN.EQ.'Y').OR.(YN.EQ.'y')) THEN
```

```
757 CONTINUE
```

```
WRITE(*,*) 'Enter Array Triple Index to Check (J,L,I)'
```

```
WRITE(*,*) ' J= x-point 1,2,...,NPTS
```

```
WRITE(*,*) ' L= y-point 1,2,...,NPTS
```

```
WRITE(*,*) ' I= 1 for TM, 2 for TE'
```

```
WRITE(*,*)
```

```
READ(*,*) J,L,I
```

```
EPM=CABS(EPHI(J,L,I))
```

```
ETM=CABS(ETH(J,L,I))
```

```
ERM=CABS(ERAD(J,L,I))
```

```
ETOT=SQRT(EPM*EPM+ETM*ETM+ERM*ERM)
```

```
C Determine local planar array coordinates
```

```
C
```

```
J1=FLOAT(J-1)-RPTS
```

```
L1=FLOAT(L-1)-RPTS
```

```
XP=J1*DX
```

```
YP=L1*DY
```

```
ZP=0.0
```

```
C If Array Tilted Then Transform Coordinates
```

```
C From Array to Core ....
```

C

```

IF(IFLG.EQ.1) THEN
  XC=A(1,1)*XP+A(1,2)*YP+A(1,3)*ZP
  YC=A(2,1)*XP+A(2,2)*YP+A(2,3)*ZP
  ZC=A(3,1)*XP+A(3,2)*YP+A(3,3)*ZP
ELSE
  XC=XP
  YC=YP
  ZC=ZP
ENDIF
WRITE(*,*) 'XP,YP,ZP:',XP,YP,ZP
WRITE(*,*) 'XC,YC,ZC:',XC,YC,ZC
WRITE(*,*)
WRITE(*,*) 'IE-RADI =' ,ERM
WRITE(*,*) 'IE-THI =' ,ETM
WRITE(*,*) 'IE-PHI =' ,EPM
WRITE(*,*) 'IE-TOTI =' ,ETOT
WRITE(*,*)
WRITE(*,*) 'Look at Another Point ? (Y/N):'
READ(*,101) YN
IF((YN.EQ.'Y').OR.(YN.EQ.'y')) go to 757
ENDIF

```

C \*\*\*\*\*

C Field representation selection menu

C \*\*\*\*\*

C

```
700 WRITE(*,701)
```

C \*\*\*\*\*

```

701 format(//////////5X,'CORFLD OUTPUT GRAPHICS PRESENTATION',/8X,
1'CORE FIELD REPRESENTATION SELECTION MENU',/5X,
2'Please select the type of field representation of interest
3',/5X,
4'CORE will display the following field representations: '/8X,
5'1. TM INCIDENT FIELD, E-THETA',/8X,
6'2. TM INCIDENT FIELD, E-PHI ',/8X,
7'3. TM INCIDENT FIELD, E-RADIAL ',/8X,
8'4. TM INCIDENT FIELD, E-TOTAL FIELD MAGNITUDE ',/8X,
9'5. TE INCIDENT FIELD, E-THETA',/8X,
1'6. TE INCIDENT FIELD, E-PHI ',/8X,
2'7. TE INCIDENT FIELD, E-RADIAL ',/8X,
3'8. TE INCIDENT FIELD, E-TOTAL FIELD MAGNITUDE ',/8X,
4'9. COMPARE COMPUTED FIELD TO INCIDENT FIELD',/8X,
5'10. CHANGE ASPECT RATIO',/8X,
6'0. FINISHED WITH THIS ANGLE OF INCIDENCE',/5X,
6'Indicate your selection entering "1","2",..., "10", or "0"
7',5X)

```

C \*\*\*\*\*

```
READ(*,*) SELECT
```

```

C   Check response to menu

      IF (SELECT.EQ.1) THEN
C   *****
C   DISPLAY TM INCIDENT FIELD, E-THETA

C   CHECK FOR DESIRED REPRESENTATION OF FIELD, MAGNITUDE/PHASE
      WRITE(*,715)
C   *****
      715 format(//////////5X,'CORE FIELD PRESENTATIONS',/5X,
1'You have selected the following field element',/5X,
2'1. TM INCIDENT FIELD, E-THETA',/8X,
3'This field can be plotted in PHASE or MAGNITUDE',/5X,
4'Please select the type of field representation of interest
5',/8X,
6'1. PHASE',/8X,
7'2. MAGNITUDE',/8X,
8'Indicate your selection entering "1" or "2"
9',/5X)
C   *****

      READ(*,*) SELCT1

C   ASSIGN AS INDICATED BY RESPONSE TO MENU

      DO 712 J=1,NPTS
      DO 711 L=1,NPTS
      CPLOT=ETH(J,L,1)
      IF (SELCT1.EQ.1) THEN
      PLOT(J,L)=(ARCTAN2(IMAG(CPLOT),REAL(CPLOT)))/DTR
      ELSE
      PLOT(J,L)=CABS(CPLOT)
      ENDIF
711 CONTINUE
712 CONTINUE
C
      IF (SELCT1.EQ.1) THEN
      TITLE2 = ' TM INCIDENT FIELD, E-THETA PHASE '
      ELSE
      TITLE2 = ' TM INCIDENT FIELD, E-THETA MAGNITUDE '
      ENDIF
C
C   *****

      ELSEIF (SELECT.EQ.2) THEN
C   *****
C   DISPLAY TM INCIDENT FIELD, E-PHI

C   CHECK FOR DESIRED REPRESENTATION OF FIELD, MAGNITUDE/PHASE
      WRITE(*,725)
C   *****

```

```

725 format(/,,,,,,,,,5X,'CORE FIELD PRESENTATIONS',/5X,
1'You have selected the following field element',/5X,
2'2. TM INCIDENT FIELD, E-PHI',/8X,
3'This field can be plotted in PHASE or MAGNITUDE',/5X,
4'Please select the type of field representation of interest
5',/8X,
6'1. PHASE',/8X,
7'2. MAGNITUDE',/8X,
8'Indicate your selection entering "1" or "2"
9',/5X)

```

C \*\*\*\*\*

```

READ(*,*) SELCT1

```

C ASSIGN AS INDICATED BY RESPONSE TO MENU

```

DO 722 J=1,NPTS
DO 721 L=1,NPTS
  CPLOT=EPHI(J,L,1)
  IF (SELCT1.EQ.1) THEN
    PLOT(J,L)=(ARCTAN2(IMAG(CPLOT),REAL(CPLOT)))/DTR
  ELSE
    PLOT(J,L)=CABS(CPLOT)
  ENDIF

```

721 CONTINUE

722 CONTINUE

C

```

IF (SELCT1.EQ.1) THEN
  TITLE2 = ' TM INCIDENT FIELD, E-PHI PHASE '
ELSE
  TITLE2 = ' TM INCIDENT FIELD, E-PHI MAGNITUDE'
ENDIF

```

C

C \*\*\*\*\*

```

ELSEIF (SELECT.EQ.3) THEN

```

C \*\*\*\*\*

C DISPLAY TM INCIDENT FIELD, E-RADIAL

C CHECK FOR DESIRED REPRESENTATION OF FIELD, MAGNITUDE/PHASE

```

WRITE(*,735)

```

C \*\*\*\*\*

```

735 format(/,,,,,,,,,5X,'CORE FIELD PRESENTATIONS',/5X,
1'You have selected the following field element',/5X,
2'3. TM INCIDENT FIELD, E-RADIAL',/8X,
3'This field can be plotted in PHASE or MAGNITUDE',/5X,
4'Please select the type of field representation of interest
5',/8X,
6'1. PHASE',/8X,
7'2. MAGNITUDE',/8X,
8'Indicate your selection entering "1" or "2"

```

```

9',/5X)
C *****

READ(*,*) SELCT1

C ASSIGN AS INDICATED BY RESPONSE TO MENU

DO 732 J=1,NPTS
DO 731 L=1,NPTS
CPLT=ERAD(J,L,1)
IF (SELCT1.EQ.1) THEN
PLOT(J,L)=(ARCTAN2(IMAG(CPLT),REAL(CPLT)))/DTR
ELSE
PLOT(J,L)=CABS(CPLT)
ENDIF
731 CONTINUE
732 CONTINUE
C
IF (SELCT1.EQ.1) THEN
TITLE2 = ' TM INCIDENT FIELD, E-RADIAL PHASE '
ELSE
TITLE2 = ' TM INCIDENT FIELD, E-RADIAL MAGNITUDE '
ENDIF
C
C *****

ELSEIF (SELECT.EQ.4) THEN
C *****
C DISPLAY TM INCIDENT FIELD, E-TOTAL FIELD MAGNITUDE

C ASSIGN AS INDICATED BY RESPONSE TO MENU

DO 742 J=1,NPTS
DO 741 L=1,NPTS
EPM=CABS(EPhi(J,L,1))
ETM=CABS(ETH(J,L,1))
ERM=CABS(ERAD(J,L,1))
PLOT(J,L)=SQRT(EPM*EPM+ETM*ETM+ERM*ERM)
741 CONTINUE
742 CONTINUE
TITLE2 = ' TM INCIDENT FIELD, E-TOTAL FIELD MAGNITUDE '

C *****

ELSEIF (SELECT.EQ.5) THEN
C *****
C DISPLAY TE INCIDENT FIELD, E-THETA

C CHECK FOR DESIRED REPRESENTATION OF FIELD, MAGNITUDE/PHASE
WRITE(*,755)
C *****

```

```

755 format(//////////5X,'CORE FIELD PRESENTATIONS',/5X,
1'You have selected the following field element',/5X,
2'5. TE INCIDENT FIELD, E-THETA',/8X,
3'This field can be plotted in PHASE or MAGNITUDE',/5X,
4'Please select the type of field representation of interest
5',/8X,
6'1. PHASE',/8X,
7'2. MAGNITUDE',/8X,
8'Indicate your selection entering "1" or "2"
9',/5X)

```

C \*\*\*\*\*

```

READ(*,*) SELCT1

```

C ASSIGN AS INDICATED BY RESPONSE TO MENU

```

DO 752 J=1,NPTS
DO 751 L=1,NPTS
CPLT=ETH(J,L,2)
IF (SELCT1.EQ.1) THEN
PLOT(J,L)=(ARCTAN2(IMAG(CPLT),REAL(CPLT)))/DTR
ELSE
PLOT(J,L)=CABS(CPLT)
ENDIF

```

```

751 CONTINUE

```

```

752 CONTINUE

```

C

```

IF (SELCT1.EQ.1) THEN
TITLE2 = 'TE INCIDENT FIELD, E-THETA PHASE '
ELSE
TITLE2 = 'TE INCIDENT FIELD, E-THETA MAGNITUDE'
ENDIF

```

C

C \*\*\*\*\*

```

ELSEIF (SELECT.EQ.6) THEN

```

C \*\*\*\*\*

```

C DISPLAY TE INCIDENT FIELD, E-PHI

```

```

C CHECK FOR DESIRED REPRESENTATION OF FIELD, MAGNITUDE/PHASE
WRITE(*,765)

```

C \*\*\*\*\*

```

765 format(//////////5X,'CORE FIELD PRESENTATIONS',/5X,
1'You have selected the following field element',/5X,
2'6. TE INCIDENT FIELD, E-PHI',/8X,
3'This field can be plotted in PHASE or MAGNITUDE',/5X,
4'Please select the type of field representation of interest
5',/8X,
6'1. PHASE',/8X,
7'2. MAGNITUDE',/8X,
8'Indicate your selection entering "1" or "2"

```

```

9'//5X)
C *****

READ(*,*) SELCT1

C ASSIGN AS INDICATED BY RESPONSE TO MENU

DO 762 J=1,NPTS
DO 761 L=1,NPTS
CPLT=EPHI(J,L,2)
IF (SELCT1.EQ.1) THEN
PLOT(J,L)=(ARCTAN2(IMAG(CPLOT),REAL(CPLOT)))/DTR
ELSE
PLOT(J,L)=CABS(CPLOT)
ENDIF
761 CONTINUE
762 CONTINUE
C
IF (SELCT1.EQ.1) THEN
TITLE2 = ' TE INCIDENT FIELD, E-PHI PHASE '
ELSE
TITLE2 = ' TE INCIDENT FIELD, E-PHI MAGNITUDE '
ENDIF
C
C *****

ELSEIF (SELECT.EQ.7) THEN
C *****
C DISPLAY TE INCIDENT FIELD, E-RADIAL

C CHECK FOR DESIRED REPRESENTATION OF FIELD, MAGNITUDE/PHASE
WRITE(*,775)
C *****
775 format(//////////5X,'CORE FIELD PRESENTATIONS'//5X,
1'You have selected the following field element'//5X,
2'7. TE INCIDENT FIELD, E-RADIAL'//8X,
3'This field can be plotted in PHASE or MAGNITUDE,'//5X,
4'Please select the type of field representation of interest
5'//8X,
6'1. PHASE'//8X,
7'2. MAGNITUDE'//8X,
8'Indicate your selection entering "1" or "2"
9'//5X)
C *****

READ(*,*) SELCT1

C ASSIGN AS INDICATED BY RESPONSE TO MENU

DO 772 J=1,NPTS
DO 771 L=1,NPTS

```

```

CPL0T=ERAD(J,L,2)
IF (SELCT1.EQ.1) THEN
PLOT(J,L)=(ARCTAN2(IMAG(CPLOT),REAL(CPLOT)))/DTR
ELSE
  PLOT(J,L)=CABS(CPLOT)
ENDIF
771 CONTINUE
772 CONTINUE
C
IF (SELCT1.EQ.1) THEN
  TITLE2 = ' TE INCIDENT FIELD,  E-RADIAL PHASE '
ELSE
  TITLE2 = ' TE INCIDENT FIELD,  E-RADIAL MAGNITUDE'
ENDIF
C
C *****
ELSEIF (SELECT.EQ.8) THEN
C *****
C  DISPLAY TE INCIDENT FIELD, E-TOTAL FIELD MAGNITUDE

DO 782 J=1,NPTS
DO 781 L=1,NPTS
EPM=CABS(EPI(J,L,2))
ETM=CABS(ETH(J,L,2))
ERM=CABS(ERAD(J,L,2))
PLOT(J,L)=SQRT(EPM*EPM+ETM*ETM+ERM*ERM)
781 CONTINUE
782 CONTINUE
  TITLE2 = ' TE INCIDENT FIELD,  E-TOTAL FIELD MAGNITUDE '
C *****
ELSEIF (SELECT.EQ.9) THEN
C *****
C *****
C Incident Field comparison representation selection sub-menu
C *****
C
800 WRITE(*,801)
C *****
801 format(//////////5X,'CORE COMPARISON TO IDEAL FIELD'//5X,
1'CORE FIELD REPRESENTATION SELECTION MENU 2'//5X,
2'Please select the type of field representation of interest
3'//5X,
4'CORE will display the following field representations:'//8X,
5'1. TM INCIDENT FIELD,  Computed Field dot Ideal Field'//8X,
6'2. TM INCIDENT FIELD,  Scaled Error component  '//8X,
7'3. TE INCIDENT FIELD,  Computed Field dot Ideal Field'//8X,
8'4. TE INCIDENT FIELD,  Scaled Error component  '//8X,
9'Indicate your selection entering "1","2","3", or "4"

```



```

1'//5X)
C *****

READ(*,*) SELCT2

C Check response to menu
*****

IF (SELCT2.EQ.1) THEN
C *****
C DISPLAY TM INCIDENT FIELD, Computed Field dot Ideal Field
C CHECK FOR DESIRED REPRESENTATION OF FIELD, MAGNITUDE/PHASE
WRITE(*,815)
C *****
815 format(//////////5X,'CORE FIELD PRESENTATIONS',/5X,
1'You have selected the following field element',/5X,
2'1. TM INCIDENT FIELD, Computed Field dot Ideal Field',/8X,
3'This field can be plotted in PHASE or MAGNITUDE',/5X,
4'Please select the type of field representation of interest
5',/8X,
6'1. PHASE',/8X,
7'2. MAGNITUDE',/8X,
8'Indicate your selection entering "1" or "2"
9',/5X)
C *****

READ(*,*) SELCT1

C ASSIGN AS INDICATED BY RESPONSE TO MENU

DO 812 J=1,NPTS
DO 811 L=1,NPTS
C PLOT=EDOT(J,L,1)
IF (SELCT1.EQ.1) THEN
PLOT(J,L)=(ARCTAN2(IMAG(CPLOT),REAL(CPLOT)))/DTR
ELSE
PLOT(J,L)=CABS(CPLOT)
ENDIF
811 CONTINUE
812 CONTINUE
C
IF (SELCT1.EQ.1) THEN
TITLE2='TM INCIDENT FIELD, Computed Field dot Ideal Field, PHASE'
ELSE
TITLE2='TM INCIDENT FIELD, Computed Field dot Ideal Field, MAGN.'
ENDIF
C
C *****

ELSEIF (SELCT2.EQ.2) THEN
C *****

```

```

C   DISPLAY TM INCIDENT FIELD,  Scaled Error component

      DO 822 J=1,NPTS
      DO 821 L=1,NPTS
        PLOT(J,L)=EDTERR(J,L,1)
821  CONTINUE
822  CONTINUE
      TITLE2 = 'TM INCIDENT FIELD,  Scaled Error component '

C   *****
ELSEIF (SELCT2.EQ.3) THEN
C   *****
C   DISPLAY TE INCIDENT FIELD,  Computed Field dot Ideal Field
C   CHECK FOR DESIRED REPRESENTATION OF FIELD, MAGNITUDE/PHASE
      WRITE(*,815)
C   *****
835 format(/,,,,,,,,/5X,'CORE FIELD PRESENTATIONS',/5X,
1'You have selected the following field element',/5X,
2'3.  TE INCIDENT FIELD, Computed Field dot Ideal Field',/8X,
3'This field can be plotted in PHASE or MAGNITUDE',/5X,
4'Please select the type of field representation of interest
5',/8X,
6'1.  PHASE',/8X,
7'2.  MAGNITUDE',/8X,
8'Indicate your selection entering "1" or "2"
9',/5X)
C   *****

      READ(*,*) SELCT1

C   ASSIGN AS INDICATED BY RESPONSE TO MENU

      DO 832 J=1,NPTS
      DO 831 L=1,NPTS
        CPLOT=EDOT(J,L,2)
        IF (SELCT1.EQ.1) THEN
          PLOT(J,L)=(ARCTAN2(IMAG(CPLOT),REAL(CPLOT)))/DTR
        ELSE
          PLOT(J,L)=CABS(CPLOT)
        ENDIF
831  CONTINUE
832  CONTINUE
C
      IF (SELCT1.EQ.1) THEN
        TITLE2='TE INCIDENT FIELD, Computed Field dot Ideal Field, PHASE'
      ELSE
        TITLE2='TE INCIDENT FIELD, Computed Field dot Ideal Field, MAGN.'
      ENDIF
C
C   *****

```

```

ELSEIF (SELCT2.EQ.4) THEN
C *****
C DISPLAY TE INCIDENT FIELD, Scaled Error component

DO 842 J=1,NPTS
DO 841 L=1,NPTS
PLOT(J,L)=EDTERR(J,L,2)
841 CONTINUE
842 CONTINUE
TITLE2 = 'TE INCIDENT FIELD, Scaled Error component '

C *****
ELSE
C *****
C ((SELCT2.LT.0).OR.(SELCT2.GT.4))
GO TO 800
ENDIF
C =====
C *****

ELSEIF (SELECT.EQ.10) THEN
C *****
C ASPECT RATIO
791 write(*,792)
792 FORMAT(/5X, '***** ASPECT RATIO *****'//5X,
1'IN ORDER TO AVOID DISTORTION ON THE SCREEN, IT IS NECESSARY'//5X,
2'TO DEFINE THE NUMBER OF ROWS PER INCH AND THE NUMBER OF'//5X,
3'COLUMNS PER INCH. THESE DEFINITIONS CHANGE AS THE'//5X,
4'RESOLUTION OF THE SCREEN, AS WELL AS THE TYPE OF SCREEN'//5X,
5'CHANGE.'//5X,
C 'THIS PROGRAM WAS WRITTEN IN MODE 16 (EGA) USING'//5X,
C 6'A GB-1 VIDEO BOARD AND A NEC MULTISYNC MONITOR. THE'//5X,
C 7'OPTIMUM ASPECT RATIO FOR THIS CONFIGURATION WAS .65'//5X,
8'PLEASE INPUT ASPECT RATIO.'//5X)

read(*,*) aspect
goto 700
C *****

ELSEIF (SELECT.EQ.0) THEN
C *****
C FINISHED WITH THIS ANGLE OF INCIDENCE
goto 999
C *****

ELSE
C *****
C ((SELECT.LT.0).OR.(SELECT.GT.9))
GO TO 700
ENDIF

```

C \*\*\*\*\*

C

```
WRITE (*,*) ' CALL PLOTTING ROUTINE'  
CALL PLOT3D(PLOT,50,50,ASPECT,GRFLAB,  
+ TITLE1,TITLE2,HDR1,HDR2,ANGINC(NAI),DTH)  
GO TO 700
```

C End of graphic output routine

C\*\*\*\*\*

999 CONTINUE

C

C Program completed

C

C I/O FORMAT STATEMENTS

C

```
10 FORMAT(/'//////////7X,'**** WELCOME TO CORFLD ****'/7X,  
1'THIS PROGRAM COMPUTES INTERIOR EM FIELD WITHIN PENETRABLE'/7X,  
2'BODIES OF REVOLUTION USING THE FIELD COMPONENT INFORMATION'/7X,  
3'OUTPUT BY THE PROGRAM EMCAD.'/7X,  
4'PLEASE PRESS ANY KEY TO CONTINUE.'/)  
14 FORMAT(/'//////////7X,  
1'THE OUTPUT DATA FILE IS THE FILE CONTAINING THE OUTPUT'/7X,  
2'RESULTS OF ALL NUMERICAL CALCULATIONS CONDUCTED BY EMCAD.'/7X,  
3'THE FORMAT FOR THIS INPUT IS FILENAME ONLY. NO EXTENSION IS'/7X,  
4'REQUIRED OR DESIRED. EMCAD AUTOMATICALLY APPENDS AN '/7X,  
5'EXTENSION OF .INT TO YOUR FILENAME.'/7X,  
6'PLEASE ENTER THE FILENAME OF THE OUTPUT DATA FILE.'/7X)  
23 FORMAT(/7X,'ENTER INC FLD ANGLE (DEG) FOR # ',I3,/7X)  
25 FORMAT(/'////////7X,'PLEASE PRESS ANY KEY TO CONTINUE.'///)  
100 FORMAT(/'***** CORE OUTPUT DATA *****'  
1'*****')  
101 FORMAT(A)  
102 FORMAT(I5)  
103 FORMAT(4(E14.6))  
104 FORMAT(' *** PROGRAM ABORTED BECAUSE ----- ***')  
107 FORMAT(/7X,I5,2(2X,'(',1PE11.3,2X,1PE11.3,')'))  
109 FORMAT(/7X,'INCIDENT FIELD ANGLES'/9X,N',10X,'ALPHA(N)')  
110 FORMAT(/7X,I3,7X,F5.0,' DEG')  
111 FORMAT(/7X,'COMPLEX Er(n) AND Ur(n)')  
112 FORMAT(/7X,'ENTER INTERIOR DATA FILE (D:FILENAME.EXTENSION): ')  
115 FORMAT(/7X,'ENTER CAPTION OR LABEL ')  
124 FORMAT(/7X,'INDEXING PROGRAM THROUGH VALUES OF M')  
125 FORMAT(7X,'M-LOOP .... M = ',I5)  
135 FORMAT(7X,'EX M-LOOP')  
136 FORMAT(/7X,'***** CORE ANALYSIS COMPLETED *****')  
204 FORMAT(/7X,'***** M = ',I5,' *****')  
300 FORMAT(7X,I5,5E12.3)
```

```

500 FORMAT(3X,I5,A64)
503 FORMAT(3X,E14.6,A64)
505 FORMAT(3X,I5,2X,I5,A64)
507 FORMAT(3X,1PE11.3,2X,1PE11.3,2X,A64)
510 FORMAT(3X,F5.0,A64)
511 FORMAT(3X,F5.0)
555 FORMAT(3X,E12.6,3X,E12.6,4X,E12.6,3X,E12.6,3X,A64)
566 FORMAT(3X,A10,E12.6,3X,E12.6)
567 FORMAT(3X,A10,E12.6)
576 FORMAT(3X,A5,I5,A2,E12.6,3X,E12.6)
577 FORMAT(3X,A5,E12.6)
578 FORMAT(3X,E12.6)

```

```

99 CONTINUE

```

```

C
C Program termination
C
C WRITE(*,136)

```

```

STOP
END

```

```

*****

```

```

SUBROUTINE CSBSL (Z,N1,CJ,DCJ)
COMPLEX Z,Z2,F1,F2,FSTO,ALPHA,CJ(*),DCJ(*)

```

```

C
C This routine computes Riccati spherical bessel functions and
C derivatives for complex Z using downward recurrence as in
C Miller's algorithm, but with highly accurate starting values
C using truncated Taylor's series.

```

```

C
C Returns CJ(n)=J[n-1] (kr) for n=1...N1
C DCJ(n)=J'[n-1] (kr)
C

```

```

C DEFINING CONSTANTS

```

```

C
C ZM2=(CABS(Z))**2
C NMX=N1+ZM2
C Z2=(Z*Z)/2.0
C D1=2.*NMX+3.
C D2=D1*(2.*NMX+5.)
C D3=D2*(2.*NMX+7.)
C D4=D3*(2.*NMX+9.)

```

```

C Using Truncated Taylor's series for relative upper starting
C values of J(NMX) and J(NMX+1) with NMX .GT. ABS(Z*Z).

```

```

C

```

```

F1=1.-Z2/D1+Z2*Z2/(2.*D2)-Z2*Z2*Z2/(6.*D3)

```

$$F2=Z*(1./D1-Z2/D2+Z2*Z2/(2.*D3)-Z2*Z2*Z2/(6.*D4))$$

C Performing downward recurrence with highest two orders in CJ(N1).

```
C
M=NMX
11 FSTO=F1
F1=(2.*M+1.)*F1/Z-F2
F2=FSTO
IF (CABS(F1).LT.1.0E20) GO TO 1
F1=F1*1.0E-20
F2=F2*1.0E-20
FSTO=FSTO*1.0E-20
1 CONTINUE
M=M-1
IF (M+2.GT.N1) GO TO 11
CJ(N1)=F2
CJ(N1-1)=F1
N0=N1-2
```

C Continuing downward recurrence to CJ(1)

```
C
DO 22 K=1,N0
J=N1-K-1
22 CJ(J)=(2.*J+1.)*CJ(J+1)/Z-CJ(J+2)
```

C Normalizing entire array wrt actual J0(Z).

```
C
ALPHA=CSIN(Z)/CJ(1)
DO 33 K=1,N1
33 CJ(K)=ALPHA*CJ(K)
```

C Computing derivatives

```
C
DCJ(1)=CJ(1)/Z-CJ(2)
DO 44 K=2,N1
44 DCJ(K)=CJ(K-1)-(K-1)*CJ(K)/Z
RETURN
END
```

\*\*\*\*\*

SUBROUTINE LPAD (M,N1,C,P,DP)

C This routine computes Normalized Legendre polynomials and derivatives.

```
C
C For m >= 1; P(n) = P(m,n+m-1)/sin(THETA)
C DP(n) = dP(m,n+m-1) / dTHETA for n=1,2,...
C For m = 0; P(n) = P(0,n)/sin(THETA)
C DP(n) = dP(0,n) / dTHETA for n=1,2,...
```

C

REAL P(\*),DP(\*)

```

KSP=N1-1
Q=1.0-C*C
S=SQRT(Q)
IF(M.GT.0) GO TO 1
P(1)=1.0
P(2)=C
DP(1)=0.0
DP(2)=-S
Q=S
GO TO 3
1 IF (M.EQ.1) GO TO 5
P(1)=-((-S)**(M-1))
DP(1)=-M*C*(-S)**(M-1)
GO TO 7
5 P(1)=-1.0
DP(1)=-M*C
7 DO 2 K=1,M
P(1)=P(1)*(2*K-1)
2 DP(1)=DP(1)*(2*K-1)
P(2)=P(1)*C*(2*M+1)
DP(2)=(C*DP(1)-Q*P(1))*(2*M+1)
3 DO 4 K=2,KSP
N=K+M-1
AK=M-N-1
P(K+1)=((M+N)*P(K-1)-(2*N+1)*C*P(K))/AK
4 DP(K+1)=((M+N)*DP(K-1)+(2*N+1)*(Q*P(K)-C*DP(K)))/AK
RETURN
END

```

FUNCTION ARCTAN2(Y,X)

```

C
C Routine returns ATAN(Y/X) for all cases
C
REAL ARCTAN2,Y,X,PI
PI=3.1415927
IF(Y.NE.0.0) GO TO 11
IF(X.EQ.0.0) GO TO 33
IF(X.GT.0.0) ARCTAN2=0.0
IF(X.LT.0.0) ARCTAN2=PI
RETURN
11 IF(X.NE.0.0) GO TO 22
IF(Y.GT.0.0) ARCTAN2=0.5*PI
IF(Y.LT.0.0) ARCTAN2=1.5*PI
RETURN
22 ARCTAN2=ATAN2(Y,X)
RETURN
33 ARCTAN2=0.0
RETURN
END

```

```

c *****
C PLOT3D Plotting subroutine

```

C REVISED: 22 NOV 1989

C

C This subroutine automatically scales and plots data as 3-D surfaces

C

C All subroutines beginning with 'Q'

C are from the Grafmatic plotting library

C

```
SUBROUTINE PLOT3D(Z,M,N,ASPECT,GRFLAB,  
+ TITLE1,TITLE2,HDR1,HDR2,ALPHA,GAMMA)  
REAL X(50,50),Y(50,50),Z(50,50),XMIN,XMAX,YMIN,YMAX,ZMAX,ZMIN  
REAL XST,XFIN,YST,YFIN,ZST,ZFIN,ZFLOOR,ZAVG  
REAL PHI,THETA,ALPHA,GAMMA,STHETA,I1,J1,M2,N2,R  
INTEGER M,N  
CHARACTER*1 YES,GRAFPRNT  
CHARACTER*5 ASTRING,GSTRING,TSTRING,PSTRING,MIN,MAX,AVG  
CHARACTER*12 name,label  
CHARACTER*64 TITLE1, TITLE2, TITLE3, TITLE4, GRFLAB, HDR1, HDR2  
CHARACTER*64 HCOPY  
DIMENSION IWORK1(640),IWORK2(640)
```

C SETTING CONSTANTS

C

BELL=CHAR(7)

FF = CHAR(12)

C Set constant for degree to radian conversion

C

PI = 3.14159265359

DTR= PI/180.

C Calculate # of points on array

C

NARRAY=PI\*( (M/2)\*\*2)

M2=FLOAT(M-1)/2.0

N2=FLOAT(N-1)/2.0

C IWORK1 and IWORK2 should have a dimension equal to the number of

C pixels (or points on a pen plotter) in the x direction.

C

NPTS=640

C NPTS is the size of the IWORK1 and IWORK2 arrays

C

MODEP=16

C Plot will be in graphics mode 16

C

C XYSET is a routine called to set up the initial x,y values (see below)

C

CALL XYSET(X,Y,M,N)



C

```
XST = X(1,1)
YST = Y(1,1)
ZST = Z(1,1)
```

```
XFIN = XST
YFIN = YST
ZFIN = ZST
```

```
ZMIN = 1000
ZMAX = -1000
ZAVG = 0.0
```

```
PHI = 45.0
THETA = 75.0
```

```
DO 10 I = 1,M
  DO 15 J = 1,N
    IF (X(I,J) .LT. XST) XST = X(I,J)
    IF (X(I,J) .GT. XFIN) XFIN = X(I,J)

    IF (Y(I,J) .LT. YST) YST = Y(I,J)
    IF (Y(I,J) .GT. YFIN) YFIN = Y(I,J)

    IF (Z(I,J) .LT. ZST) ZST = Z(I,J)
    IF (Z(I,J) .GT. ZFIN) ZFIN = Z(I,J)
```

C Check if point is on the antenna array

C

```
I1=FLOAT(I)-1.0
J1=FLOAT(J)-1.0
R= SQRT( ((I1-M2)/M2)**2.0 + ((J1-N2)/N2)**2.0 )
IF (R.LT.1.0) THEN
  IF (Z(I,J) .LT. ZMIN) ZMIN = Z(I,J)
  IF (Z(I,J) .GT. ZMAX) ZMAX = Z(I,J)
  ZAVG = ZAVG + Z(I,J)/(FLOAT(NARRAY))
ENDIF
```

15 CONTINUE

10 CONTINUE

```
XFIN = XFIN + .2
YFIN = YFIN + .2
```

C The following parameters set the axes values, etc. (see documentation  
C for Q3DXAX, Q3DYAX, Q3DZAX)

C

```
XBEG=XST
YBEG=YST
XEND=XFIN
YEND=YFIN
```

```
XSTEP = .2
```

```

YSTEP = .2
IF ((XFIN-XST).GE. 0.9) XSTEP = .5
IF ((YFIN-YST).GE. 0.9) YSTEP = .5

ZDIF=ZFIN-ZST

IF (ZDIF.LE. 0.3) THEN
  ZSTEP = 0.05
  ZFIN = FLOAT(INT(10*ZFIN))/10+2*ZSTEP
  ZST = FLOAT(INT(10*ZST))/10-ZSTEP
  ZMINOR = 1
ELSEIF (ZDIF.LE. 1.0) THEN
  ZSTEP = 0.25
  ZFIN = FLOAT(INT(ZFIN+0.5))+2*ZSTEP
  ZST = FLOAT(INT(ZST-0.5))-ZSTEP
  ZMINOR = 1
ELSEIF (ZDIF.LE. 2.0) THEN
  ZSTEP = 0.5
  ZFIN = FLOAT(INT(ZFIN+0.5))+2*ZSTEP
  ZST = FLOAT(INT(ZST-0.5))-ZSTEP
  ZMINOR = 1
ELSEIF (ZDIF.LE. 5.0) THEN
  ZSTEP = 1.0
  ZFIN = FLOAT(INT(ZFIN+0.5))+2*ZSTEP
  ZST = FLOAT(INT(ZST-0.5))-ZSTEP
  ZMINOR = 1
ELSEIF (ZDIF.LE. 10.0) THEN
  ZSTEP = 2.0
  ZFIN = FLOAT(INT(ZFIN+0.5))+2*ZSTEP
  ZST = FLOAT(INT(ZST-0.5))-ZSTEP
  ZMINOR = 1
ELSE
  ZSTEP = 30.0
  ZFIN = INT(ZFIN+ZSTEP)
  ZST = INT(ZST-15.0)
  ZMINOR = 1
ENDIF
ZFLOOR=0.0

```

C Clear the screen and enter input data

C

```
CALL QSMODE(2)
```

C 3D-stick is a "wire-frame" figure with hidden lines removed.

C 3D-fill is similar, except that the interior regions of each

C "panel" making up the surface is filled in with color "klrin"

C and the boundary of each panel is drawn with color "klredg".

C NOTE: The two routines use different hidden line removal algorithm.

C Which you use is a matter of taste. However the equivalent

C of Q3DFIL is not available on the pen plotter since it is

C based on an overpainting scheme which isn't practical on a plotter.

```

C
C The angles phi and theta specify the view direction as shown in the
C   appropriate figure in your GRAFMATIC/PLOTMATIC manual.
C The parameter icross is one if you wish cross-grid lines in both the
C   x and y directions or zero for grid lines only parallel to
C   the x axis (as may be appropriate in creating a spectral plot).
C
C
C
16  WRITE(*,*) ' Enter 0 for 3D-stick or 1 for 3D-fill option'
C    READ(*,*) IFIL
    IFIL=0
    WRITE(*,*)
    WRITE(*,*) ' Default view angles are: phi=-45.,theta=70.'
    IF (IFIL.EQ.1) THEN

C      KLRIN is the color inside the panel
C
      KLRIN=2

C      KLREDG is the panel border color
C
      KLREDG=1
    ELSE
C      ICROSS is 1 for cross-grids in both directions
C
      ICROSS=1
    ENDIF

C Continuation point to loop through desired angles of observation
C
17  CONTINUE
    CALL QSMODE(MODEP)

C Modify THETA to reflect YFIN/ZFIN
C
    STHETA = ATAN( (YFIN/ZFIN)*TAN(THETA*DTR) )/DTR

C Q3DROT changes the view perspective as described in the documentation
C
    CALL Q3DROT(X,Y,Z,M,N,PHI,STHETA)
C
    CALL Q3DWIND(XST,XFIN,YST,YFIN,ZST,ZFIN,XMIN,XMAX,YMIN,YMAX)
    IOPT=0
    IF ( (XMAX-XMIN).NE.0.0) THEN
      YOVERX = (YMAX-YMIN) / (XMAX-XMIN)
    ELSE
      YOVERX = 999
    ENDIF
    XORG=0.0
    YORG=0.0

```

```
CALL QPLOT(100,550,30,270,XMIN,XMAX,YMIN,YMAX,
1 XORG,YORG,IOPT,YOVERX,ASPECT)
```

- C The next 3 routines create the x, y, and z axes
- C If Q3DFIL is used, then draw the axes AFTER the 3D plot is drawn
- C so that the 3D plot does not overwrite the x/y axes.

```
C
  IF (IFIL.EQ.1) GO TO 66
```

```
C
  CALL Q3DXAX(XST,XFIN,XSTEP,9,1,2,YBEG,YEND,ZFLOOR,1.0)
  CALL Q3DYAX(YST,YFIN,YSTEP,9,1,2,XBEG,XEND,ZFLOOR,1.0)
  CALL Q3DZAX(ZST,ZFIN,ZSTEP,9,-1,2,XBEG,YBEG,1.0)
```

```
66 CONTINUE
```

- C Finally draw the 3D plot, using the appropriate option.

```
C
  IF(IFIL.EQ.1) CALL Q3DFIL(X,Y,M,N,KLRIN,KLREDG)
  IF(IFIL.NE.1) CALL Q3DSTk(X,Y,M,N,IWORK1,IWORK2,NPTS,ICROSS)
```

- C Draw the axes if using Q3DFIL routine

```
C
  IF(IFIL.NE.1) GO TO 67
  CALL Q3DXAX(XST,XFIN,XSTEP,9,1,2,YBEG,YEND,ZFLOOR,1.0)
  CALL Q3DYAX(YST,YFIN,YSTEP,9,1,2,XBEG,XEND,ZFLOOR,1.0)
  CALL Q3DZAX(ZST,ZFIN,ZSTEP,9,-1,2,XBEG,YBEG,1.0)
```

```
67 CONTINUE
```

```
C *****
```

- C WRITE TEXT ON SCREEN

```
NCHAR = 64
KOLOR = 10
ICOL = 10
IROW = 24
CALL QPTXT(NCHAR,TITLE1,KOLOR,ICOL,IROW)
```

```
C *****
```

- C WRITE TEXT ON SCREEN

```
NCHAR = 64
KOLOR = 10
ICOL = 10
IROW = 23
CALL QPTXT(NCHAR,HDR1,KOLOR,ICOL,IROW)
```

```
C *****
```

- C WRITE TEXT ON SCREEN

```
NCHAR = 64
KOLOR = 10
ICOL = 10
IROW = 22
CALL QPTXT(NCHAR,HDR2,KOLOR,ICOL,IROW)
```

```
C *****
```

- C WRITE TEXT ON SCREEN

```

NCHAR = 64
KOLOR = 10
ICOL = 10
IROW = 21
CALL QPTXT(NCHAR,GRFLAB,KOLOR,ICOL,IROW)
C *****
C WRITE TEXT ON SCREEN
NCHAR = 64
KOLOR = 10
ICOL = 15
IROW = 20
CALL QPTXT(NCHAR,TITLE2,KOLOR,ICOL,IROW)
C *****
C MAGNITUDES INTO A STRING
C
CALL NUMSTR(ZMIN,MIN)
CALL NUMSTR(ZMAX,MAX)
CALL NUMSTR(ZAVG,AVG)
TITLE3='min. Z = '//MIN//'; max. Z = '//MAX
+ //'; average Z = '//AVG
C WRITE TEXT ON SCREEN
C
NCHAR = 64
KOLOR = 10
ICOL = 17
IROW = 3
CALL QPTXT(NCHAR,TITLE3,KOLOR,ICOL,IROW)
C *****
C ANGLES INTO A STRING
C
CALL NUMSTR(ALPHA,ASTRING)
CALL NUMSTR(GAMMA,GSTRING)
CALL NUMSTR(THETA,TSTRING)
CALL NUMSTR(PHI,PSTRING)
TITLE4='Inc. A = '//ASTRING//';Plane G = '//GSTRING
+ //'; View: phi='//PSTRING// theta='//TSTRING
C WRITE TEXT ON SCREEN
C
NCHAR = 64
KOLOR = 10
ICOL = 10
IROW = 2
CALL QPTXT(NCHAR,TITLE4,KOLOR,ICOL,IROW)
C *****
C Hardcopy Query
NCHAR = 30
KOLOR = 12
ICOL = 1
IROW = 1
HCOPY='Hardcopy ---> Enter P or p'
CALL QPTXT(NCHAR,HCOPY,KOLOR,ICOL,IROW)
CALL QCMOV(32,1)

```

```

CALL QINKEY(IEXTEND,IKEY)
NCHAR = 40
KOLOR = 1
ICOL = 1
IROW = 1
HCOPY='
CALL QPTXT(NCHAR,HCOPY,KOLOR,ICOL,IROW)
C If 'P' or 'p' then prtsc
C
IF( IKEY.EQ.80 .OR. IKEY.EQ.112 ) THEN
  CALL QPSCRN
ENDIF
C *****
CALL Q3DINV(X,Y,Z,M,N)
CALL QSMODE(2)
WRITE(*,*)'ENTER NEW ANGLES PHI & THETA (DEG) OR (9,9) WHEN DONE'
READ(5,*)PHI,THETA
IF ( (PHI.NE.9.).AND.(THETA.NE.9.) ) GOTO 17
999 CONTINUE
100 FORMAT(A1)
520 FORMAT(3X,I5)
578 FORMAT(3X,E12.6)

101 FORMAT(A)
RETURN
END

*****
C *****
C
SUBROUTINE XYSET(X,Y,M,N)
C
REAL X(M,N),Y(M,N),I1,J1,N2,M2
C
C define x,y values over the m by n grid
C
M2=FLOAT(M-1)/2.0
N2=FLOAT(N-1)/2.0
DO 111 I=1,M
DO 121 J=1,N
I1=FLOAT(I)-1.0
J1=FLOAT(J)-1.0
X(I,J)= (I1-M2)/M2
Y(I,J)= (J1-N2)/N2
121 CONTINUE
111 CONTINUE
RETURN
END
C*****
C
C SUBROUTINE NUMSTR
C

```

C ACCEPTS NUMBER AND RETURNS CHAR\*5 WITH SIGN AND THREE DIGIT STRING

C

```
SUBROUTINE NUMSTR(ANUM,STR)
REAL ANUM,VNUM
INTEGER NUM,HUN,TEN,ONE,ORDER
CHARACTER*5 STR
```

```
ORDER = 0
```

C Get sign information

C

```
IF (ANUM.GE.0.0) THEN
  STR(1:1)='+'
ELSE
  STR(1:1)='- '
ENDIF
```

C Strip sign values

C

```
VNUM=ABS(ANUM)
```

C

```
IF (VNUM .LT. 1.0) THEN
  ORDER=0
  VNUM=VNUM*1000.0
ELSEIF (VNUM .LT. .10.0) THEN
  ORDER=1
  VNUM=VNUM*100.0
ELSEIF (VNUM .LT. 100.0) THEN
  ORDER=2
  VNUM=VNUM*10.0
ELSE
  ORDER=3
ENDIF
```

C Use integer part of shifted VNUM

C

```
NUM=VNUM
IF (NUM.GE.1000) THEN NUM=999
HUN=INT(NUM/100.)
TEN=(NUM-100*HUN)/10
ONE=(NUM-100*HUN-10*TEN)
```

C PLACE DECIMAL

C

```
IF (ORDER .EQ. 0) THEN
  STR(2:2)='.'
  STR(3:3)=CHAR(48+HUN)
  STR(4:4)=CHAR(48+TEN)
  STR(5:5)=CHAR(48+ONE)
ELSEIF (ORDER .EQ. 1) THEN
  STR(2:2)=CHAR(48+HUN)
  STR(3:3)='.'
```

```
STR(4:4)=CHAR(48+TEN)
STR(5:5)=CHAR(48+ONE)
ELSEIF (ORDER .EQ. 2) THEN
STR(2:2)=CHAR(48+HUN)
STR(3:3)=CHAR(48+TEN)
STR(4:4)='.'
STR(5:5)=CHAR(48+ONE)
ELSE
STR(2:2)=CHAR(48+HUN)
STR(3:3)=CHAR(48+TEN)
STR(4:4)=CHAR(48+ONE)
STR(5:5)='.'
ENDIF
```

C

```
RETURN
END
```



## Appendix D

### SOFTWARE SOURCES

#### Microsoft FORTRAN

16011 NE 36th Way  
Box 97017  
Redmond, WA 98073-9717

#### West Coast Consultants CURVE DIGITIZER

4202 Genesee Avenue, Suite 309  
San Diego, CA 92117  
(619) 565-1266

#### Microcompatibles, Inc. GRAFMATIC

301 Prelude Drive  
Silver Spring, MD 20901  
(301)593-5151

#### Prof. M.A. Morgan

Code 62Mw  
Naval Postgraduate School  
Monterey, CA 93943

## LIST OF REFERENCES

1. J. D. Walton, Jr., Radome Engineering Handbook , Marcel Dekker, Inc., New York, 1970.
2. H. L. Hirsch and D. C. Grove, Practical Simulation of Radar Antennas and Radomes , pp. 169-173, Artech House, Norwood, Massachusetts, 1987.
3. M. A. Morgan, "Numerical computation of electromagnetic scattering by inhomogeneous dielectric bodies of revolution," Ph.D. dissertation, University of California at Berkeley, 1976.
4. E. M. Connolly, " Finite-element electromagnetic scattering: an interactive micro-computer algorithm," Master's thesis, Naval Postgraduate School, Monterey, California, 1988.
5. M. A. Morgan, and K. K. Mei, "Finite-element computation of scattering by inhomogeneous penetrable bodies of revolution," IEEE Transactions on Antennas and Propagation, Vol. AP-27, No. 2, pp. 202-214, March 1979.
6. K. K. Mei, "Unimoment method of solving antenna and scattering problems," IEEE Transactions on Antennas and Propagation, Vol. AP-22, pp. 760-766, November 1974.
7. M. A. Morgan, S.-K. Chang, and K. K. Mei, "Coupled azimuthal potentials for electromagnetic field problems in inhomogeneous axially-symmetric media," IEEE Transactions on Antennas and Propagation, Vol. AP-25, pp. 413-417, May 1977.
8. F. D. Groutage, "Radome development for broadband RF missile sensor," Technical Report No. TR2023, Naval Electronics Laboratory Center, San Diego, California, January 1977.
9. D. A. James, Radar Homing Guidance for Tactical Missiles , pp. 38-55, John Wiley & Sons, New York, 1986.

10. M. A. Morgan, "Finite element calculation of microwave absorption by the cranial structure," IEEE Transactions on Biomedical Engineering, Vol. BME-28, No. 10, pp. 687-695, October 1981.
11. R. F. Harrington, Time-Harmonic Electromagnetic Fields , pp. 264-269, McGraw-Hill Book Company, Inc., New York, 1961.
12. P. L. Overfelt, "Radome analysis and design capabilities of the RF and Microwave Technology Branch," Technical Report No. NWC TP 6636, Naval Weapons Center, China Lake, California, April 1985.

## INITIAL DISTRIBUTION LIST

	No. Copies
1. Defense Technical Information Center Cameron Station Alexandria, Virginia 22304-6145	2
2. Library (Code 0142) Naval Postgraduate School Monterey, California 93943-5002	2
3. Chairman, Code 62 Department of Electrical and Computer Engineering Naval Postgraduate School Monterey, California 93943-5000	1
4. Chairman, Code 67 Department of Aeronautics and Astronautics Naval Postgraduate School Monterey, California 93943-5000	1
5. Professor Michael A. Morgan (Code 62MW) Naval Postgraduate School Monterey, California 93943-5000	10
6. Professor James Hauser (Code 67HS) Naval Postgraduate School Monterey, California 93943-5000	5
7. Dr. Rabiner Madan (Code 1114SE) Office of Naval Research 800 N. Quincy Street Arlington, Virginia 22217	1

8. Dr. Arthur Jordan (Code 1114SE) 1  
Office of Naval Research  
800 N. Quincy Street  
Arlington, Virginia 22217
9. Mr. Joseph A. Mosko (Code 35203) 1  
RF Components Division  
Naval Weapons Center  
China Lake, California 93555
10. Ms. Pamela L. Overfelt (Code 3814) 1  
Naval Weapons Center  
China Lake, California 93555
11. Professor Kenneth K. Mei 1  
EECS Department  
University of California  
Berkeley, California 94720
12. LT Robert Vince 3  
2878 Christ Road  
Warsaw, New York 14569





Thesis

V684 Vince

c.1 An electromagnetic ra-  
dome model using an inter-  
active micro-computer fi-  
nite element algorithm.

27 APR 93

38042

Thesis

V684 Vince

c.1 An electromagnetic ra-  
dome model using an inter-  
active micro-computer fi-  
nite element algorithm.



thesV684

An electromagnetic radome model using an



3 2768 000 89543 7  
DUDLEY KNOX LIBRARY